Program

<table>
<tr><th>May 27 (Sun)</th><th colspan="2">May 28 (Mon) @ A204</th><th colspan="2">May 29 (Tue) @ A204</th></tr>
<tr><td rowspan="18">Field Trip</td><td rowspan="6">9:00～11：50</td><td rowspan="6">Qualifying Exam. of GP-EES students</td><td>9:00～9:10</td><td>Opening Remarks</td></tr>
<tr><td>9:10～9:40</td><td>Shanaka de Silva</td></tr>
<tr><td>9:40～10:10</td><td>Georg Zellmer</td></tr>
<tr><td>10:10～10:30</td><td>Coffee Break</td></tr>
<tr><td>10:30～11:00</td><td>Fidel Costa</td></tr>
<tr><td>11:00～11:30</td><td>Satoshi Okumura</td></tr>
<tr><td rowspan="3">11:50～14：50</td><td rowspan="3">Poster Session & Lunch Break @ A205 & 2F Hall</td><td rowspan="2">11:30～13:00</td><td rowspan="2">Group Photo & Poster Session & Lunch Break @ A205 & 2F Hall</td></tr>
<tr><td>13:00～13:30</td><td>Tatsuki Tsujimori</td></tr>
<tr><td>13:30～14:00</td><td>Inna Safonova</td></tr>
<tr><td rowspan="6">14:50～17：40</td><td rowspan="6">Qualifying Exam. of GP-EES students</td><td>14:00～14:30</td><td>Daniel Frost</td></tr>
<tr><td>14:30～14:50</td><td>Coffee Break</td></tr>
<tr><td>14:50～15:20</td><td>Stephen Kirby</td></tr>
<tr><td>15:20～15:50</td><td>Hisashi Nakahara</td></tr>
<tr><td>15:50～16:20</td><td>Marcel Thielmann</td></tr>
<tr><td>16:20～16:40</td><td>Coffee Break</td></tr>
<tr><td rowspan="3">18:00～20：00</td><td rowspan="3">Discussion @AOSIS</td><td>16:40～17:10</td><td>Bo Qiu</td></tr>
<tr><td>17:10～17:40</td><td>Shusaku Sugimoto</td></tr>
<tr><td>17:40～17:50</td><td>Closing Remarks</td></tr>
</table>

Access

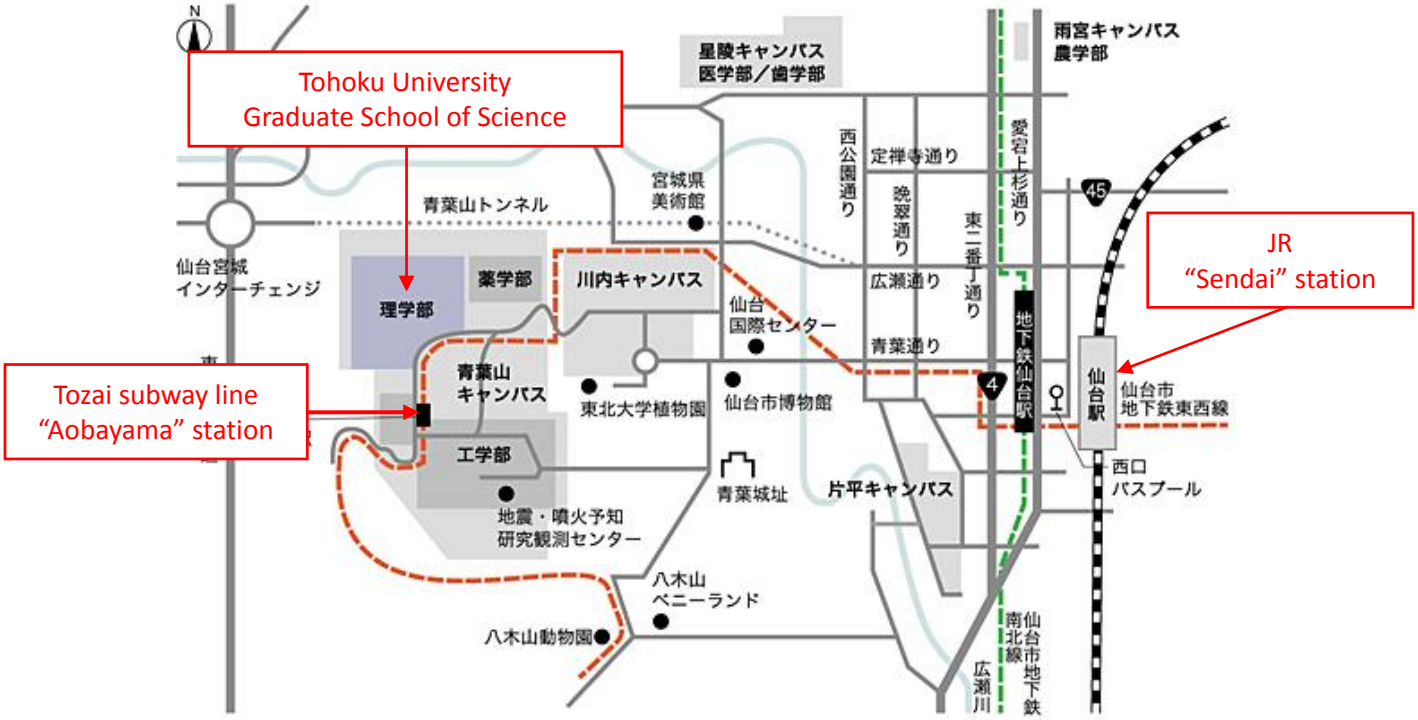

Campus map

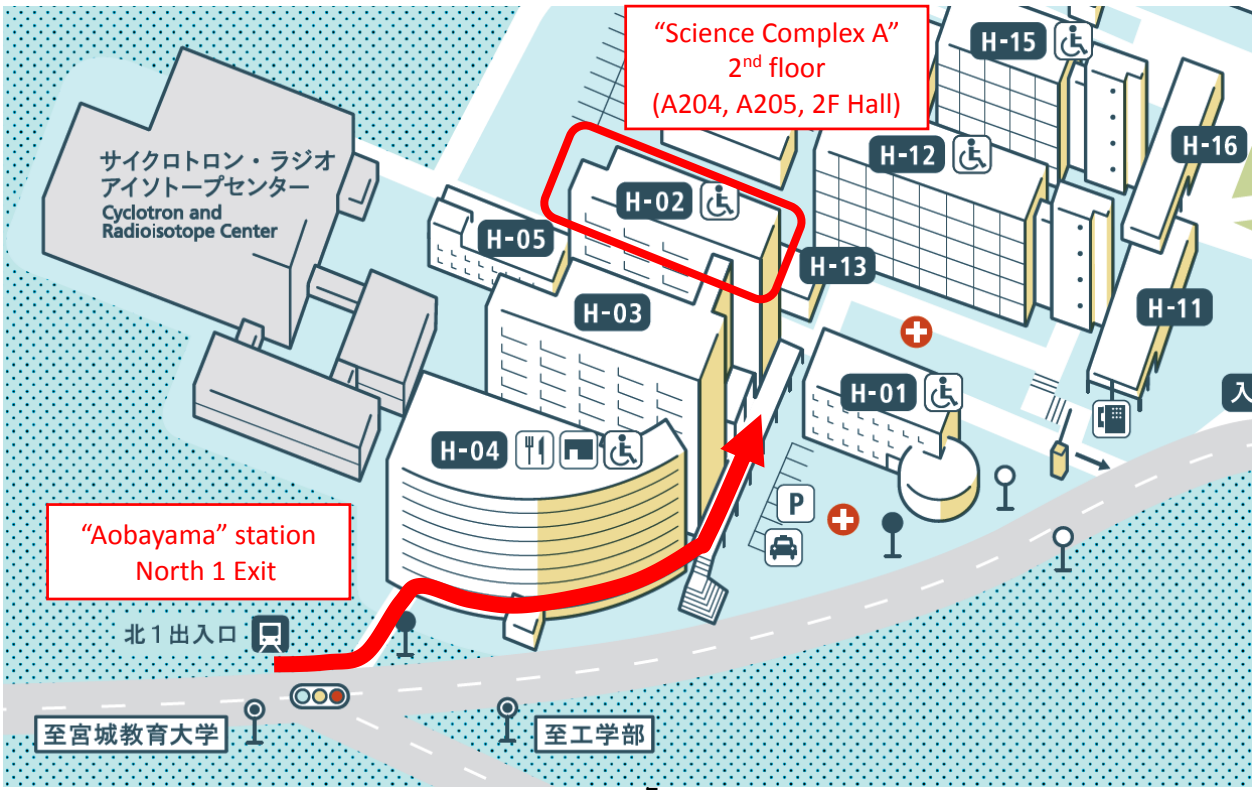

Oral presentations

Earth, Sea and Sky III:
International Joint Graduate Program Workshop in Earth and Environmental Sciences
co-hosted by The International Joint Graduate Program in Earth and Environmental Sciences, Tohoku University
andJSPS-DFG Japanese-German Graduate Externship for Research on Deep Earth Volatile Cycle
May 27-29, 2018. Tohoku University Aobayama Campus

Zircon constraints on magmatic evolution: Application to the Unzen magmatic system

SHANAKA DE SILVA[1], BETHANY MURPHY[1], SHINJI TAKARADA[2]

[1] College of Earth Ocean and Atmospheric Science, Oregon State University, Corvallis, OR 97333. U.S.A
[2] Geological Survey of Japan, AIST Site 7, 1-1-1, Higashi, Tsukuba, Ibaraki 305-8567, JAPAN

One of major goals of igneous petrology is to understand the long-term thermal evolution or thermal history of pre-eruptive magmas. This is a key to understanding the behavior of crustal magmatic systems and understand their hazard potential. While progress has been made on diffusive time scales that pertain to syn-eruptive and immediately pre-eruptive times scales (Druitt et al., 2013; Nakamura, 1995), the time scales of eruptible magma accumulation and longevity have been more challenging. In the last two decades studies of the mineral zircon has provided many advances because of the rare capability to combine temporal, thermal and chemical data in this one phase. This offers the opportunity to track pre-eruptive evolution of magmas and assess the role of thermal and chemical drivers of magma dynamics and eruption. Recent work (Tierney et al., 2016; Kent and Cooper, 2017) has led to the development of integrated geochronological, thermal, and chemical models that allows pre-eruptive magma dynamics to be explored at the previously elusive magma system longevity. Here we explore the application of zircon chronochemistry to one of Japan's iconic volcanic systems, Unzen volcano, Kyushu, Japan.

Crystal-rich (40-50 vol.%) intermediate lava has been the primary eruptive product of Unzen, Japan (1990-1995). Despite the association with devastating eruptions, the formation, timing, and evacuation of such magma is not well understood: do such eruptions tap a long-lived, multi-cycle crystal mush, or, is it generated in a single magmatic cycle prior to eruption? We explored these questions through U/Th zircon geochronology and zircon chemistry studies (zircon chronochemistry) on several eruptions, spanning in age from the most recent (Heisei-Shinzan; 1990-1995) to lavas of the Older Unzen period (≥200 ka).

Our work has revealed the protracted history and evolution of the crystal mush zone at the Unzen Volcanic Complex. Individual zircon surface-interior age pairs, together with zircon age spectra, suggest that portions of this crystal mush have been present in the crust since at least the late Older Unzen period (≥200 ka). Significant zircon growth appears to occur throughout the eruptive hiatus (200-100 ka), suggesting that magmatic activity continued uninterrupted through this period. Ti-in-zircon temperatures show that zircon crystalizes from a low temperature (≤790˚C) magma. Subtle variations in trace element chemistry are observed in titanium and hafnium content through time: titanium contents show a moderate negative correlation with time, while hafnium shows a moderate positive correlation. This suggests that the crystal mush zone has evolved towards a more mature, heterogeneous system. Using integrated thermochemical models we show that the Unzen magmatic system could be maintained in a melt-present state for extended periods of time through periodic recharge. Thus eruptions tap a long-lived crystal mush and eruptions maybe controlled by non-magmatic factors.

[References]
[1] Druitt, T H, F Costa, E Deloule, M Dungan, and B Scaillet. 2013. "Decadal to Monthly Timescales of Magma Transfer and Reservoir Growth at a Caldera Volcano." Nature 482 (7383). Nature Publishing Group: 77–80. doi:10.1038/nature10706.
[2] Kent, Adam J R, and Kari M Cooper. 2017. "How Well Do Zircons Record the Thermal Evolution of Magmatic Systems?." Geology 46 (2). 111–14. doi:10.1130/G39690.1.
[3] Nakamura, M. 1995. "Continuous Mixing of Crystal Mush and Replenished Magma in the Ongoing Unzen Eruption." Geology 23 (9): 807–10.
[4] Tierney, Casey R, Axel K Schmitt, Oscar M Lovera, and Shanaka L de Silva. 2016. "Voluminous Plutonism During Volcanic Quiescence Revealed by Thermochemical Modeling of Zircon." Geology 44 (8): 683–86. doi:10.1130/G37968.1.

Earth, Sea and Sky III:
International Joint Graduate Program Workshop in Earth and Environmental Sciences
co-hosted by The International Joint Graduate Program in Earth and Environmental Sciences, Tohoku University
andJSPS-DFG Japanese-German Graduate Externship for Research on Deep Earth Volatile Cycle
May 27-29, 2018. Tohoku University Aobayama Campus

Deciphering magma ascent and eruptive processes through microanalytical investigations of the tephra record of Tongariro Volcanic Centre, North Island, New Zealand

C. LORMAND[1], G. F. ZELLMER[1], K. NEMETH[1], S. MEAD[1]

[1] Volcanic Risk Solutions, Massey University, Private Bag 11222, Palmerston North 4442, New Zealand

Crystals within erupted volcanic rocks record geochemical and textural signatures during magmatic evolution prior to the onset of an eruption. Deriving residence time of microlites using growth rate and CSDs may constrain time windows between geophysical unrest and the onset of explosive eruptions. We developed a new method to automate CSD image processing, using the Trainable Weka Segmentation (TWS) plugin in ImageJ. We obtained back-scattered electron images (BSE) of a range of volcanic deposits from the Taupo Volcanic Zone, New Zealand. Deposits record a wide range of eruption styles (Strombolian, phreatomagmatic, Vulcanian, sub-Plinian and Plinian). Three samples, consisting of different crystal content and imaged using variable resolution scanning electron microscopes, were tested using TWS. Crystal measurements and CSDs obtained from the automatically segmented images are then be compared with that of the manual segmentation. The three samples tested with the TWS plugin are successfully segmented, but manual segmentation for the crystal-rich sample (>85 vol. % of microlites) is not achievable, as crystal boundaries are difficult to distinguish. Accuracy performance tests for the TWS classifiers yield F-scores between 0.930 and 0.951, hence, the TWS is a successful and fast-computing tool for outlining crystals from BSE images of volcanic glass shards. A total of 200 plagioclase and pyroxene microlites CSDs were generated from individual tephra shards, and CSDs from the same tephra were combined. All combined pyroxene CSDs exhibit concave-up shape, similar intercepts and slopes at the smallest sizes. Combined with a well-constrained pyroxene microlite growth rate, they yield similar growth durations of 13±9 (2σ) to 29±20 (2σ) hours, regardless the eruptive style or source. Further geothermometry and barometry calculations may provide additional constraints on physical parameters such as decompression rate, depth of crystallization, and thus ascent rates. Our study shows that pyroxene microlite CSDs can be generated relatively rapidly, and provide insights into the rapid timescales of magma ascent at active arc volcanoes.

Earth, Sea and Sky III:
International Joint Graduate Program Workshop in Earth and Environmental Sciences
co-hosted by The International Joint Graduate Program in Earth and Environmental Sciences, Tohoku University
andJSPS-DFG Japanese-German Graduate Externship for Research on Deep Earth Volatile Cycle
May 27-29, 2018. Tohoku University Aobayama Campus

Processes driving eruptions at Open Vent volcanoes

F. COSTA[1], D. RUTH[2], T. GIRONA[3]

[1] Earth Observatory of Singapore, Nanyang Technological University. fcosta@ntu.edu.sg
[2] Department of Geology and Environmental Science. College of Charleston. USA
[3] Jet Propulsion Laboratory, California Institute of Technology.USA

Mafic open vent volcanoes are among the most active on Earth. They display prominent volcanic plumes which during quiescence can passively release several thousand of ktones of gas per day. They produce frequent, mildly explosive and small eruptions every few months or years. Their typically produce the same magma composition and phenocryst content for decades (e.g. Arenal, Mayon, Llaima). This monotonous activity may be punctuated by subplinian or plinian eruption every hundred years or so. Why do these volcanoes erupt so often? What processes drive the repetitive eruptions of the same magma composition for decades at these volcanoes? What is the role of magma replenishment versus degassing? How can we anticipate their eruptions? We will address these questions with a close look to the phenocryst zoning patterns, monitoring datasets, and physical model of the plumbing system.

A physical model of magma ascent during lava effusion

SATOSHI OKUMURA[1], TOMOFUMI KOZONO[2]

[1] Department of Earth Science, Graduate School of Science, Tohoku University
[2] Department of Geophysics, Graduate School of Science, Tohoku University.

Non-explosive volcanism shows various types of magma effusion to the surface. The type of effusion has been known to have a rough correlation with the magma flux. Under low magma flux, the magma is nearly crystallized and effuses as lava spine. On the other hand, high magma flux leads to effusion of relatively low viscosity magma and sometimes, causes explosions[1]. Physical models of magma ascent to the surface have been proposed to model and predict lava effusion behavior. However, these models do not include an important property of magma, namely the ductile-brittle transition (DBT) of magma. Silicic magma exhibits brittle behavior under high deformation rates[2]. The brittle behavior during magma ascent results in the formation of magmatic faults along conduit rims, and the type of magma ascent changes from viscous flow to friction-controlled flow, as observed at Mt. Unzen, Japan, and Mt. St. Helens, USA. In this study, we have experimentally investigated the friction of magmatic faults and incorporated the DBT in the physical model of magma ascent. Our experiments indicate that the flow type depends on the deformation rate, magma viscosity, and normal stress on the fault[3]. The physical model proposed can reproduce the transition from viscous flow to friction-controlled flow, i.e., the various types of lava effusion, and the cause of explosion under high magma flux. We have investigated the rheology of magmatic faults under the assumption of crystal-free magma, although actual magma consists of crystals and causes crystallization during ascent. Thus, additional studies on magmatic faults are necessary to improve the physical model and our understanding of lava effusion behavior.

[References]
[1] Watts et al. (2002) Geological Society, London, 21, 115–152.
[2] Dingwell (1996) Science, 273, 1054–1055.
[3] Okumura et al. (2015) JGR, 120, doi:10.1002/2014JB011532.
[4] Okumura&Kozono (2017) GRL, 44, doi:10.1002/2017GL072875.

Earth, Sea and Sky III:
International Joint Graduate Program Workshop in Earth and Environmental Sciences
co-hosted by The International Joint Graduate Program in Earth and Environmental Sciences, Tohoku University
andJSPS-DFG Japanese-German Graduate Externship for Research on Deep Earth Volatile Cycle
May 27-29, 2018. Tohoku University Aobayama Campus

Nature of slab-derived fluids: Stable isotope records in metasedimentary phengite

TATSUKI TSUJIMORI [1,2], DANIEL PASTOR-GALÁN [1],
ANTONIO M. ÁLVAREZ-VALERO [3]

[1] Center for Northeast Asian Studies, Tohoku University
[2] Department of Earth Science, Tohoku University
[2] Department of Geology, Universidad de Salamanca

Phengite is the most common metamorphic mineral in H*P*–UH*P* metasedimentary rocks, which can convey H_2O and LILEs (especially K, Ba, Cs and Rb) plus Li, B and N to subarc and/or rear arc depths. The breakdown of phengite in a downgoing slab causes fluid-induced element transport into overlying mantle wedge. *What are the oxygen and hydrogen isotope signatures of phengite in metasedimentary rocks in Pacific type subduction zone? What are the stable isotopic compositions of fluids equilibrated with the phengite? Do they evolve during continuous dehydration reactions?* We have investigated the $^{2}H/^{1}H$ (D/H) and $^{18}O/^{16}O$ ratios of phengites from pelitic schists of the Devonian–Carboniferous Renge and Cretaceous Sambagawa H*P* belts, SW Japan.

Phengite separates from the lawsonite- and/or epidote-grade blueschist-facies pelitic schists of the Osayama mélange (central Chugoku Mtns) of the Renge belt are characterized by very low δD_{VSMOW} ranging from –113 to –93.9‰; $\delta^{18}O_{VSMOW}$ values range from +12.9 to +14.6‰. Phnegites from the garnet-bearing pelitic schists of the Sambagawa belt also show low δD values (–95.6 to –60.5‰) with $\delta^{18}O$ = +12.3 to + 14.4‰.

Assuming 250–350°C and 450°C for metamorphic temperatures of the Osayama and Sambagawa schists respectively, the inferred metamorphic fluid compositions in 'blueschist-facies' depth in fossil slabs have a compositional range of δD = ~–40 to –75‰ and $\delta^{18}O$ = ~+13 to +15‰. These values are significantly lower than the slab-fluid induced from the Arima hot spring water in a forearc region of modern SW Japan subduction. Our study suggests that slab-derived fluids in Pacific-type subduction zone are characterized by light hydrogen isotope and also suggests that the phengite breakdown can affect hydrogen isotope of nominally anhydrous minerals (NAMs) in deep mantle.

Earth, Sea and Sky III:
International Joint Graduate Program Workshop in Earth and Environmental Sciences
co-hosted by The International Joint Graduate Program in Earth and Environmental Sciences, Tohoku University
andJSPS-DFG Japanese-German Graduate Externship for Research on Deep Earth Volatile Cycle
May 27-29, 2018. Tohoku University Aobayama Campus

Tectonic erosion at Pacific-type convergent margins: evidence from the western Central Asian Orogenic Belt

INNA SAFONOVA[1,2], SHIGENORI MARUYAMA[1,3], PAVEL KOTLER[1], ALINA PERFILOVA[1]

[1] Novosibirsk State University
[2] Sobolev Institute of Geology and Mineralogy SB RAS
[3] Earth-Life Science Institute, Tokyo Institute of Technology

Pacific-type convergent margins (PCM) and their related orogenic belts exist/form over subduction zones. PCM are places of major continental growth by island-arc juvenile magmatism and accretion, but they are also places of strong plate interactions and crust destruction. Accordingly there are two contrast types of PCM: accreting ones accompanied by the formation of accretionary complexes, and eroding ones accompanied by the tectonic erosion of accretionary wedge, fore-arc prism and volcanic arc and even by direct subduction of intra-oceanic arcs (Safonova et al., 2015). PCM are the only ways on the Earth surface to deliver surface materials to the deep mantle. The longer are the periods of tectonic erosion and subduction, the larger will be the volume of the material arriving to the mantle. Therefore, it is very important to highlight the periods of tectonic erosion in fossil PCMs to evaluate the amount of the surface material eroded in the past.

The objectives of our study were Pacific-type orogenic belts of the Central Asian Orogenic Belt (CAOB). There are dozens of accretionary complexes formed during the late Neoproterozoic-early Paleozoic (Transbaikalia, Altai-Sayan, central Kazakhstan, N. Tienshan), the Middle Paleozoic-early Carboniferous (S. Tienshan, East Kazakhstan, Mongolia); the late Carboniferous-Permian (Sikhote-Alin), and the Triassic-Neogene (Russian Far East). The most promising areas of tectonic and subduction erosion in the CAOB are eastern and central Kazakhstan, northern Tienshan and Transbaikalia (Safonova et al., 2017).

We have sampled and studied greywacke and/or turbiditic sandstones in three orogenic belts of the CAOB: the Char ophiolite belt and the Zharma arc terrane in eastern Kazakhstan, and Itmurundy ophiolite/accretionary belt in central Kazakhstan. In total, we analyzed 11 samples for bulk rock geochemistry and U-Pb detrital zircon ages and four samples for Hf-in-zircon isotopes. The rocks have andesitic to dacitic major element composition. The samples from Char, Zharma and Itmurundy (early stage) have andesitic major element compositions; they yielded unimodal distributions of U-Pb ages peaked at 340-320 and 390-340 (Char), 350-330 (Zharma) and 470-450 (Itmurundy-1) Ma suggesting their intra-oceanic arc origin. More evidence for this comes from their positive Hft values –5.5-16.7, 7.2-15.2, 9.2-17.6, respectively –and the occurrence of sparse outcrops of volcanic rocks possessing supra-subduction geochemical affinities. In addition, the Char samples show positive epsilon Ndt values: 6.0-7.6. Two younger samples from Itmurundy-2 have dacitic compositions and yielded multi-model U-Pb age probability curves peaked at 500-480, 1000-900, and 2500-2400 Ma suggesting a continental arc origin. Thus, on the one hand, the unimodal U-Pb age probability curves and the positive epsilon Nd and Hf values suggest an Ordovician intra-oceanic arc in the Itmurundy-1 area, and a late Devonian and possibly two early Carboniferous arcs in east Kazakhstan. On the other hand, the scarcity of outcrops of supra-subduction rocks suggests that those arcs were tectonically eroded during oceanic subduction.

The study was supported by the Ministry of Education and Science of the Russian Federation (project no. 14.Y26.31.0018).

[References]

[1] Safonova, I., Maruyama, S., Litasov, K. (2015). Generation of hydrous-carbonate plumes in the mantle transition zone linked to tectonic erosion and subduction. Tectonophysics 662, 454-471.
[2] Safonova I., Maruyama, S., Kruk N., Obut O., Kotler P., Gavryushkina O., Khromykh S., Kuibida M., Krivonogov S., in press. Pacific-type orogenic belts: linking evolution of oceans, active margins and intra-plate magmatism. Episodes.

Earth, Sea and Sky III:
International Joint Graduate Program Workshop in Earth and Environmental Sciences
co-hosted by The International Joint Graduate Program in Earth and Environmental Sciences, Tohoku University
andJSPS-DFG Japanese-German Graduate Externship for Research on Deep Earth Volatile Cycle
May 27-29, 2018. Tohoku University Aobayama Campus

Evolution of the Earth's redox state

DANIEL FROST[1]

[1] Bayerisches Geoinstitut, University of Bayreuth, Bayreuth, D95447, Germany

During accretion and core-mantle differentiation mantle silicates must have equilibrated with iron metal. This would have fixed the oxygen fugacity of the earliest mantle at a level where the volatile species degassing to the surface would have been dominantly CH_4 and H_2. The oldest rocks on Earth, however, indicate a more oxidised mantle, similar to todays, where H_2O and CO_2 are the dominant degassing species. This rapid increase in the oxidation state of the mantle after core formation finished was one of the most important events in the Earth's development towards a habitable planet. The mechanism by which this increase, essentially in the Fe_2O_3 content of the mantle, occurred is important for the formation of the early atmosphere and the timing of volatile element arrival to the mantle and Earth as a whole.

There are a number of possible mechanisms that can be explored to explain the oxidation of the mantle. H_2O, Fe_2O_3 or CO_2-rich material accreted in the final stages of growth after core formation had ceased could potentially oxidize the mantle. Although H_2O could have oxidized FeO to Fe_2O_3, the reaction would have produced H_2 in the mantle which would tend to reduce the already oxidized material. It is questionable whether accreting material contained sufficient Fe_2O_3 to oxidize the mantle and CO_2 would have had trouble entering the mantle as temperatures were presumably too high after core formation to allow carbonates to exist.

One very effective mechanism is the disproportionation of FeO at high pressures to produce Fe_2O_3 and Fe metal. Experiments on mineral phases such as garnet and the lower mantle mineral bridgmanite show that with increasing pressure the proportion of Fe_2O_3 in these minerals, when they are in equilibrium with iron metal, increases. Bridgmanite for example contains approximately 50 % of its iron in the ferric state in equilibrium with iron metal. If bridgmanite therefore crystallized from a mantle initially poor in Fe_2O_3 then it would have to form through the partial reduction of FeO to form metallic iron i.e. $3FeO = Fe + Fe_2O_3$. If some of this iron were lost to the core during the final stages of core formation, then the mantle would be left with a higher overall proportion of Fe_2O_3.

The stabilization of Fe_2O_3 and iron metal in preference to FeO results from a smaller molar volume of the Fe_2O_3 component compared to FeO. This is seen for both both garnet and bridgmanite iron components, which raises the question of whether silicate melt components might show a similar behavior. Although with initially increasing pressure the molar volume of Fe_2O_3 in silicate melts is larger than that of the FeO melt component, experimental evidence indicates that this situation reverses at approximately 15 GPa. This implies that a sufficiently deep magma ocean formed during accretion that was initially Fe_2O_3-poor may similarly have precipitated iron metal near its base. This is due to the requirement of the silicate melt to contain a raised level of Fe_2O_3 even in equilibrium with iron metal at high pressure. Convective mixing could have then rendered the magma ocean with an Fe_2O_3 content compatible at its surface with H_2O and CO_2 degassing but in equilibrium with iron metal at its base. Such a scenario would be also consistent with the apparently more reduced mantle of Mars because an early magma ocean would have been too shallow to reach pressures where the difference in molar volumes between the two iron components reverses.

Earth, Sea and Sky III:
International Joint Graduate Program Workshop in Earth and Environmental Sciences
co-hosted by The International Joint Graduate Program in Earth and Environmental Sciences, Tohoku University
andJSPS-DFG Japanese-German Graduate Externship for Research on Deep Earth Volatile Cycle
May 27-29, 2018. Tohoku University Aobayama Campus

Adventures in the History of the Geosciences: What We Can Learn from the Research of the Past

STEPHEN KIRBY[1, 2]

[1] Research Center for Prediction of Earthquakes and Volcanic Eruptions, Tohoku University
[2] U.S. Geological Survey, Menlo Park, California, USA

I give two examples from research published in the past that give important scientific data and insights that cannot easily be found in digital form on the internet and that show how the then new technical developments and inventions can lead to important new scientific discoveries. These historical investigations were often motivated by practical needs for societies.

1. The Discovery of the Japan and Kurile Oceanic Trenches.

As late as 1870, the shape of the ocean basins and the nature of the rocks of the seafloor were largely unknown. In particular, there were no reliable methods for measuring depths greater than a few kilometers. In 1873, English physicist J.J. Thomson announced the completion of the design and construction of an apparatus using piano wire and a spooling wheel that counted the number of rotations of the wheel and hence the amount of wire line deployed from the ship. When the seafloor was reached, a bottom weight was released and the change in the total weight of the line allowed the observer to confirm that the seafloor had been reached. Depths as great as 8500 m could be measured. Thin (~ I mm) piano wire was used in this apparatus instead of rope because of its high strength and availability of this steel wire in great lengths.

Motivated by the need for a trans-Pacific telegraphic cable from the USA to Japan, the U.S. Navy sailing/steamship *Tuscarora* was equipped with the Thompson wireline sounder under the command of George Belknap. It departed California in January 1874 and took wireline soundings all of the way to Tokyo and then north to Alaska. On this northern leg of the cruise, deep soundings were recorded off the Pacific coast of Honshu and Hokkaido Islands at a certain distance from the shoreline. In Commander Belknap's own words, *"... as a rule the deepest water is found, not in the central parts of the great oceans, but near or approximately near the land whether of the continental mass or island isolation."*.

Building on this hypothesis, Belknap subsequently recorded 16 depths greater than 7000 m off the Kurile Islands. These soundings were the first evidence of deep ocean trenches that we now know are the consequence of the subduction process and the cause of Japan's earthquakes and arc volcanic eruptions. These discoveries were made possible by new technology, advanced wireline materials manufacture, and the need for global communications.

[References]
[1] Belknap, George E., Commander USN, 1874. Deep-Sea Soundings in the Northern Pacific Ocean – Obtained in the United States Steamer Tuscarora in 1874. U.S. Bureau of Navigation Office 54 Washington U.S. Printing Office, 51 p. and Plates I through XVI.
[2] Theberghe, Albert, 2014. "George Belknap and the Thomson Sounding Machine. Hydro International eNewsletter, 07/04/2014 Issue

2.Mercury Mining, Detailed Subsurface Geologic Mapping Using Electrical Lights, and the Rheology of Serpentinites in California.

Mercury was widely used before the 1960's in the refinement of gold from disseminated gold deposits. Mercury ores are a byproduct of metasomatism of serpentinite bodies. Serpentinites, in turn, are formed from the hydration of peridotites beginning at mantle depths and in the crust. In California serpentinites are typically in tectonic contact with the Franciscan Complex, an assemblage of oceanic rocks thought to be accreted to the California margin during subduction. Careful surface and subsurface mapping of serpentinites in mercury ore mining districts by the U.S. Geological Survey from the late 1930's into the 1960's showed that these serpentinites were intruded into host rocks by cold injection from depth. Blocks of metamorphic rocks such as blueschists and eclogites that are entrained by such intrusions demonstrate that the source of these serpentinites is likely in the former forearc mantle. Although there were more than 40 such USGS investigations (1935-1964) based on mining geology that confirmed the cold intrusion model, these reports have been completely ignored in more recent papers on the emplacement mechanisms of serpentinites in California. Nearly all of the mines described in these earlier USGS reports are now covered or closed, so these mining papers are crucial to the interpretation of these serpentinites.

[References]
[3] Bailey, E. H. and Everhart, D.L. 1964. Geology and quicksilver deposits of the New Almaden district. Santa Clara County, California: U.S. Geological Survey Professional Paper 360, 206 p.
[4] Kirby, S.H., Wang, K., and Brocher, T. M., 2014. A large mantle water source for the northern San Andreas fault system: a ghost of subduction past. Earth, Planets and Space 66: 67, 18 p.

Earth, Sea and Sky III:
International Joint Graduate Program Workshop in Earth and Environmental Sciences
co-hosted by The International Joint Graduate Program in Earth and Environmental Sciences, Tohoku University
andJSPS-DFG Japanese-German Graduate Externship for Research on Deep Earth Volatile Cycle
May 27-29, 2018. Tohoku University Aobayama Campus

Improving seismic-interferometry-based monitoring techniques

HISASHI NAKAHARA[1]

[1] Department of Geophysics, Graduate School of Science, Tohoku University.

Seismic interferometry is a technique to retrieve Green's function between two points from cross correlation functions of noise records at the two points. This technique is cost-effective because no expensive active sources are necessary. After it was developed in seismology in early 2000s (e.g. Campillo and Paul, 2003), it has been widely used to image and monitor the Earth medium. Such monitoring techniques have successfully detected temporal changes in the Earth medium in association with some large earthquakes and/or volcanic eruptions.

However, there are at least a few issues to be solved for further improving these monitoring techniques. Firstly, though temporal changes in medium properties such as seismic velocity and seismic scattering strength have been detected, physical mechanisms for these changes are not clear yet. So far, stress or strain changes, temperature changes, and material changes have been raised as these candidates. However, these mechanisms have not been identified yet. If different mechanisms operate at the same time, it is not easy to distinguish one from the others by observations. I just point out here that multi-parameter observations are necessary to disentangle the contributions of the respective mechanisms.

Secondly, techniques to locate where these medium changes took place are not developed well. Sensitivity kernels play a central role for that purpose that relate medium property changes at one location to changes in travel times or waveform similarity of coda waves at a certain lapse time for a source-receiver pair. By using these relations, we can set up an inverse problem to locate regions of medium-property changes from observed changes in travel times or waveform similarity of coda waves. The sensitivity kernels can be calculated from seismogram envelopes based on the radiative transfer theory (e.g. Pacheco and Snieder, 2005). So far, different assumptions are made to synthesize seismogram envelopes in terms of single scattering, multiple scattering, two dimensional case, three dimensional case, and so on. The most serious problem is that all these calculations are based on scalar waves, though seismic waves are vector waves having three different components. Therefore it is necessary to perform more realistic modeling of seismogram envelopes for vector wave cases. I have started a trial toward that direction. If we consider polarization of vector waves only at the receiver, we can approximately treat vector waves. Though under the single scattering regime, the vector-wave sensitivity kernels can be analytically derived. The kernels show two peaks at the source and the receiver as scalar-wave cases, but the shape of the peaks are found to be different from different components. These characteristics of the vector-wave sensitivity kernels will impose more constrains on locations of medium property changes.

Last but not least, quantitative monitoring would be necessary to detect large changes (or anomalies) to issue alerts or warnings. In order to detect anomalies, characteristics of medium properties during normal time periods should be known. I propose a following strategy. I first calculate statistical distributions of seismic velocity changes during normal periods. Such statistical distributions are the basis for providing a probability to a current value of seismic velocity change, and accordingly enable us to subjectively judge if the current value is normal or abnormal. I have investigated statistical distributions of observed seismic velocity changes (Nakahara, 2018), and have found that Gaussian distribution is plausible for most cases. Such information can be exploited to quantify and automate the monitoring of seismic velocity changes.

Solving the issues listed above, we will be able to improve seismic-interferometry-based imaging techniques.

[References]
[1] Campillo, M., and A. Paul (2003), Science.
[2] Pacheco, C., and R. Snieder (2005), JASA.
[3] Nakahara, H., (2018), SSJ.

Earth, Sea and Sky III:
International Joint Graduate Program Workshop in Earth and Environmental Sciences
co-hosted by The International Joint Graduate Program in Earth and Environmental Sciences, Tohoku University
andJSPS-DFG Japanese-German Graduate Externship for Research on Deep Earth Volatile Cycle
May 27-29, 2018. Tohoku University Aobayama Campus

From ductile shear zones to earthquakes

M. THIELMANN[1], T. DURETZ[2], B. J. P. KAUS[3], A. ROZEL[4], Y. RICARD[5]

[1] Bayerisches Geoinstitut, University of Bayreuth
[2] Geosciences Rennes, Université de Rennes
[3] Institut für Geowissenschaften,Johannes Gutenberg-Universität Mainz
[4] Departement Erdwissenschaften, ETH Zürich
[5] Laboratoire de Géologie de Lyon, ENS Lyon

Deformation in the Earth's lithosphere mostly occurs in narrow shear zones. At shallow depths, these shear zones form due to brittle processes, but at larger depths, brittle failure becomes increasingly unlikely due to elevated pressures and temperatures and rocks deform via solid-state ductile creep. The physical mechanisms through which localization occurs in solid-state creep are not yet fully understood. Several mechanisms such as grain size reduction, anisotropy development, shear heating etc. have been proposed to govern weakening and thus localization in ductile creep, but no consensus has been reached on their relative efficiency.

Here I will give an overview of ductile weakening mechanisms, with particular focus on shear heating and grain size reduction. The term shear heating describes the process of converting deformational work to heat. It has been shown that shear heating is a viable mechanism to generate ductile shear zone. Depending on pressure and temperature conditions, it may even result in thermal runaway, which has been proposed as a mechanism to generate intermediate-depth earthquakes. Recent studies have shown that grain size reduction assists thermal runaway, thus enabling this process at lower stresses than previously thought. I will show how these two processes form a positive feedback loop and use numerical models to apply the concept of grain size assisted thermal runaway to a recent lithospheric mantle earthquake.

Dynamical links between the decadal Oyashio and Kuroshio Extension variability

BO QIU[1], SHUIMING CHEN[1], NIKLAS SCHNEIDER[1]

[1] Department of Oceanography, University of Hawaii at Manoa

Rather than a single and continuous boundary current outflow, long-term satellite observations reveal that the Oyashio Extension (OE) in the North Pacific subarctic gyre is comprised of two independent, northeast-southwest slanted, front systems. With a mean latitude along 40°N, the western OE front exists primarily west of 153°E and is a continuation of the subarctic gyre western boundary current. The eastern OE front, also appearing along 40°N, is located between 153°E and 170°E, whose entity is disconnected from its western counterpart. During 1982–2016, both of the OE fronts exhibit prominent decadal fluctuations, although their signals show little contemporaneous correlation. An upper ocean temperature budget analysis based on the ECCO2 state estimate reveals that the advective temperature flux convergence plays a critical role in determining the low-frequency temperature changes relating to the OE fronts. Specifically, the western OE front variability is controlled by the decadal mesoscale eddy modulations in the upstream Kuroshio Extension (KE). An enhanced eddy activity increases the poleward heat transport and works to strengthen the western OE front. The eastern OE front variability, on the other hand, is dictated by both the meridional shift of the KE position and the circulation intensity change immediately north of the eastern OE. Different baroclinic adjustment speeds for the KE and OE are found to cause the in-phase changes between these latter two processes. Lack of contemporaneous correlation between the decadal western and eastern OE variability is found to be related to the interaction of meridionally migrating KE jet with the Shatsky Rise near 159°E.

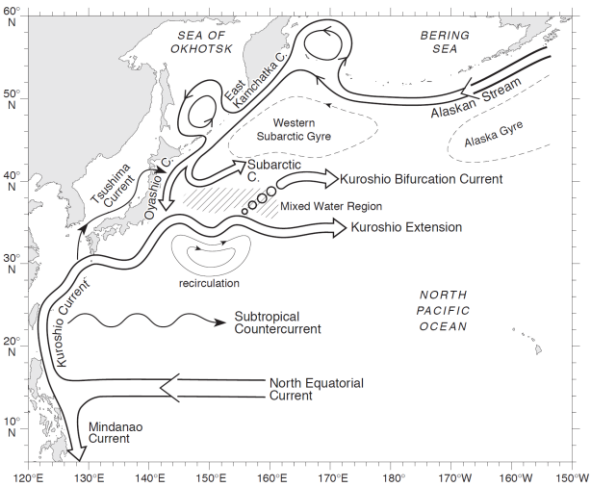

Schematic current patterns associated with the subtropical and subarctic gyres in the western North Pacific Ocean. Updated based on Qiu (2001): Kuroshio and Oyashio Currents. In *Encyclopedia of Ocean Sciences*, Academic Press, p.1413-1425.

Earth, Sea and Sky III:
International Joint Graduate Program Workshop in Earth and Environmental Sciences
co-hosted by The International Joint Graduate Program in Earth and Environmental Sciences, Tohoku University
andJSPS-DFG Japanese-German Graduate Externship for Research on Deep Earth Volatile Cycle
May 27-29, 2018. Tohoku University Aobayama Campus

New perspective on air-sea interaction off the east coast of Japan

SHUSAKU SUGIMOTO[1]

[1] Creative Interdisciplinary Research Division, Frontier Research Institute for Interdisciplinary Sciences, Tohoku University

In this earth, there are ocean and its overlying atmosphere. Both ocean and atmosphere exchange heat with each other, through the sea surface. Through modern climate science, it is becoming clear that the heat exchange between the ocean and atmosphere greatly influences the global climate. Numerous climate scientists have undertaken the challenge to reveal the heat exchange processes between the ocean and atmosphere. They suggested that the atmosphere drives the heat exchange in mid- and high-latitude regions, such as where we live in Japan. That is, "strong winds on the sea surface enhance heat release from the ocean, resulting in a cooling of the waters".

Recently, available ocean and atmosphere dataset, e.g., satellite-derived data with a high spatial resolution, have increased and the regional atmospheric models have been developed. We attempted to reveal a role of ocean for a determination of the heat exchange between the ocean and atmosphere, and then to detect the impact of ocean on the overlying atmosphere.

Vigorous heat related to the turbulent heat flux (sum of latent and sensible heat fluxes) is released from the ocean to the atmosphere during winter off the east coast of Japan; the value and variance are one of the largest in the world's oceans. Our observational studies based on satellite-derived data revealed that the warm (anticyclonic) ocean eddies with a horizontal extent of a few hundred kilometers and a thickness of a few hundred meters, which pinched off from the warm Kuroshio Extension in a northward direction, released a huge amount of heat, exceeding 600 W m^{-2} (Sugimoto and Hanawa 2011, Sugimoto 2014). Furthermore, the satellite measurements showed that surface winds were enhanced over the warm eddy. Our observation studies indicated, "the warm surface waters enhance upward heat release, leading to enhanced surface winds" over the warm eddies off the east coast of Japan. Our scenario differs greatly from that outlined in the previous studies; strong winds on the sea surface enhance a heat release from the ocean, resulting in ocean cooling.

The satellite measurements are able to observe the sea surface conditions over the warm eddies, but unable to capture vertical atmospheric structures over the warm eddies. In order to reveal atmospheric response to warm ocean eddies quantitatively, we conducted regional atmospheric model experiments using the Japan Meteorological Agency nonhydrostatic model (JMA–NHM). The results showed, off the east coast of Japan, wintertime warm eddies heat the overlying atmosphere and accelerate winds in the near-surface atmosphere due to the vertical momentum mixing process, leading to wind convergence. Then, the warm-eddy-induced convergence forms a local ascending motion where convective precipitation is enhanced (Sugimoto et al. 2017).

Our findings based on observational data and atmospheric model experiments indicated that warm eddies off the east coast of Japan influences the overlying atmosphere not only near the surface but also into high altitude. A detailed understanding of warm eddy-atmosphere interaction is necessary to improve in weather and climate projections.

[References]

[1] Sugimoto, S., and K. Hanawa, 2011: Roles of SST anomalies on the wintertime turbulent heat fluxes in the Kuroshio-Oyashio Confluence Region: Influences of warm eddies detached from the Kuroshio Extension. J. Climate, 24 (24), 6551-6561.

[2] Sugimoto, S., 2014: Influence of SST anomalies on winter turbulent heat fluxes in the eastern Kuroshio-Oyashio Confluence region. J. Climate, 27 (24), 9349-9358.

[3] Sugimoto, S., K. Aono, and S. Fukui, 2017: Local atmospheric response to warm mesoscale ocean eddies in the Kuroshio-Oyashio Confluence region. Scientific Reports, 7, 11871, 1-6.

Poster presentations

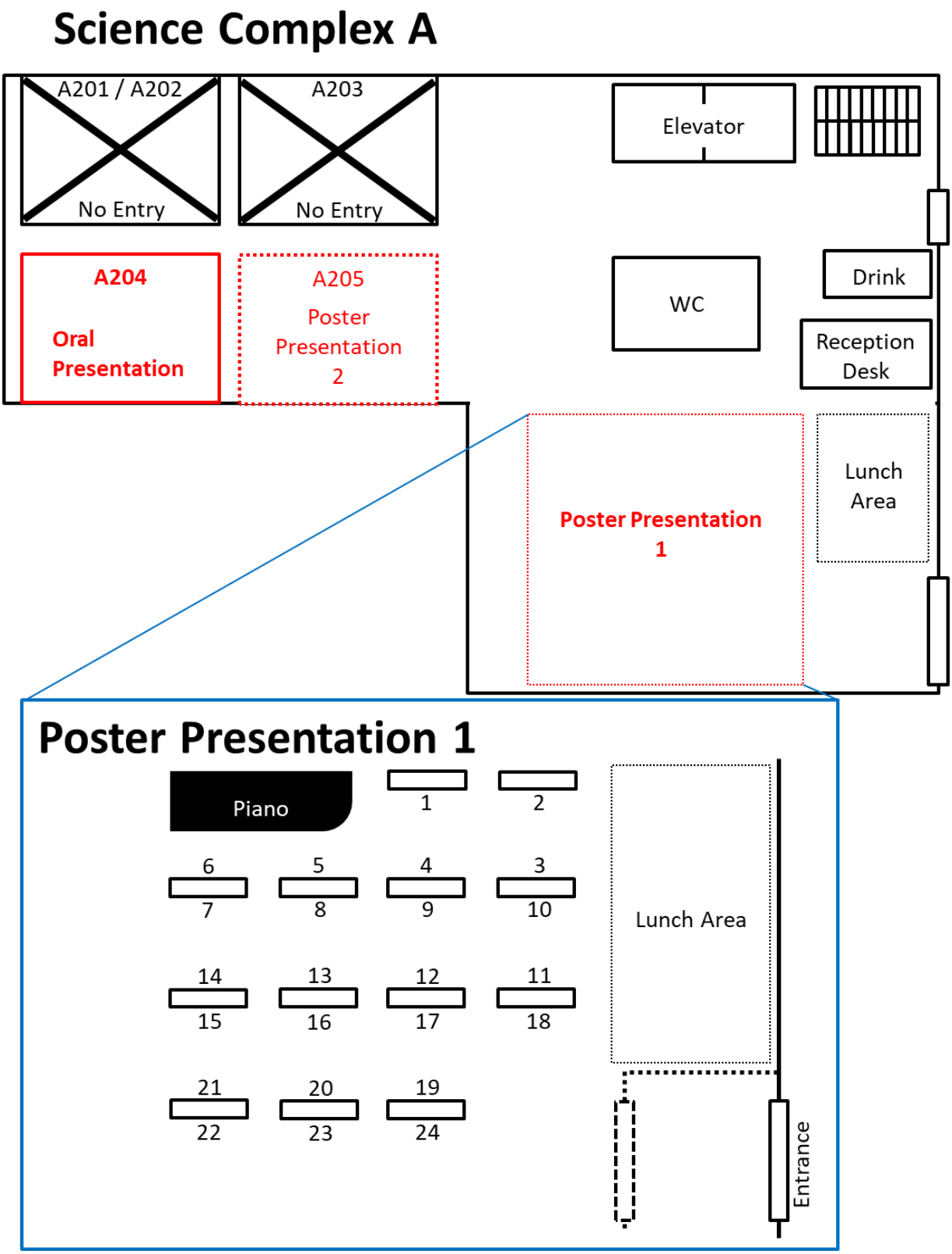
Science Complex A
A201 / A202
No Entry
A203
No Entry
Elevator
A204
Oral Presentation
A205
Poster Presentation 2
WC
Drink
Reception Desk
Poster Presentation 1
Lunch Area
Poster Presentation 1
Piano
1
2
6
5
4
3
7
8
9
10
14
13
12
11
15
16
17
18
21
20
19
22
23
24
Lunch Area
Entrance

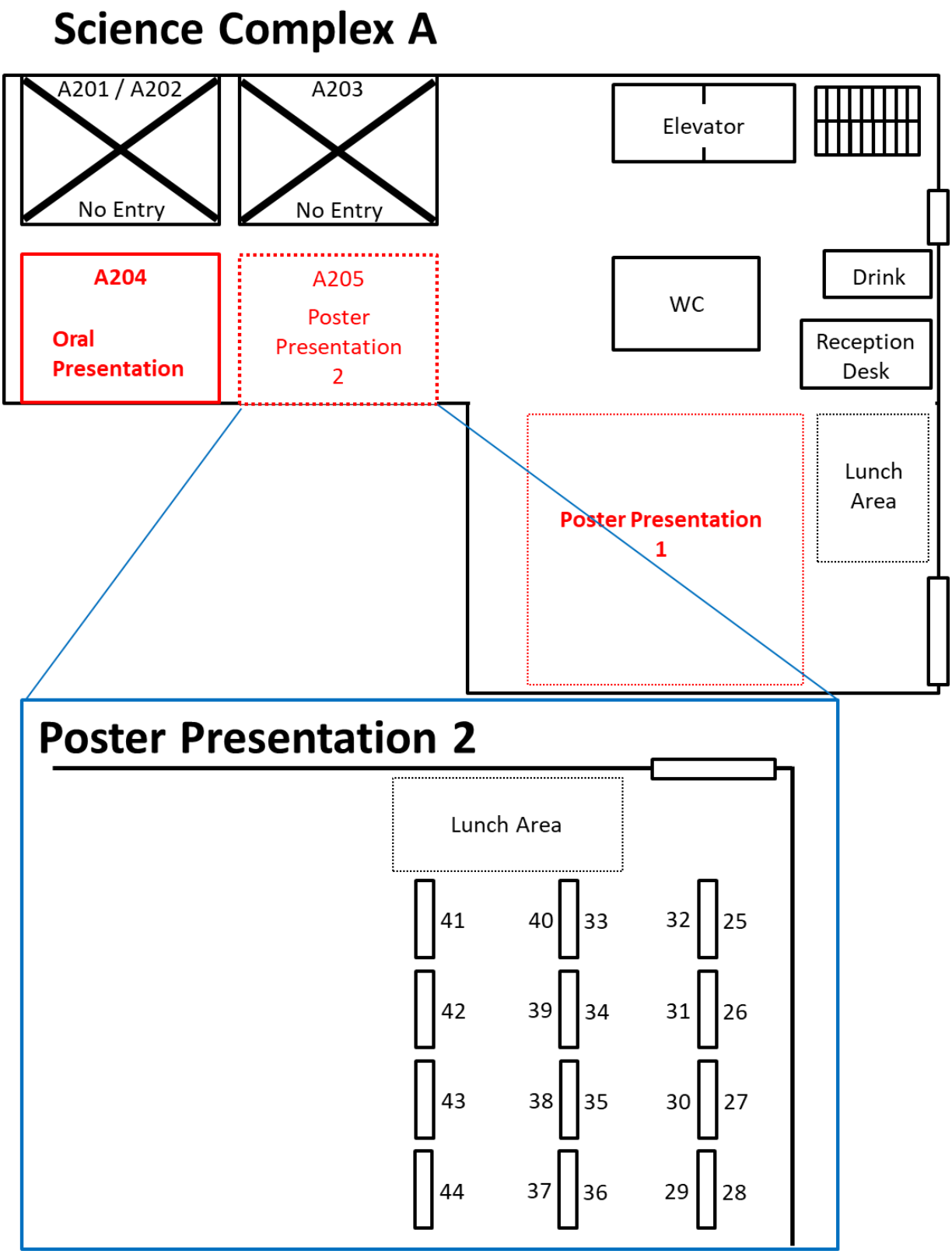
Science Complex A
A201 / A202
No Entry
A203
No Entry
Elevator
A204
Oral Presentation
A205
Poster Presentation 2
WC
Drink
Reception Desk
Lunch Area
Poster Presentation 1
Poster Presentation 2
Lunch Area
41
40
33
32
25
42
39
34
31
26
43
38
35
30
27
44
37
36
29
28

Poster list

q	Name (Family, First, Middle)			Title
1	Aizawa,	Sae		Ion dynamics in the magnetospheric flanks of Mercury
2	Arai,	Shun		Mechanical property of rocks at the Brittle-Ductile transition zone: experimental approach with Griggs apparatus
3	Araya,	Naoki		Very shallow magma storage at the Sakurajima volcano
4	Budiati,	Masyitha	R.	Regional-scale cross-correlation analysis of seismic ambient noise in the Central Indonesia
5	Diana,	Mindaleva		Time scales of Cl-bearing fluid infiltration and permeability estimated by reactive transport modelling for granulite/amphibolite-hosted reaction zones, Sør Rondane Mountains, East Antarctica
6	Emanuel,	Sara		Paleoenvironmental settings and Assemblage changes of foraminifera and palynomorphs across Eocene-Oligocene boundary of southern Tanzania
7	Fujita,	Wakana		Permeability benchmark using 3D modelling and quantification of intergranular fluids connectivity in synthetic quartzite
8	Goto,	Kenichi		The melting behavior in albite – brine system at 1.5 GPa: the effect of NaCl on melting temperature
9	Hara,	Tomomi		*In-situ* Sr–Pb isotope geochemistry of lawsonite: A new method to investigate slab fluid
10	Hasib,	Mohammad		Topography effect on spectral ratio analysis of explosion earthquakes at Sakurajima volcano
11	Hirose,	Takashi		A passive method for the estimation of scattering and intrinsic absorption parameters using envelopes of ambient seismic noise cross-correlation functions
12	Huang,	Yongsheng		Experimental constraints on the dihedral angles in the system of olivine-multicomponent aqueous fluids at 800-1000℃ and 1-4 GPa
13	Ishikawa,	Ayumu		Characteristic behavior of ground tilt motions associated with repeated small explosions at Stromboli volcano
14	Iskandar,	Mochamad	R.	Seasonal to inter-decadal variability of temperature and salinity in the Indonesian Seas and their adjacent ocean
15	Jayawickrama,	Eranga		Contact theory based power-law relation to represent the pressure dependence of elastic wave velocity
16	Jensen	Kasper	B.	In-situ observation in a FE-SEM of crystallization of natural basalt glass with emphasis on olivine dendrites
17	Kasahara,	Hisamu		Direct measurement of reaction-induced stress during hydration reaction of periclase
18	Katsuragi,	Yuki		H_2O / F ratios in asthenosphere inferred from volatile compositions of petit-spot lavas
19	Maeda,	Fumiya		Stability of $MgCO_3$ in Fe-rich hydrous lower mantle
20	Masuti,	Sagar		Anisotropic creep in hydrous olivine single crystals and its application to earthquake cycle
21	McDonough,	William	F.	Th, U and Pb in the Earth
22	Mori,	Keiko		Origin and metamorphic evolution of corundum (or kyanite)-bearing amphiboites from the Paleoproterozoic Usagaran belt, Tanzania
23	Netsu,	Yusuke		Synthesis of garnet by hydrothermal metamorphism in basalt-water system
24	Nurdiana,	Astin		Fluids transport and magma-driven metamorphism related to Granitic Pegmatite Complex in Kinka-san Island, NE Japan
25	Obase,	Tomoya		Solar wind noble gases in the Rumuruti chondrite PRE95410 and heliocentric distance of the meteorite parent body: implication to inward migration
26	Ohashi,	Tomonori		Structures of basaltic glass under high pressure by in-situ x-ray and neutron diffraction investigations
27	Permana,	Theodorus		Source location determination based on seismic cross-correlations: application to simulated tremor using volcano-tectonic earthquakes
28	Puji,	Anggraini		Reexamination in northern Haramachi Segment of Futaba Fault delineation and its activity
29	Sakai,	Shunta		Cretaceous OIBs and MORBs into the Tokoro accretionary complex, NE-most of Japan
30	Sawa,	Sando		Mechanism of olivine-spinel transformation and microstructural development under differential stress by phase field method

#	Name (Family, First, Middle)		Title
31	Sawayama,	Kengo	Evaluation of mining effects to river water in abandoned mining area by statistical analysis
32	Sharygin	Igor	Interaction of peridotite with Ca-rich carbonatite melt at high pressure: Implication for merwinite formation in the upper mantle
33	Shibata	Tsuyoshi	S-wave velocity and attenuation structure as estimated from deconvolution analysis at CHBH10, in Chiba prefecture, KiK-net station
34	Shinji	Yuzuki	Pumpellyite-bearing retrograde mineral assemblage of the Yunotani eclogite and the areal extension of eclogite-facies metamorphism in the Omi area, Japan
35	Suzuki	Kento	Forecasting Coastal Front by numerical simulation
36	Suzuki	Manami	Distribution of localized fluid inferred from S wave reflectors beneath the earthquake swarm in Yonezawa-aizu area, NE Japan
37	Takahashi	Miki	Dark inclusion in the NWA2900 carbonaceous chondrite: CI-like material with large hydrothermal diopside veins
38	Takahashi	Naoya	Seasonality and co-variability of sea surface temperature front and low cloud cover in the mid-latitude North Pacific
39	Takahashi	Naoya	Defining subsegments and testing their roles by comparing with actual rupture extent: an example from the Kamishiro fault, Japan
40	Wang	Tong	Evolutions of water mass anomalies in the upper North Pacific based on Argo
41	Yamaguchi	Ryohei	Diagnostic of the development of seasonal stratification using potential energy anomaly in the North Pacific
42	Yoshizaki	Takashi	Refractory lithophile composition of chondrites and their components: Implications for planetary compositions
43	Yuan	Liang	Chemical reactions between Fe and H_2O up to megabar pressures and implications for water storage in the Earth's mantle and core
44	Yuan	Liang	Compressibility and structure of hydrous silicate melts from first-principles

Poster #1

Ion dynamics in the magnetospheric flanks of Mercury

SAE AIZAWA[1,2], DOMINIQUE DELCOURT[2], NAOKI TERADA[1]

[1] Department of Geophysics, Graduate School of Science, Tohoku University, Japan
[2] Laboratoire de Physique des Plasmas, CNRS-UPMC, France

1. Introduction

At the magnetized planet, the solar wind flow interacts with planetary magnetosphere and thus, the magnetopause is the boundary layer of these two-different plasmas. Under the circumstance, these different plasmas have a velocity shear across the magnetopause and the Kelvin-Helmholtz instability (KHI) can occur because of its velocity shear and make the KH vortex when it fully developed. In fact, many KH vortices have been observed by spacecrafts at the Earth's magnetopause and Mercury's magnetopause [e.g., Slavin et al., 2008]. The evolution of the KHI have been studied numerically for a long time by various authors. Some authors have suggested that the KH vortex play a role of momentum and energy transportation and mixing of two plasmas which have different properties at the planet's magnetopause.

Previous observations have revealed that Mercury has the weak magnetic field compared that of Earth, and collisionless exosphere with neutral particle, Na, K and Ca. These particles will be ionized by various processes and thus, ionized particle is picked up by the magnetic field and travels the magnetosphere.

Due to the weak magnetic field of Mercury, charged particle motion is significantly different from that of Earth. The kinetic effect of the particle motion becomes more efficient on physical phenomena. If the magnetic field or electric field varies in space or time and if its scale is comparable to the particle motion, the MHD approximation is not valid. Many authors have discussed about the particle motion in the spatial and temporal variations of the magnetic field [e.g., Delcourt et al., 2003], but few people studied that of the electric field. In particular, the evolution of KHI produces complex field variations. No one have studied the particle motion inside vortex.

Purpose of this study is to reveal the role of the KHI for the heavy ions by numerical approach and understand deeply how particle behaves with the spatial and temporal variation of the electric field. And also this study contributes the forthcoming study of the BepiColombo mission by ESA/JAXA.

2. Result

In order to investigate particle behavior via KH vortex, we developed new numerical code which is combined MHD code and test particle calculation. By using the code, we injected many particles on the KH field with various initial conditions, then we got each particle trajectory. We found that particle may be energized by the complex KH field nonadiabatically and particle can gain energy up to around the energy which is determined by the field (see figure 1).

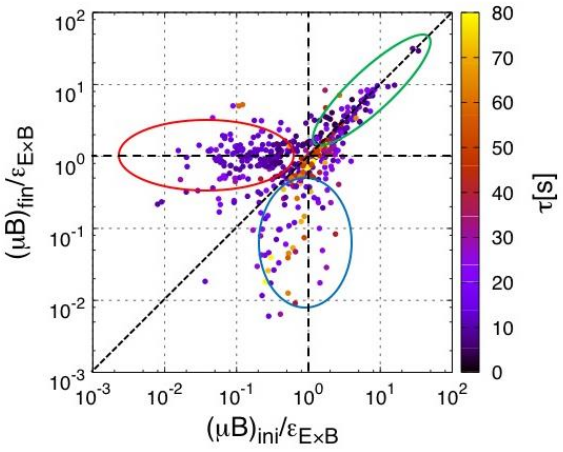

figure 1. Statistical distribution of the particle energization. Each particle was launched with various initial position and perpendicular energy in the fixed MHD field. X-axis (Y-axis) shows the initial (final) perpendicular energy normalized by $\mathcal{E}_{E\times B}$, where $\mathcal{E}_{E\times B} = \frac{1}{2}m(\frac{E_{max}}{B})^2$ and E_{max} is the maximum electric field intensity along the particle trajectory. [Aizawa et al.,2018]

Here initial and final show the time before(t-τ) and after(t+ τ) the electric field variation, here τ is defined by the half with 1 over e of Gaussian Fit. we have 3 categories for the particle energization: group 1 circled by red, particles with a smaller energy compared to $\mathcal{E}_{E\times B}$ will be energized up to around $\mathcal{E}_{E\times B}$. Group 2 circled by blue, particles with an energy around $\mathcal{E}_{E\times B}$ may lose its energy because they move against the electric field. Group 3 in green, particles with an energy above $\mathcal{E}_{E\times B}$ do not gain energy because they already have enough energy compare to the net energy change by the electric field variation. Our result shows that there seems to have a threshold energy determined by the maximum electric field along the particle path. Such a nonadiabatic energy gain may leads the transport of planetary material and mixing of magnetosphere and magnetosheath populations in the magnetospause vicinity. Here we performed sodium ion dynamics as a representative of planetary materials. We are surveying other particle species behavior in order to investigate the dependence of the different scale of particle motion, and the escape and mixing ratio via the KH vortex.

[References]
[1] Aizawa et al., Sodium Ion Dynamics in the Magnetospheric Flanks of Mercury, Geophys. Res.Lett., 45, 595-601, 2018.
[2] Delcourt et al., A quantitative model of planetary Na+ contribution to Mercury's magnetosphere, Annales Geophys., 21, 1723, 2003.
[3] Slavin et al., Mercury's magnetosphere after MESSENGER's first flyby, Science, 321, 85, 2008.

Poster #2

Mechanical property of rocks at the Brittle-Ductile transition zone: experimental approach with Griggs apparatus

SHUN ARAI[1], MASANORI KIDO[1], JUN MUTO[1], HIROYUKI NAGAHAMA[1]

[1] Department of Earth Science, Graduate School of Science, Tohoku University

In the deeper part of the upper crust, the deformation behaviors of rocks change from brittle to ductile. The area is known to be the Brittle-Ductile (BD) transition zone where the rocks have the highest shear strength[*1], and large earthquakes nucleate as well. To investigate the physical properties around this area is lead to quantitative understanding of the strength of continental crust. From old days, many experimental studies aimed to understand the BD transition[*2] have been conducted. However, there are not so much studies on poly-minerals (e.g. natural rocks), and enough mechanical data are not collected. There is previous study for brittle to semi-brittle zone[*3], while the mechanical properties in ductile zone are not revealed in detail. To resolve these problems, we conducted the shear experiment with poly-minerals using Griggs apparatus and obtained mechanical data.

Griggs deformation apparatus can impose the confining pressure around middle to lower crust on the experimental material. The sample is the Gneiss Minuti which mainly consists of quartz, plagioclase and biotite[*4]. This sample is suitable as the experimental material because its mineral composition is resembled to granitic rocks without K-feldspar. The experiments are performed at these conditions (Pc: 1.5 GPa, T: 800° $\dot{\gamma}$: 2×10^{-5} /s). After the experiment, deformed samples are filled up with resin and polished with diamond paste for microstructural observation.

The peak shear strength is 600~900MPa, and the strength decreased with increase in strain and does not attain the steady state even at γ of 7.9. The shear strength is smaller than the previous study[*1] despite same material and conditions). With SEM-EDS analysis, the development of weak S-C structure is observed. As the result of image analysis, our sample have much more content of biotite than previous study[*4]. We consider that the reduction in shear strength is caused by the content and distribution of biotite.

In the presentation we describe the results of deformation experiments and microstructural observations. Then we discuss the role and the content and deformation behavior of biotite at high pressure and high temperature conditions.

[References]
[1] Brace W.F. and Kholstedt, D.L., 1980, Limits on the lithospheric stress imposed by laboratory experiments. *JGR volume, page*
[2] Shimamoto, T., 1989, The origin of S-C mylonites and a new fault zone model. *JSG*
[3] Pec, M., Stünitz, J., Heilbronner, R., 2012, Semi-brittle deformation of granitoid gouges in shear experiments at elevated pressures and temperatures. *JSG*
[4] Holyoke, C.W. III. and Tullis, J., 2006, Mechanisms of weak phase interconnection and the effects of phase strength contrast on fabric development. *JSG*

Poster #3

Very shallow magma storage at the Sakurajima volcano

N. ARAYA[1], M. NAKAMURA[1], S. OKUMURA[1],
A. YASUDA[2], D. MIKI[3], M. IGUCHI[3], N. GESHI[4]

[1] Department of Earth Science, Graduate School of Science, Tohoku University
[2] Earthquake Research Institute, University of Tokyo
[3] Sakurajima Volcano Research Center, Disaster Prevention Research Institute, Kyoto University
[4] Geological Survey of Japan, National Institute of Advanced Industrial Science and Technology

To constrain pre-eruptive magma storage depths of historic Plinian and recent Vulcanian eruptions at the Sakurajima volcano, we analyzed water contents of melt inclusions and calculated melt water contents with a plagioclase-liquid hygrometer. In the Plinian eruptions, melt inclusions have 1.4–3.5 wt% H_2O, which are in good agreement with melt water contents calculated from the hygrometer (1.1–3.6 wt%). On the other hand, measured water contents of melt inclusions (0.7–2.3 wt%) were lower than the hygrometer melt water contents (1.5–3.0 wt%) in the Vulcanian eruptions. This result is interpreted as a result of diffusive dehydration of the melt inclusions during magma ascent without mineral-melt reequilibration.

Our petrological investigation demonstrated that the Plinian and Vulcanian magmas have almost the same equilibrated water contents (i.e., final storage depths). The water saturation pressure calculated from >95% melt inclusions of the Plinian eruptions is 19–74 MPa (0.9–3.3 km in depth). Because this storage depth is shallower than the shallowest magma reservoir inferred from geophysical observations (4 km), magmas should have been stored in a conduit connected to the surface. The diameter of the present conduit inferred from hypocenter distribution has a thickness capable of supplying the historic Plinian magmas. Thus, a ground subsidence detected around the Aira caldera after the 1914–15 Plinian eruption was probably caused by magma recharge from a main deep magma reservoir beneath the caldera (~10 km in depth) to the shallow magma feeding system.

Poster #4

Regional-scale cross-correlation analysis of seismic ambient noise in the Central Indonesia

MASYITHA RETNO BUDIATI[1], GENTI TOYOKUNI[1], TOMOMI OKADA[1]

[1] Department of Geophysics, Graduate School of Science, Tohoku University

The central Indonesia has a complex tectonic structure which is characterized by several subduction zones (e.g., double subduction zones beneath Molucca Sea) and active faults (e.g., Palu Koro, Matano and Hamilton faults). However, due to the limitation of studies, the information of seismic velocity changes beneath the desired regions is needed for monitoring those structures. Currently, cross-correlation functions (CCFs) retrieved from ambient seismic noise are assumed as the representation of the surface wave green function that can show the response of the Earth. Our previous study at Sulawesi Island **(Budiati et al., 2017)** observed the dominant energy of CCFs at period of 10 s - 30 s with velocity around 2 - 3km/s which were interpreted as Rayleigh waves. Currently, we enhanced the station pairs in order to further investigate the propagation direction of the surface waves and to extract 1D velocity structure beneath the station pairs by comparing the observed dispersion curves of the Rayleigh waves and the calculated crustal model obtained from CRUST 1.0 **(Laske et al., 2013)**. In the present study, we used the vertical component of continuous and broadband (20 sps) seismograms recorded at eight permanent stations in and around Sulawesi Island (station codes: APSI, BKB, KMSI, LUWI, SANI, TNTI, TTSI, and TOLI2). The data period encompasses 1 January to 31 May 2015 (five months). The data were divided into 20 minutes segments with time shift in every 5 minutes to enhance the signal to noise ratio (SNR). We applied taper, whitening, band-pass filter at the frequency band of 0.01 Hz - 1 Hz and binalization in each data segment as the preprocessing steps, then selected the feasible segments and calculated CCF between two contemporaneous segments from two stations. We further stacked the CCFs for 1 day to obtain day-averaged CCFs, and finally stacked the day-averaged CCFs over 5 months to retrieve stabilized Rayleigh wave signals. The 5 months CCFs were then filtered at center period of 0.25 s - 32 s to find the dominant energy of the CCFs. Our recent findings suggest that the SNR measurements are enhanced at up to 12 station pairs after calculating 5-month-averaged CCFs and represent clear Rayleigh waves. The asymmetric shapes of the CCFs indicate that the Rayleigh waves propagated towards Sulawesi Island not only from eastern to northwestern **(Budiati et al., 2017)**, but also from northeastern to southwestern and vice versa.

[References]
[1] Budiati, M. R., G. Toyokuni, T. Okada (2017), *Regional-scale Cross-correlation Analysis of Seismic Ambient Noise in The Central Indonesia*, Poster session presented at JpGU-AGU Joint Meeting, Makuhari Messe, Chiba, Japan, May 20 - 25, 2017.
[2] Laske, G., G. Masters, Z. Ma, M. Pasyanos (2013), *Update on CRUST1.0 – A 1-degree Global Model of Earth's Crust*, Geophys. Res. Abstracts, 15, Abstract EGU2013-2658, 2013.

Poster #5

Time scales of Cl-bearing fluid infiltration and permeability estimated by reactive transport modelling for granulite/amphibolite-hosted reaction zones, Sør Rondane Mountains, East Antarctica

MINDALEVA DIANA[1], MASAOKI UNO[1], FUMIKO HIGASHINO[1], TAKAYOSHI NAGAYA[1], ATSUSHI OKAMOTO[1], NORIYOSHI TSUCHIYA[1]

[1] Department of Environmental Studies for Advanced Society, Graduate School of Environmental studies, Tohoku University

Fluids in arc crusts are important for crust evolution, ore deposit formation and geothermal activities. Hydrologic properties in the crust, such as permeability to aqueous fluids, control advection and mass transport. However, permeability in the crust is of great uncertainty, because of its heterogeneity as well as experimental difficulties in high P-T conditions (Ingebritsen and Manning, 2010). Abundant evidence of Cl-bearing fluids in Sør Rondane Mountains (SRM), East Antarctica (e.g., Higashino et al., 2013; Kawakami et al., 2017; Uno et al., 2017) make this area as one of the most suitable areas to study activities of Cl-bearing fluids. However, permeability, elemental transport mode, mechanism of fluid infiltration, as well as duration of fluid infiltration in the SRM are still unknown.

This study aims to investigate Cl-bearing fluids infiltration under crustal P-T conditions by examining hydrous veins in the mafic granulite and amphibolite samples from Mefjell, southern SRM, East Antarctica. Studied area is metamorphosed under granulite facies.

Mafic granulite and amphibolite are cut by numerous randomly-oriented veins. Mafic granulite and amphibolite samples are partially hydrated along veins and associated with mm-sized hydration reactions zones. Based on the local mineral assemblage and the minerals mode, samples were divided into vein, reaction zone and host rock domains. Mafic granulite was divided as follows: vein (1 mm width; plagioclase (pl)+hornblende (hbl)+quartz (qtz), minor orthopyroxene (opx)+biotite (bt)+ilmenite (ilm)+clinopyroxene (cpx)+magnetite (mag)+apatite (ap)+potassium feldspar (kfs)+chlorite (chl)), host rock (pl+cpx+opx, minor bt+ilm+mag+kfs+ap).

In amphibolite, vein, reaction zones, and host rock domains are identified as follows: vein (2 mm width; act+hbl+cum, minor ilm+ap+ep+serp), actinolite zone (2.3mm; act+hbl+cum, minor opx+ilm+ap+ep+mus), muscovite zone (2.5mm; hbl+opx, minor act+cum+ilm+ap+ep+mus+pl), host rock (hbl+opx, minor ilm+ap+ep+mus+pl). P-T conditions were identified using pseudosections, Al-in-hornblende geobarometry and hornblende–plagioclase geothermometry, and estimated as 6±0.5 kbar, 635±50°C for the veins, and 770–820°C, 5.5-10 kbar for the host rock. For amphibolite, vein temperature was estimated by magnetite-ilmenite thermometer to be around 400±50°C. Distribution of Cl in apatite in the reaction zones were measured by EPMA and used to estimate type of mass transport and duration of fluids infiltration. Cl-contents in apatite decrease from 0.2 mass% in vein to 0.02 mass% in host rock for mafic granulite, and from 1.54 mass% to 0.1 mass% for amphibolite. The Cl distribution profiles were analyzed by a reactive-transport model with local equilibrium. The Cl profile was fit using Peclet number (Pe# = vL/D, where v is pore velocity, L is length of reaction zone, D is hydrodynamic dispersion). For mafic granulite Pe# is around 0.05, for amphibolite is around 90. Duration of fluid infiltration was estimated to be 6×10^{-3} yr for granulite, and 6×10^{-5} yr for amphibolite, which is short in geological time scales.

These results are combined to constrain permeability, transport mechanism and to show a comprehensive model for fluid activities in lower-middle crustal conditions in the SRM. Infiltration conditions, transport mechanism is defined by Pe# and duration of fluid infiltration are different for mafic granulite and amphibolite. Diffusion transport was dominant for mafic granulite. Contrary, in amphibolite, transport by advection was greater, influencing the time-scale of fluid infiltration.

[References]
[1] Ingebritsen and Manning. (2010) Geofluids 10.1-2: 193-205.
[2] Higashino et al. (2013) Precambrian Research 234: 229-246.
[3] Kawakami et al. (2017) Lithos 274: 73-92.
[4] Uno et al. (2017) Lithos 284: 625-641.

Poster #6

Paleoenvironmental settings and Assemblage changes of foraminifera and palynomorphs across Eocene-Oligocene boundary of southern Tanzania

SARA EMANUEL[1], CHARLES KASANZU[2], AMINA KAREGA[3]

[1] Department of Earth Science, Graduate School of Science, Tohoku University
[2] Department of Geology. University of Dar es Salaam
[3] Biostratigraphy Unit. Tanzania Petroleum Development Corporation

Purpose

A quantitative micropaleontological analysis was performed on core samples across a shallow borehole drilled in the southern coastal basin of Tanzania with the aim of characterizing foraminifera and palynomorphs assemblage changes aiming at reconstructing paleoenvironmental settings across the Eocene-Oligocene transition (EOT).

Experimental method

This study utilized core samples from TDP 11 provided by Tanzania Petroleum Development Corporation (TPDC). For the purpose of studying foraminifera, samples were prepared using standard micropaleontological techniques as in Hess et al. (2014). TDP 11 core samples were also analysed for palynomorphs (dinoflagellate, spores and pollens). Samples were prepared by using palynological standard technique and for quantitative palynological analysis according to Vega (1992).

Result

Foraminifera and palynomorphs results are presented in terms of abundance percentages.

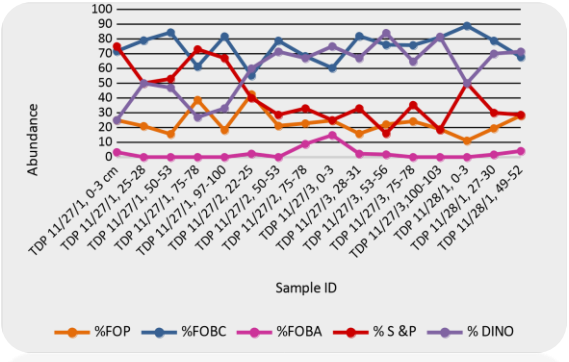

Figure 1; A chart showing the abundance distribution of foraminifera and palynomorphs across TDP 11 borehole.

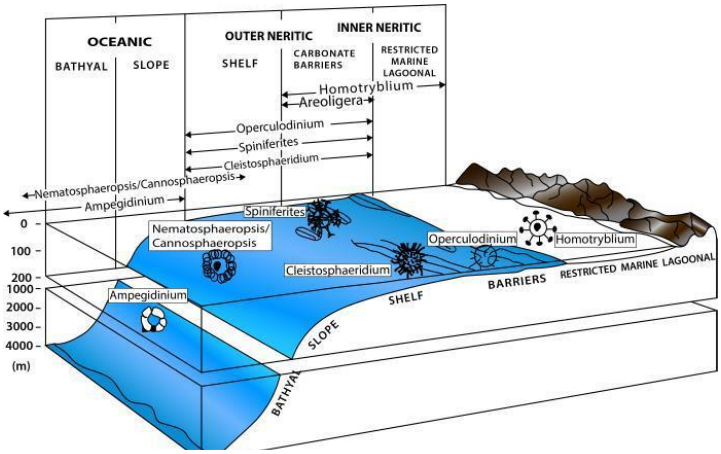

Figure 2; Trends in bathymetry and global palynomorphs content of sediments from the shelf to the abyssal plain. Palynomorph types obtained in our study are also indicated in the diagram (modified after Haq and Boersma 1998).

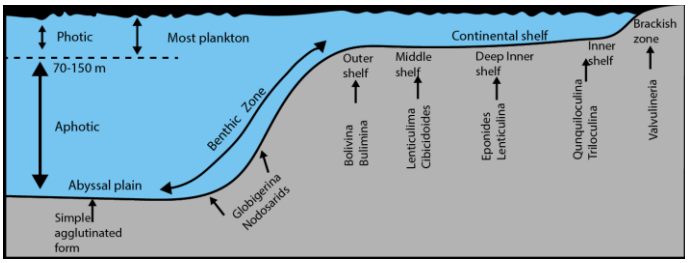

Figure 3; Trends in bathymetry and foraminifera content of sediments from the shelf to the abyssal plain (modified after Haq and Boersma, 1998).

The P:B ratio data together with the foraminifera and palynomorphs assemblages suggest that the Eocene–Oligocene boundary paleoenvironment settings was generally shallow marine of inner to outer shelf environment.

Future Plan

My plan is to engage myself more on micropaleontology specifically foraminifera and nannofossils of Neogene to Quaternary sediments.

The aim is to analyze the assemblage changes with respect to glacial-interglacial cycling period influenced by winter monsoon.

[References]
[1] Murray JW 1991 Ecology and distribution of benthic foraminifera. Biology of Foraminifera. Academic Press, London, 221-253.
[2] Sluijs A, Pross J and Brinkhuis H 2005 From greenhouse to icehouse; organicwalled dinoflagellate cysts as paleoenvironmental indicators in the Paleogene. Earth-Science Reviews, 68(3), 281-315.
[3] Haq BU and BoersmaA (Eds.) 1998 Introduction to marine micropaleontology. Elsevier.pp. 356.

Poster #7

Permeability benchmark using 3D modelling and quantification of intergranular fluids connectivity in synthetic quartzite

WAKANA FUJITA[1], PHILIPP EICHHEIMER[2], MARCEL THIELMANN[2], ANTON POPOV[3], GREGOR J. GOLABEK[2], BORIS KAUS[3], MICHIHIKO NAKAMURA[1], KENTARO UESUGI[4]

[1] Department of Earth Science, Graduate School of Science, Tohoku University
[2] Bayerisches Geoinstitut, University of Bayreuth, Bayreuth, Germany
[3] Johannes Gutenberg Universität Mainz, Institute for Geosciences, Mainz, Germany
[4] Japan Synchrotron Radiation Research Institute (JASRI/SPring-8)

The connectivity of intergranular fluids in a subducting slab controls efficiency of fluid segregation and thus pore fluid pressure to lead increase of seismic activities within the slab. Some previous experiments have shown that the dihedral angles between fluid and relevant minerals are too high to allow pervasive flow along grain edges and corners in a subducting slab (e.g., Watson & Lupulescu, 1993; Mibe at al., 2003). However, recent studies report that sintering experiments with rock-forming minerals + melt show considerable deviations from geometry predicted by dihedral angles. This "disequilibrium feature" results from grain boundary migration and Ostwald ripening during grain growth (e.g., Walte et al., 2003).

To quantify the effect of grain growth on pore fluid connectivity, we conducted sintering experiments of fluid-bearing quartzite using a piston cylinder apparatus. The experiments were conducted at 900□ and 1.0 GPa for up to 192 hours with two fluid compositions, X_{CO_2}= 0 and 0.75 which correspond to θ< 60°and θ> 60°respectively. After quenching, the microstructure of run products were investigated using x-ray synchrotron microtomography. We measured porosity and connectivity from the 3D CT data.

To quantify the permeability of the run products, we conducted benchmark test of 3D thermomechanical code LaMEM (Lithospheric and Mantle Evolution Model, Kaus et al., 2016). We calculated fluid flow through single and multiple pipes by computing the flow velocities and then plugged them into Darcy's law using LaMEM. Resulting permeabilities with different grid resolutions were compared against analytical solution for Hagen-Poiseuille flow. In a next step we computed the permeability of Fontainbleau sandstone digitalized by Andra et al. (2012). We obtained 2171 mD, which is higher than 1100 mD from laboratory measurement (Keehm 2003). However, our result is almost consistent with numerical results by Andra et al. (2012) which are 1503 mD (Lattice-Boltzmann method) and 1914 mD (Explicit Jump method), respectively.

This work was supported by the JSPS Japanese–German Graduate Externship.

[References]

[1] Watson & Lupulescu, (1993). Aqueous fluid connectivity and chemical transport in clinopyroxene-rich rocks, Earth and Planetary Science Letters, 117, 279-294
[2] Mibe et al., (2003). Connectivity of aqueous fluid in eclogite and its implications for fluid migration in the Earth's interior, Journal of Geophysical Research, 108, B6, 2295
[3] Walte et al., (2003). Disequilibrium melt distribution during static recrystallization, Geology, 31, 1009-1012
[4] Andra et al,(2013). Digital rock physics benchmarks—Part I: Imaging and segmentation Computers and Geoscience, 50 25-32
[5] Andra et al,(2013). Digital rock physics benchmarks—part II: Computing effective properties Computers and Geoscience, 50 33-43
[6] Kaus, B., Popov, A., Baumann, T., Pusok, A., Bauville, A., Fernandez, N., Collignon, M., (2016). Forward and inverse modeling of lithospheric deformation on geological timescales. In: Binder, K., Mller, M., Kremer, M., Schnurpfeil, A. (Eds.), NIC Proceedings. Vol. 48. pp. 299–307.
[7] Keehm, Y., (2003). Computational Rock Physics: Transport Properties in Porous Media and Applications. Ph.D. Dissertation, Stanford University. 135 pp.

Poster #8

The melting behavior in albite – brine system at 1.5 GPa : the effect of NaCl on melting temperature

KENICHI GOTO[1], AKIO SUZUKI[1]

[1] Department of Earth Science, Graduate School of Science, Tohoku University

The aqueous fluid released from the subducting plate causes a melting temperature depression of the rock and a decrease in strength, thus it has the influence on the volcanic and seismic activity[1]. In addition, the aqueous fluid can also be the carrier of elements, it is considered to affect the chemical composition of igneous rocks generated in the subduction zone. It is therefore important to investigate the nature of the fluid released from the subducting plate.

It is suggested that chlorine is contained in the fluid released from the subducting plate by analysis of natural samples[2].

Therefore, when discussing the melting temperature in the subduction zone, it is necessary to think of water to which sodium chloride is added instead of pure water.

Recently, it has been confirmed that the decrease of the melting temperature drop due to the addition of NaCl for the internal minerals of the earth, and it is suggested the influence on magma generation inside the earth[3].

In addition, the rise in melting temperature in water-containing systems also affects the composition of magmas and aqueous fluids that can be released from the subducting plate. For example, it is thought that supercritical fluid has the effect of changing the chemical composition of igneous rock[4], but the second critical end point indicated at the intersection of hydrous solidus and critical curve becomes lower pressure due to increase of hydrous solidus by addition of NaCl.

Thus, NaCl has an influence on whether the fluid released from the slab is water, magma or supercritical fluid.

In this study, the experiments have been carried out at 1.5 GPa to determine the influence of NaCl on melting temperature by conducting melting experiment in albite–brine system. The composition and texture of the sample which was quenched and recovered at 1.5 GPa ・ 973 K, 1.5 GPa ・ 1013 K are shown. From these results, it was revealed that the melting temperature exists between 973 K and 1013 K at 1.5 GPa, which is above the melting temperature of the conventional albite-H_2O system.

This work was supported by the JSPS Japanese–German Graduate Externship.

[References]
[1] Tatsumi and Eggins. *Subduction zone magmatism*. Vol.1. (1995)
[2] Fu, Touret, and Zheng. *J. Metamorphic Geol.* 19 (2001): 531-547
[3] Makhluf, Newton, and Manning. *Contrib Mineral Petrol* 171 (2016): 75
[4] Mibe et al. *Proceedings of the National Academy of Sciences* 108 (2011): 8177-8182.

Poster #9

In-situ Sr–Pb isotope geochemistry of lawsonite: A new method to investigate slab fluid

TOMOMI HARA[1], TATSUKI TSUJIMORI[1,2], QING CHANG[3] JUN-ICHI KIMURA[3]

[1] Department of Earth Science, Graduate School of Science, Tohoku University
[2] Center for Northeast Asian Studies, Tohoku University
[3] Department of Solid Earth Geochemistry, JAMSTEC

Lawsonite is a hydrous Ca–Al silicate mineral which is broadly stable in a typical subduction-zone geotherm after late Neoproterozoic. In order to understand the elemental fractionation and the sources of subducted materials, lawsonite crystals in basaltic and sedimentary lawsonite-eclogites from South Motagua Mélange of Guatemala [1] were investigated using LA-ICPMS and LA-MC-ICPMS. Mass balance calculation using *in-situ* trace element and modal compositions in an eclogite with a low-variance mineral assemblage confirmed that lawsonite hosts most of the LREE, Sr, Pb, Th and U in the bulk rock as has been reported elsewhere. *In-situ* Sr–Pb isotope analyses of the lawsonite crystals revealed isotopic variations reflecting their protoliths. Isotopic zoning is also detected in some crystals. Lawsonite crystals in a phengite-rich metabasaltic eclogite have relatively low $^{87}Sr/^{86}Sr$ = 0.70335–0.70355 with variations in $^{207}Pb/^{206}Pb$ = 0.840–0.851 and $^{208}Pb/^{206}Pb$ = 2.076–2.091. Lawsonite crystals from another metabasaltic eclogite are remarkably zoned. The cores have $^{87}Sr/^{86}Sr$ = 0.70558-0.70601 and the rims have elevated $^{87}Sr/^{86}Sr$ = 0.70636-0.70662. The Pb in the cores has MORB-like compositions $^{207}Pb/^{206}Pb$ = ~0.843–0.844, whereas rims have more enriched $^{207}Pb/^{206}Pb$ = ~0.839–0.841. The radiogenic Sr isotope composition would have been derived from sea-floor alteration before subduction. In fact, lawsonite crystals in a metachert have higher $^{87}Sr/^{86}Sr$ = 0.70697–0.70757 with $^{208}Pb/^{206}Pb$ = ~2.07. However, Considering geological contexts, tthe isotopically zoned metabasaltic lawsonite crystals with MORB-like core compositions suggest metasomatism by an `external' fluid from sediment protolith occurred during overgrowth of their rims. Our study indicates that lawsonite crystals record both the isotopic composition of the protoliths and fluid metasomatism from different protoliths. The *in-situ* Sr–Pb isotope analysis has a potential to reveal such complicated metamorphic processes.

[References]
[1] Tsujimori *et al.* (2006) *GSA Special Paper* **403**, 147-168.

Poster #10

Topography effect on spectral ratio analysis of explosion earthquakes at Sakurajima volcano

MOHAMMAD HASIB[1], TAKESHI NISHIMURA[1], HISASHI NAKAHARA[1]

[1] Department of Geophysics, Graduate School of Science, Tohoku University

Spectral ratio method is often used for examining the source spectrum characteristics of tectonic earthquakes, but we applied the spectral ratio method to explosion earthquakes at Sakurajima volcano. The spectral ratio of larger explosion earthquakes are about 2 times higher than those of small explosion earthquakes at about 1-3 Hz, and there is no significant changes in corner frequencies. The spectral ratios further change with lapse time, which may represent the source time function difference between the initial explosion and continuous ash emission. These results are not recognized in the tectonic earthquakes. To understand the origins of the characteristics in the observed spectral ratios of explosion earthquakes, we examine the topography effect of Sakurajima volcano by using numerically simulated explosion earthquakes.

We calculate explosion earthquake waveforms by using OpenSWPC (Meada et al, 2017). We input the ground surface topography data from GSI with a resolution of 10 m and bathymetry data from JODC with a resolution of 500 m. We set a 12 km x 12 km x 9 km grids around the center of coordinate at Showa crater. A vertical single force is exerted to generate explosion earthquakes, which has a source duration T_R of 0.5 s and a unit force. A homogeneous medium with Vp of 2.5 km/s, Vs of 1.3 km/s, density ρ of 2.0 g/cm^3, Qp of 100 and Qs of 70 is assumed. We simulate the explosion earthquake waveforms for different source depths from 0.1 km beneath the summit of Showa crater down to 1 km from the sea level every 0.1 km. The simulated 3-components seismograms are obtained at the three stations (SKRB, SKRC and SKRD), which are located about 3 km away from the active crater (Showa crater). Then, we calculate spectral ratio of the waveforms calculated for shallow depths to the deepest one (1 km from the sea level).

The result shows that the spectral amplitude ratios of simulated waveform of the vertical component are smaller than those from the horizontal components. Amplitude ratios for vertical component at shallow depth from the summit of 0.1 km is about 2 times larger than that for deeper depth of 1 km below the sea level. On the other hand, Amplitude ratios for horizontal component at shallow depth is about 4 times larger than that for deeper depth of 1 km below the sea level. Although the spectral ratios become large with shallowing the source depths, overall characteristics are different from the observed features. Therefore, the spectral ratio changes are not simply caused by the depths change of the sources generating initial explosions and continuous ash emission.

[References]
[1] Maeda, T., Takemura, S., and Furumura, T. (2017) An open-source integrated parallel simulation code for modeling seismic wave propagation in 3D heterogeneous viscoelastic media. *Earth, Planets and Space.,*69-101.

Poster #11

A passive method for the estimation of scattering and intrinsic absorption parameters using envelopes of ambient seismic noise cross-correlation functions

TAKASHI HIROSE[1], HISASHI NAKAHARA[1], TAKESHI NISHIMURA[1]

[1] Department of Geophysics, Graduate School of Science, Tohoku University

Scattering and intrinsic absorption parameters are measures of medium heterogeneities. Those of S waves have been estimated by using seismogram envelopes of natural earthquakes (e.g., Carcole and Sato, 2010) or active shots (e.g., Yamamoto and Sato, 2010). However, it is hard to estimate those parameters in the region where seismicity is low or where no active seismic experiment is conducted. To overcome this problem, we propose a passive estimation method for estimating scattering and intrinsic absorption parameters from envelopes of ambient seismic noise cross-correlation functions (CCFs).

We used ambient seismic noise records in 1 – 2 Hz and 2 - 4 Hz bands recorded at 6 JMA stations in 2014. Daily CCFs were calculated using ambient noise on the vertical-vertical (ZZ), vertical-radial (ZR, RZ), and vertical-transverse (ZT, TZ) component, and were stacked as the following procedures: We simply averaged causal (positive lag time) and acausal (negative lag time) part of ZZ, and averaged causal parts of ZR (ZT) and acausal parts of RZ (TZ). Then, we stacked these averaged daily CCFs over 3 months, and calculated mean squared envelopes by smoothing squared amplitude with 2 s (1 - 2 Hz) or 1 s (2 - 4 Hz) long time windows.

Rayleigh waves were dominant in those CCFs. Hence, scattering and intrinsic absorption parameters were estimated by modelig the space-time distribution of energy density calculated from CCFs with 2-D radiative transfer theory. We determined the best-fit parameters every 3 months.

The value ranges of best-fit parameters were asfollows: Mean free path of Rayleigh waves were 1.6 - 2.0 km both in the 1 - 2 Hz and the 2 - 4 Hz bands, and parameters of intrinsic absorption b ($b = Q_I^{-1}\omega$) were 0.08 - 0.10 s^{-1} in the 1 - 2 Hz and 0.15 - 0.16 s^{-1} in the 2 - 4 Hz. To validate our method, we estimated these parameters using active shot records at Sakurajima volcano. Since the source is located near the ground surface (about 60 m depth), we can directly compare the results with those of using CCFs that may represent the waveforms from a source at one station to the other one. The mean free path of Rayleigh waves was estimated as 1.2 km in the 1 – 2 Hz and 2.0 km in the 2 - 4 Hz, and the values of b were estimated as 0.1 s^{-1} in the 1 - 2 Hz and 0.15 s^{-1} in the 2 - 4 Hz. They are almost consistent with those of using CCFs. This confirms that we can estimate scattering and intrinsic absorption parameters of Rayleigh waves by using envelopes of ambient seismic noise CCFs without active sources.

[References]
[1] Carcole, E. and Sato, H. (2010), Spatial distribution of scattering loss and intrinsic absorption of short-period S waves in the lithosphere of Japan on the basis of the Multiple Lapse Time Window Analysis of Hi-net data, Geophys. J. Int. 118, 286-290
[2] Yamamoto, M. and Sato, H. (2010), Multiple scattering and mode conversion revealed by an active seismic experiment at Asama volcano, Japan, J. Geophys. Res. 115, B07304

Poster #12

Experimental constraints on the dihedral angles in the system of olivine-multicomponent aqueous fluids at 800-1100°C and 1-4 GPa

YONGSHENG HUANG[1], TAKAYUKI NAKATANI[1], MICHIHIKO NAKAMURA[1], CATHERINE MCCAMMON[2]

[1] Department of Earth Science, Graduate School of Science, Tohoku University, Aramaki-Aza-Aoba, Aoba-ku, Sendai, Miyagi 980-8578, Japan
[2] Bayerisches Geoinstitut, University of Bayreuth, 95440 Bayreuth, Germany

In subduction zone, generation and migration of aqueous fluid are important to understand the global geodynamics including arc volcanism, seismic activities, and element recycling. In fluid-bearing rocks, the dihedral angle, θ, formed by two intersecting walls of a pore at a junction with two solid grains, is one of the key parameters to determine the distribution and connectivity of fluid phases that strongly affect the physical properties of rocks such as permeability, elasticity, and electrical conductivity. Theoretically, the dihedral angle of 60° is a critical value to constrain whether an interconnected network could be formed in an isotropic system. An interconnected network can be established migrating fluids if θ <60°, whereas the fluids will be closed at grain corns transporting to the deep mantle if the θ≥60°(Bargen and Waff, 1986; Watson and Brenan, 1987, Holness, 1991, 1992; Laporte and Watson, 1995; Watson et al.,1982; Nakamura and Watson, 2001). Dihedral angles are dependent on not only temperature and pressure, but also on the composition of fluid. Fluid released from a subducting slab is often assumed to be composed of pure H_2O in previous studies. However, recent researches of fluid inclusions in the mantle xenolith (Kawamoto et al., 2013), melt inclusion from primitive arc basalts (Wallace, 2005; Keppler, 2017), and upwelling slab-derived fluid in fore-arc arc regions (Morikawa et al., 2016) suggested that CO_2 and NaCl could be the important constituents of aqueous fluid in subduction zones. The effect of H_2O-CO_2-NaCl fluid on dihedral angle is, however, still poorly understood.

We conducted the annealing experiments in the systems olivine-H_2O-CO_2-NaCl at 1.0-4.0 GPa and 800–1100°C for 72–192 hours by using piston cylinder apparatus at Tohoku University and Bayerisches Geoinstitut, University of Bayreuth. More than 200 dihedral angles were measured from secondary electron or backscattered images taken by FE-SEM at magnifications above×6,000 ~×150,000, depending on the size of grains and pores. Because our research is still in progress, here we present only the results obtained at 1 GPa and 1000°C. In this P-T condition, the olivine-fluid dihedral angles in the H_2O, H_2O-NaCl (~27.5 wt% NaCl), CO_2-rich fluid ($(COOH)_2$), H_2O-CO_2 (H_2O:CO_2 = 2:1 in mol) and H_2O-CO_2-NaCl systems were 64.1°, 56.1°, 78.2°, 62.7° and 58.2°, respectively. Since Watson and Brenan (1987) also investigated the olivine-fluid dihedral angle in the H_2O, H_2O-NaCl (~27.5wt% NaCl), and CO_2 system at the same P-T conditions, we can compare our results with theirs. In the H_2O system, the dihedral angle of 64.1° is in accordance with their study—65°. The dihedral angles of 56.1°in the H_2O-NaCl system is slightly smaller than that reported in the previous study (60°). The dihedral angle in the $(COOH)_2$ system (78.2°) is clearly lower that the pure CO_2 system (90°) in which $Ag_2C_2O_4$ was used as a starting material. NaCl-bearing aqueous fluid decreased the olivine-fluid dihedral angle and CO_2 also slightly decreased the angle in the H_2O-CO_2 system although the angle in the CO_2-rich system is much larger than that in the H_2O system. In the H_2O-CO_2-NaCl system, the dihedral angle fell between the values in the H_2O-NaCl and H_2O-CO_2 systems. One of the key factors to understand these results can be the olivine solubility in the aqueous fluid. For a solid-liquid system, the free energy can be decreased by adsorption of surface active species (Holness, 1997). Takei and Shimizu (2003) employed a lattice-like model to investigate the dihedral angle in the binary eutectic systems and they clarified that the solid-liquid interfacial tension decreases with increasing the concentration of solid phase in the bulk liquid phase because solid surface preferentially adsorbs the solid component. Yoshino et al., (2007) demonstrated that olivine-fluid dihedral angle decreased with increasing pressure, which was caused by the increase of olivine solubility. Recent experimental studies indicated that the solubility of olivine can be high in both H_2O-NaCl and H_2O-CO_2 systems compared to that in the H_2O system (Wykes et al., 2011; Tiraboschi et al., 2018), which could explain the low dihedral angles in both systems. According to this relationship, we expect that in the H_2O-CO_2-NaCl system CO_2 limited the olivine solubility in H_2O-NaCl fluid. The results of this research could provide indispensable information on the interpretation of seismic tomography and electric conductivity imaging

and also forward geodynamic modeling in subduction zones.

This work was supported by the JSPS Japanese-German Graduate Externship.

Poster #13

Characteristic behavior of ground tilt motions associated with repeated small explosions at Stromboli volcano

AYUMU ISHIKAWA[1], TAKESHI NISHIMURA[1], HIROSHI AOYAMA[2], RYOHEI KAWAGUCHI[3], EISUKE FUJITA[4], TAKAHIRO MIWA[4], TAISHI YAMADA[4], MAURIZIO RIPEPE[5], RICCARDO GENCO[5]

[1] Graduate school of science, Tohoku University,
[2] Faculty of Science, Hokkaido University,
[3] Meteorological Research Institute,
[4] National Research Institute for Earth Science and Disaster Prevention,
[5] The Department of Earth Sciences, University of Florence

Stromboli volcano in Italy is a typical volcano where intermittent small eruption (Strombolian eruption) occurs.

We report characteristic behavior of tilt records associated with small intermittent eruptions and its temporal change before the activity transition to flank lava effusion on August 7, 2014.

We installed 3 tiltmeters near the summit crater of Stromboli volcano from the end of May 2014. We obtained continuous tilt records with a sampling frequency of 100Hz. Down-sampled data of 1 Hz are analyzed from June 1 to July 30 divided each 15 days. To extract volcano deformation associated with small explosion from tilt records, we firstly applied 6h high-pass filter for noise removal, and then smoothed them by 50s low-pass filter. As a result, the signals associated with VLP seismic signal, which is rapid uplift and the following subsidence toward the active crater, are repeatedly observed. In addition, gradual uplift toward the active carter which has a few hundred second durations were observed, as reported in Genco and Ripepe [2010]. We extracted these three ground deformations as follows. First, we performed 20s - 100s band-pass filter on the north component of a station RFR. Secondly, we determined the onset time and end time of VLP signal by imposing a low threshold amplitude level. Finally, we extracted tilt signals that have a long interval time and a high amplitude level. The extracted tilt signals are characterized by azimuth from the north and amplitude of the tilt vector. We examined the parameters' distribution at each observation site every a half month.

Rapid uplift and subsidence tilt motion of PZZ (ESE direction from the crater) and RFR (SSE from the crater) point to the active crater, while those of CPL (NE from the crater) deviate about 30 degrees north from the crater. This suggests that the pressure source generating rapid uplift and subsidence associated with small explosion is not approximated as a point source but has a finite size. Direction of the gradual uplift prior to small explosion has large variation in the azimuth, but the directions averaged every two weeks are almost same to the average directions of rapid uplift and subsidence. During the observation period from June to July, there is no significant temporal change of averaged azimuth in any site or deformation phenomenon.

These results suggest the gradual uplift prior to small explosion and rapid deformation associated with small explosion averagely share an almost same pressure source. Although transition phenomenon of flank lava effusion occurred in the beginning of August, 2014, the pressure source location did not change significantly for time scale of two weeks.

[References]
[1] Genco, R., and M. Ripepe (2010), Inflation□deflation cycles revealed by tilt and seismic records at Stromboli volcano, Geophys. Res. Lett., 37, L12302, doi:10.1029/2010GL042925.

Poster #14

Seasonal to inter-decadal variability of temperature and salinity in the Indonesian Seas and their adjacent ocean

MOCHAMAD RIZA ISKANDAR[1], TOSHIO SUGA[1]

[1] Department of Geophysics, Graduate School of Science, Tohoku University.

The Indonesian region, also known as a major part of the "Maritime Continent," is located at the tropical zone between the Pacific and Indian Oceans. It plays an essential role in the climate system, with being identified as an area of major climatic importance both locally and globally. Changes in the Indonesian Throughflow (ITF) transport have been investigated by many researchers, through the temporal variability and its dependencies on climate mode such as El Nino/Southern Oscillation (ENSO) and Indian Ocean Dipole (IOD). However, variability of the water mass structure in term of temperature and salinity has not been fully described yet in each subregion of Indonesian Seas, which is regarded as a fingerprint to understand the climate changes as well as changes in inter-basin water exchanges. Here we demonstrate the changes of temperature and salinity within Indonesian Seas based on the potential density coordinate on the TS diagram.

Using temperature and salinity data from World Ocean Database 2013 and cruise data collected by the Indonesian Institute of Sciences (Lembaga Ilmu Pengetahuan Indonesia or LIPI), we found that during El Nino years the water in the Indonesia Seas tends to become fresher and cooler in the pycnocline especially at $22.0 \leq \sigma_\theta \leq 25.0$ kg/m^3. During the negative phase of the IOD, the majority of subregion within Indonesian Seas tends to be fresher. Generally, the conditions are vice versa during La-Nina and positive IOD events. On inter-decadal timescales in the same pycnocline ($22.0 \leq \sigma_\theta \leq 25.0$ kg/m^3). During last decade, the upper layer water in South Eastern Indian Ocean tend to be fresher. The changes of precipitation, as well as the regulation if ITF play the role to force the condition.

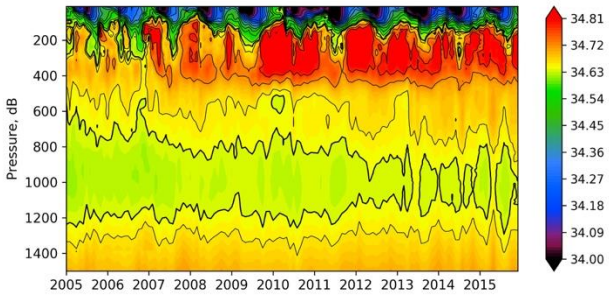

Fig 1. Interannual evolution of salinity in the upper 1500 m of the South Eastern Indian Ocean

[References]
[1] Du, Y., Y. Zhang, M. Feng, T. Wang, N. Zhang and S. Wijffels (2015). *Scientific Reports* 5: 16050.
[2] Gordon, A. L., C. F. Giulivi and A. G. Ilahude (2003). *Deep Sea Research Part II: Topical Studies in Oceanography* 50(12): 2205-2228.
[3] Hu, S. and J. Sprintall (2016). *Journal of Geophysical Research: Oceans* 121(4): 2596-2615.

Poster #15

Contact theory based power-law relation to represent the pressure dependence of elastic wave velocity

ERANGA JAYAWICKRAMA[1], JUN MUTO[1], HIROYUKI NAGAHAMA[1]

[1] Department of Earth Science, Graduate School of Science, Tohoku University

The pressure dependence of elastic wave velocity through fractured media has been of great interest for many decades. Abundant experimental studies have been conducted to observe the velocity variation (Birch, 1960) and theoretical explanations have been provided on velocity variation (Walsh, 1965). However, the pressure dependence of wave velocity was not well represented till Eberhart-Phillips et al. (1989) introduced the empirical relationship,

$$V = V^* + KP - B\ exp(-DP) \quad (1)$$

where V is the velocity and V^*, K, B and D are constants for a given rock type. Since the relationship was derived using low-pressure (<40 MPa) velocity measurements of Han (1986), the reliability of it at high pressure is questionable and this was in fact discussed by later studies. Jones (1995) showed that this relationship is unable to predict the quality factor of P-wave and S-wave at high effective stress, and Khaskar et al. (1999) showed that it is unable to represent the negative K at elevated pressures. Moreover, this empirical relationship can only be applied for the sedimentary rocks. Therefore, other relationships which are able to represent the pressure dependence of elastic velocity at both low and high pressure that are independent of rock types are needed.

As an alternative, we developed the below power-law, combining Nagumo (1963)'s contact state relationships and a one-dimensional longitudinal elastic wave velocity equation based on Hertz theory (Hertz, 1881).

$$V^2 = V_0^2 + A'P^{\mu}, \quad (2)$$

where the parameters P, V, V_0, μ and A' represent the effective pressure, wave velocity at given and zero effective pressures, the multiple contact state and a pressure dependent variable, respectively. The relationship however is similar in its form to the Kobayashi and Furuzumi (1977) empirical relationship.

Experimental and theoretical studies have shown that the pressure dependence of elastic wave velocity highly depends on fractures in rock. Therefore, the multiple contact state in the current power-law relation is an important parameter as it enables the representation of the velocity variation with respect to the fracture behavior. The two end values of μ represent fracture open (μ=2/3) and close (μ=1/2) states while the values in between show partly open state of fractures. Any μ value greater than 2/3 indicates open fractures which appears in the low-pressure regions until the fractures gradually close and increase velocity. The exponential part in relationship (1) is representing this gradual change. Once the fractures are closed the velocity increases intrinsically and is represented by μ values less than 1/2. This slope is shown by K in relationship (1). But in rocks with high porosity, after reaching a steady increment in the velocity at high pressure the velocity drops by pore collapsing. This velocity drop cannot be represented by relationship (1). But relationship (2) is able to represent this through contact state variation. While μ gives the multiple contact state, the physical properties of the contacts and the elastic properties of the rock are given by A'.

Thus, as an alternative to the empirical relationship (1) we introduce the derived power-law (2) which can represent the velocity at both low and high pressures for any given rock.

[References]
[1] Eberhart□Phillips D, Han D, Zoback M (1989) Empirical relationships among seismic velocity, effective pressure, porosity, and clay content in sandstone. Geophys. 54:82–89.
[2] Kobayashi R, Furuzumi M (1977) Study on elastic wave velocity of rocks during failure process in compression. J Min Metal Inst Japan 93:7-11. (English Abstract)
[3] Nagumo S (1963) On the elastic property of granular media (III) – Static response and stress dependency of deformation coefficient. Geophys Explor 16:13-20. (English Abstract)
[4] Hertz H (1881) On the contact of elastic solids. J Reine Angew Math 92:156-171. English translation: Hertz H (1896) Miscellaneous Papers. Macmillan: New York, 146p

Poster #16

In-situ observation in a FE-SEM of crystallization of natural basalt glass with emphasis on olivine dendrites

KASPER B. JENSEN[1], MAYUMI MUJIN[1]

[1] Department of Earth Science, Graduate School of Science, Tohoku University

Crystallization of basalt is a big and important topic in geology as it is the most common magmatic rock on earth. This study will emphasise on crystallization and specific the formation of olivine dendrites in basaltic magma. The dendritic texture in olivine is a process of undercooling of a melt. These processes have been observed however new equipment allows for in-situ observation at smaller scale. Sample used for current experiment is EPR-G3 (East pacific rise), and chemistry and volatile content have been analyzed in a SIMS by Shimizu et al. (2017). There were two different preparations for the experiments. First experiment the sample was crushed in an agate mortar, for other experiment sample has been double polished beforehand. All heating experiment is conducted on a FE-SEM (JEOL JSM-7100F) with a connected heating module placed at Tohoku University, afterwards observation with BSE have been conducted on same machine. Experiments have been conducted at various temperature, however no pressure can be applied to the experiment. For observations after heating Os-coating has been done to sample after heating experiment. Current experiments have different results to how fast nucleation occurs and crystal shape. However, more experiments are being conducted at different conditions such as different maximum temperature, cooling rate and time. To observe the conditions at which olivine dendrites form.

[References]

[1] Shimizu, K., Ushibuko, T., Hamada, M., Itoh, S., Higashi, Y., Takahashi, E., Ito, M., 2017, H_2O, CO_2, F, S, Cl, and P_2O_5 analysis of silicate glasses using SIMS: Report of volatile standard glasses, Geochemical Journal, Vol. 51, pp. 299-313

Poster #17

Direct measurement of reaction-induced stress during hydration reaction of periclase

HISAMU KASAHARA[1], MASAOKI UNO[1],
ATSUSHI OKAMOTO[1], NORIYOSHI TSUCHIYA[1]

[1] Tohoku University

Hydration reactions in the crust and mantle accompany large solid volume increase (several to tens vol%). Solid volume increase by hydration may generate stress, strain and fracturing. Thermodynamic estimation of maximum reaction-induced stress for serpentinization reaction is as high as 1.5 GPa (Kelemen and Hirth, 2012), which well exceeds the tensile strength of rocks. Actual hydration reactions observed in the field, however, have variations raging from reaction-induced fracturing (e.g., Jamtveit and Austrheim, 2010) to non-fracturing pseudomorphic replacement (e.g., Centrella et al., 2015). Suggesting that actual stress generation differs from the thermodynamic estimation. To understand the process controlling such variations in stress generation, we have conducted direct measurement of reaction-induced stress in MgO- H_2O system.

In MgO- H_2O system, periclase (MgO) reacts with H_2O to from brucite. The volume expansion of this reaction is 119%. Pressed powder pellet (initial porosity, φ_0 ~55%) and sintered (φ_0 ~14%) periclase were used as starting material. The samples were set in a uniaxial reaction cell, reacted with H_2O under fluid pressure of 0.2 MPa, and the solid pressure generated by the reaction was measured by load cell. We conducted experiments from 80 °C to 120 °C to change reaction rate and observe the difference of mechanical behavior.

During the pellet hydration experiments, stress increased to approximately ~40 MPa. Different behaviors of stress generation was observed for a temperature change. Particularly, stress increased monotonously at 80 °C, whereas remarkable stress relaxation was observed after peak stress at 120 °C. This finding suggests that reaction rate and deformation rate have temperature dependence. The additional experiments were conducted for investigating the temperature dependency of reaction rate and deformation rate in this system. As a result, it was revealed that temperature dependence of the shrinking strain rate was about four times larger than that of the reaction. The expansion strain rate by reaction was larger than shrinkage strain rate at <110 °C. Whereas shrinkage strain rate gets larger than expansion strain rate at 110 °C. Therefore, observed changes of stress generation (monotonous stress increase at 80 °C and stress relaxation at 120 °C) was explained by the balance between reaction rate and deformation rate.

Hydration of sintered periclase generated higher stress than hydration of pellet (60 MPa). In the run product, brucite was observed at the periclase grain boundary. It is considered that the hydration occurred in initial porosity fractured periclase grain boundaries and fracture promoted additional hydration.

According to the result of experiments, it is suggested that the behavior of stress generation depend on the balance of reaction rate and deformation rate. The volume expansion during initial hydration may induce fracture along grain boundaries and promote additional hydration.

[References]
[1] Kelemen and Hirth (2012) , Earth and Planetary Sciences, 345-348, 81-89
[2] Jamtveit and Austrheim (2010) , Elements, vol. 6, 153-158
[3] Centrella et al. (2015) , Lithos, 236-237, 245-255

Poster #18

H_2O / F ratios in asthenosphere inferred from volatile compositions of petit-spot lavas

YUKI KATSURAGI[1], NAOTO HIRANO[2], YUKI SATO[1], KENJI SHIMIZU[3]

[1] Faculty of Science, Tohoku University.
[2] Center for Northeast Asian Science, Tohoku University.
[3] Kochi Institute for Core Sample Research, JAMSTEC.

Mid-oceanic ridge basalts (MORBs) have ever been a key to understand the compositions of oceanic upper mantle. Although it is well known about depleted source mantle below the MORBs, they are largely limited area of youngest part of oceanic lithosphere. Some previous studies have tried to estimate the volatile compositions of upper mantle by MORBs.

Petit-spot volcano, a newly recognized volcanism into tectonic processes on the Earth, erupts by tectonic force associated with plate-flexure of outer rise. The lavas (foidite to hawaiite) are highly enriched in incompatible elements, likely originated from asthenosphere. Their samples show high vesicularity in spite of the eruption under high hydrostatic pressure at approximately 6000 meters below the sea level, indicating high levels of volatile contents in magma.

We report the volatile compositions in quenched glass rinds of petit-spot lavas from the northwestern Pacific Plate in order to recognize the volatile compositions of asthenospheric mantle below the older part of oceanic lithosphere. They are much higher than most of the previously reported MORBs without seawater alteration. The H_2O / F ratio of the studied samples is relatively constant (average: 14.6 ± 1.4, 1 s.d.). It may represent the ratio of asthenosphere below both of young and old lithosphere, because H_2O and F in magma behave similar incompatibility during mantle melting. The obtained H_2O / F ratio is consistent with those of average MORB glasses, but higher than those of OIBs (H_2O/F < 10).

Poster #19

Stability of $MgCO_3$ in Fe-rich hydrous lower mantle

FUMIYA MAEDA[1], SEIJI KAMADA[1,2], NOBUYOSHI MIYAJIMA[3], SYLVAIN PETITGIRARD[3],NAOHISA HIRAO[4], CATHERINE MCCAMMON[3], DANIEL J. FROST[3], TATSUYA SAKAMAKI[1], AKIO SUZUKI[1]

[1] Department of Earth Science, Graduate School of Science, Tohoku University
[2] Frontier Research Institute for Interdisciplinary Sciences, Tohoku University
[3] Bayerisches Geoinstitut, University of Bayreuth.
[4] Japan Synchrotron Radiation Research Institute

Carbonate minerals are important through the deep interiors of the Earth [1]. Subducting oceanic plates and lithospheric mantle carry carbonates into the deep Earth and various phenomena related to carbon-bearing phases have been expected during subduction process [e.g., 1–6].

A possible carbonate in the mantle is $MgCO_3$ magnesite. The stability of magnesite depends on redox conditions represented by oxygen fugacity (f_{O2}) in addition to pressure and temperature [e.g., 2,3]. The mantle below 250-km depth can be reduced due to precipitation of 1-wt% metallic iron through iron disproportionation in silicates [e.g., 7] and hence magnesite is expected to break down to diamond in the mantle transition zone or lower mantle [2,3]. However, existence of $MgCO_3$ is not completely ruled out in subducted slabs which may be oxidized relative to the average mantle [e.g., 8]

We should note the phase transition of $MgCO_3$ at the deep lower-mantle pressure [9–11]. Such phase transition of magnesite can enhance the stability of $MgCO_3$ under the reduced conditions [3]. We investigated the stability of $MgCO_3$ under the lower-mantle *P–T* conditions existing metallic iron in order to seek the depth where carbonates can survive.

$MgCO_3$ is a natural sample of magnesite from Bahia, Brazil. The composition is almost pure $MgCO_3$ with including a small amount of Fe and Ca. Powdered magnesite was loaded in a metallic-iron capsule with MgO powder in a sample chamber. An iron capsule was separated from diamond anvils and a W gasket by MgO, which play roles of pressure medium and thermal insulator. We consider that this configuration of the sample chamber is efficient to reduce thermal gradients on the sample even in a LHDAC experiment.

The high *P–T* experiments at 60–100 GPa and 1800–2200 K was performed using a double-sided laser-heated diamond anvil cell (LHDAC) combined with *in situ* synchrotron X-ray diffraction technique (XRD). XRD patterns were acquired at beamline BL10XU of SPring-8 in Hyogo, Japan. A sample will be recovered from high *P–T* after quenching to ambient conditions and be observed using a transmission electron microscope (TEM). A TEM lamella is going to be prepared to be ~100-nm thickness using a focused ion beam (FIB) system. The TEM and FIB are equipped at Bayerisches Geoinstitut in Germany.

We observed peaks from FeH_x, Fe_3C, and (Mg,Fe)O in the *in situ* XRD patterns. This means that metallic Fe reacts with $MgCO_3$ to form MgO-FeO solid solution and Fe_3C. Existence of FeH_x may suggest that MgO pressure medium absorbed H_2O in atmosphere, which can diffuse into the iron capsule during heating. Some additional peaks appear in the XRD patterns. These peaks can be explained by a monoclinic high-pressure phase of carbonate [10,11]. These results indicate that high-pressure polymorphs of $(Mg,Fe)CO_3$ is possible carbon-bearing phases in the reduced lower mantle though we need more detailed information from the recovered sample.

This work was supported by the JSPS Japanese-German Graduate Externship.

[References]
[1] Dasgupta and Hirschmann (2010) Earth Planet. Sci. Lett. 298, 1–13.
[2] Rohrbach and Schmidt (2011) Nature 472, 209–212.
[3] Stagno et al. (2011) Geophys. Res. Lett. 38, L19309.
[4] Thomson et al. (2016) Nature 529, 76–79.
[5] Harte and Richardson (2012) Gond. Res. 21, 236–245.
[6] Maeda et al. (2017) Sci. Rep. 7, 40602.
[7] Frost et al. (2004) Nature 428, 409–412.
[8] McCammon et al. (2004) Phys. Earth Planet. Inter. 143–144, 157–169.
[9] Isshiki et al. (2004) Nature 427, 60–63.
[10] Oganov et al. (2008) Earth Planet. Sci. Lett. 273, 38–47.
[11] Boulard et al. (2011) Proc. Natl. Acad. Sci. U.S.A. 91, 104101.

Poster #20

Anisotropic creep in hydrous olivine single crystals and its application to earthquake cycle

SAGAR MASUTI[1], JENNIFER GIRARD[2], SYLVAIN BARBOT[1], SHUN KARATO[2]

[1] Asian school of Environment, Nanyang Technological University, Singapore
[2] Yale University, Department of Geology & Geophysics, New Haven, USA

Olivine, the most abundant and weakest upper mantle mineral, has been one of the extensively studied mineral in the last few decades. From these studies, we know the strength of polycrystalline olivine is greatly reduced by the addition of water. A similar study on the single crystal olivine shows that the effect of water is not same in all direction (Mackwell et al. 1985). Here we gather the experimental data from different studies to quantify the effect of water and pressure on olivine single crystal. The data collected from different studies include wide pressure range of 0.1 MPa to 6 GPa at temperatures around 1200ºC to 1300ºC and generally on three different orientations viz., [110]c, [101]c and [011]c. The normal stress is applied in between the [100] and [010] direction for [110]c orientation to activate the [100](010) slip system. Similarly, for [011]c orientations [001](010) slip system and for [101]c orientation [100](001) and [001](100) slip systems are activated. We show the effect of water on the [110]c orientation or [100](010) slip system is substantially smaller (r[110]~0.3) than the [011]c orientation or [001](010) slip system (r[011]~1.3).

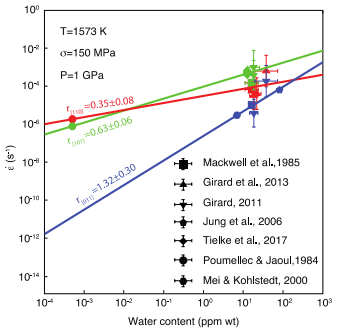

Figure 1 Strain-rate versus the water content relationships for three different orientations. Color of symbol and the profile indicated different slip systems. Different symbols correspond to the different studies.

Using the flow law values, if we plot the viscosity versus the depth profile, we can see that the easiest slip system and strongest slip system changes with depth. In other words, the transient creep of olivine aggregates at shallower depths is dominated by the soft slip system and at deeper depths it switches to the hard slip system and vice versa for the steady-state creep.

When there are multiple slip systems with largely different strength, plastic deformation and deformation microstructures of a polycrystalline aggregate are connected to different slip systems in different ways for different properties. With more than one slip system is active at a time, deformation is not free. Instead, it is constrained by the orientation of the neighbouring grains. Some grains may be favourably oriented to the soft slip system ($[110]_c$ orientation) and others may be favourably oriented to the hard slip system ($[011]_c$ orientation). The slower slip system blocks the faster slip system by creating the internal stress, this behaviour can be captured by invoking the work-hardening rheology. We will discuss such rheology and its geodynamic application to model the earthquake cycle.

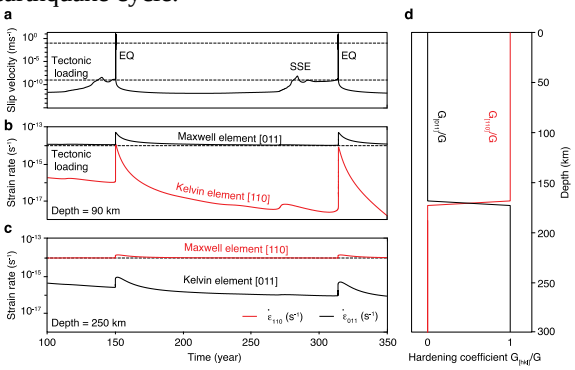

Figure 2 Slip velocity, [110]c and [011]c strain rates as a function of time at specific depths and hardening coefficients. (a) Slip velocity at depth of 11 km on the fault. (b) Strain rates of easy and hard slip systems at depth 90 km (c) Same as (b) but at depth 250 km. (d) Ratio of hardening coefficients.

[References]
[1] Mackwell, S. J., Kohlstedt, D. L., & Paterson, M. S. (1985). The role of water in the deformation of olivine single crystals. Journal of Geophysical Research: Solid Earth, 90.

Poster #21

Th, U and Pb in the Earth

W. F. McDonough[1,2], Meng Guo[2]

[1] Department of Earth Science, Graduate School of Science, Tohoku University
[2] Department of Geology, University of Maryland

Many thousands of $^{232}Th/^{238}U$ ratios (aka, K_{meas}) and time-integrated Pb isotopic ratios (aka, K_{Pb}) of the continental crust (CC) and modern mantle (MM) document two complementary reservoirs, ${}^{CC}K_{Pb} = 3.94\ ^{+0.20}_{-0.11}$ and ${}^{MM}K_{Pb} = 3.87\ ^{+0.15}_{-0.07}$, that tightly bracket the solar system (SS) initial ${}^{SS}K_{Pb} = 3.890 \pm 0.015$ (Blichert -Toft et al., 2010) and define a bulk silicate Earth (BSE) composition of ${}^{BSE}K_{Pb} = 3.90\ ^{+0.13}_{-0.07}$. The indistinguishable statistically nature of ${}^{CC}K_{Pb}$, ${}^{MM}K_{Pb}$, ${}^{BSE}K_{Pb}$, and ${}^{SS}K_{Pb}$ confirms that negligible Th/U fractionation accompanied planetary accretion, core-mantle separation, and crust-mantle differentiation. Accordingly, given significantly different metal-silicate partition coefficients for Th and U under all potential core forming conditions as yet explored, the core therefore has negligible quantities of Th and U (i.e., <ng/g).

The present day U, Th, and Pb abundances and Pb isotopic composition of the CC and MM reveal that continental crustal growth started early, likely in the Hadean to early Archean, and probable exceed the present-day mass by a factor of 3 before reaching its present state and mass. This finding requires significant recycling of continental crust during the Archean and Proterozoic.

The Earth's depleted budget of moderately volatile elements (e.g., alkali metals, S, Pb, etc.) is a product of accretion processes. The excess depletion of chalcogenes in the BSE is consistent with core formation extracting much of the Earth's sulfur budget. Although it is recognized as having negligible quantities of Th and U, the core, which during it formation sequestered thiophilic ligands, contains about half of the Earth's budget of Pb. Updated models for the Pb budget of the Earth find a BSE with 150 ppb and a core with 450 ppb Pb and a Pb isotopic composition for the bulk Earth that places it on the solar system's 4.57 Ga isochron.

Poster #22

Origin and metamorphic evolution of corundum (or kyanite)-bearing amphiboites from the Paleoproterozoic Usagaran belt, Tanzania

Keiko Mori[1], Tatsuki Tsujimori[1], Nelson Boniface[3]

[1] Department of Earth Science, Graduate School of Science, Tohoku University
[2] Center for Northeast Asian Studies
[3] University of Dar es Salaam

Occurrence of Paleoproterozoic eclogitic rocks have been known in the Usagaran belts of Tanzania. Due to severe retrogression and high-variance mineral assemblage of eclogitic rocks, however, the regional metamorphism is not fully constrained. In order to better understand the metamorphism, we studied corundum (or kyanite)-bearing aluminium-rich amphibolites occurring near the locality of Paleoproterozoic 'eclogitic rocks'. The amphibolites are characterized by the mineral assemblage of Ca-amphibole + kyanite ±corundum + talc ±garnet ±plagioclase ±quartz. Bulk-rock major and trace elements geochemistry of the investigated three samples suggest that the protolith was troctolic or anorthositic cumulates; they have high values of normative plagioclase and olivine, and show a negative correlation between Ni and Sr, and positive Eu and Sr anomalies in spidergram. The presence of talc + kyanite and the abundance of cordierite and yoderite indicate the minimum pressure of a peak metamorphic condition of P> 1.1GPa and T= 700-850 ºC. In a quartz-bearing sample, kyanite contains precursor corundum as inclusion. Relict orthopyroxene was found in a plagioclase-rich sample. Our petrological study indicates that the amphiboles recorded a metamorphic trajectory from low-pressure granulite-facies (or igneous) stage, where orthopyroxene was stable, to a high-pressure stage characterized by the mineral assemblage talc + kyanite ±garnet. Bulk-rock compositions, P-T pseudosection analyses and the talc + kyanite stability suggest that the studied amphibolites formed by a collision/subduction of the Archean continental crust at a high-pressure granulite-facies condition rather than eclogite-facies. Such a high geothermal gradient is an indicative of 'hot' subduction-zone geotherm in Paleoproterozoic.

Poster #23

Synthesis of garnet by hydrothermal metamorphism in basalt-water system

YUSUKE NETSU[1], ATSUSHI OKAMOTO[1], MASAOKI UNO[1], RYOSUKE OYANAGI[2], NOBUO HIRANO[1], NORIYOSHI TSUCHIYA[1]

[1] Graduate School of Environmental Studies, Tohoku University
[2] Japan Agency for Marine-Earth Science and Technology Department of Solid Earth Geochemistry

The Island Deep Drilling Project (IDDP-2) reached 427 °C and 34 MPa, which exceeds the critical point of seawater. The cores revealed that intense water-rock interaction with mineral assemblage of greenschist to amphibolite facies metamorphism. Although such deep drilling provides us direct information of active metamorphic processes; however, it is still unclear that conventional petrological analyses could apply to reaction processes in open systems at high temperature hydrothermal alteration at seafloor.

In this study, we conducted hydrothermal flow-through experiments on basalt-H_2O system at 410 °C and 35 MPa for 810 h. We used a powder of MORB (Island, 250-500 μm), which is composed of plagioclase, olivine phenocrysts and clinopyroxnene, plagioclase groundmass, were enclosed in a Ti inner tube (I.D.= 4.35 mm). During the run, distilled water was continuously pumped into the reaction vessel at a constant flow rate of 14.4 ml/day, and the output solution was collected every day. The concentration of Si, Al, Ti, Fe, Mg, Ca, Na, and K in the output solution was analyzed by ICP-AES and AA. For comparison, we also conducted experiments on the gabbro-H_2O system. The speciation of aqueous species and saturation index were calculated by using SOLVEQ-XPT (Reed, 1982).

In the basalt-H_2O experiment, notable spatial variations of products mineral were observed in basalt. At the inlet of the inner tube, grossular was formed preferentially in the groundmass, chlorite was formed around olivine grains, and porous anorthite (XCa = 0.98) grain was formed (Fig 1.). At the middle and outlet part of the inner tube, amphibole and chlorite were formed as replacing groundmass. In the gabbro-H_2O experiment, the extent of reaction was very low, with producing a subtle amount of biotite.

The pH of the output solution (25 °C) in basalt-H_2O experiment increased from 6.5 at ~190 h to 7.5 at ~357 h. Concentration of Na and Al increased with time from 0.1 - 1.0 mg/kg H_2O at ~190 h to 5.0 - 9.0 mg/kg H_2O at ~334 h. We performed the principal component analysis on the solution chemistry, and revealed that the PC1 represents pH, Al, and Na, PC2 represents Mg and Ca, and PC3 represents silica. The temporal variation of PC1 is consistent with that of saturation index of albite as well as linked to anorthite and grossular, indicating that (1) leaching of albite component from plagioclase predominantly controls the reactions and causes an increase of pH in the solution was increased, and (2) anorthite and grossular was formed as a residue of the leaching. Similarity between PC2 and the saturation index of Mg-bearing minerals (such as diopside, amphibole, and chlorite) suggests that PC2 represent the precipitation of these minerals under elevated pH. Our results suggest that preferential dissolution of specific minerals controls the progress and pathway of the reactions, and the principal component analyses of solution would be useful for extracting information of main reaction system under the hydrothermal conditions.

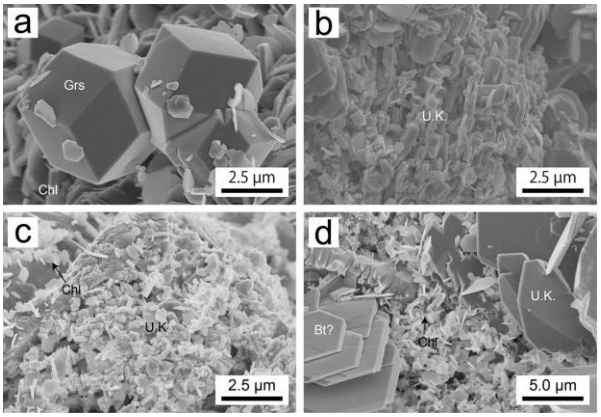

Fig 1. The surface morphology of the product during the basalt – pure water reaction. (a) Inlet part. (b - c) Middle part. (d) Outlet part. Grs : grossular, Chl : chlorite, Bt : biotite, U.K. : Unknown.

[References]
[1] Reed, M. H.(1982) Calculation of multi-component chemical equilibria and reaction processes in systems involving minerals, gases and an aqueous phase. Geochimica et Cosmochimica Acta, 46(4), 513-528.

Poster #24

Fluids transport and magma-driven metamorphism related to Granitic Pegmatite Complex in Kinka-san Island, NE Japan

A. NURDIANA[1], A. OKAMOTO[1], M. UNO[1], N. TSUCHIYA[1]

[1] Graduate School of Environmental Studies, Tohoku University

Fluid transport plays the important role on various geological processes within the crust. Recently, several geophysical observations suggest the existence of the deep-seated fluids or melts in the crusts [e.g. Wannamaker et al., 2009]. However, the detail mechanisms of aqueous fluid transport are poorly understood. Pegmatite commonly forms at the late stage of the granitic systems which associated with crust metamorphism. In order to gain a better insight of the magmatic-hydrothermal transition systems and the dynamic behaviors of aqueous fluids through the crusts, we investigated the petrology and mineralogy of pegmatite complex in the Kinka-san Island, Northeast Japan.

The Kinka-san Island is located in the southern Kitakami mountains which consists of the Cretaceous granitoid bodies. At the north-western side of the island, a small amount of metamorphic sequences, biotite (Bt) schist and mafic schist, are exposed in contact with the quartz diorite (Qz diorite) body with abundant pegmatite dikes. The Qz diorite is composed of quartz(Qz)-plagioclase(Pl)-K-feldspar(Afs)-hornblende(Hbl)-Bt-apatite(Ap)-titanite(Ttn)-ilmenite(Ilm)-magnetite(Mag). Based on the Hbl-Pl thermometer (Holland & Blundy, 1994) and Al-in-Hbl barometer (Anderson & Smith, 1995), the P-T condition of the Qz diorite is estimated to be 700-750°C and 0.37-0.42 GPa, which is close to the P-T condition of the wet solidus of granitic rocks. The pegmatite dikes, whose mineral assemblage are Qz-Pl-Afs-Bt-Grt-Ilm-Mag, cut the Qz diorite. Assuming the similar pressure to the Qz diorite, the temperature of the mafic schist (Hbl-Pl±Qz±Afs±Ttn±Apt), and amphibole- bearing veins in mafic schist (Hbl-Qz-Afs) are estimated to be 610-660°C and 600-630°C, respectively. A Qz vein hosted by the mafic schists showed a mm-scale reaction zone, which was composed of Pl-aluminosilicate (Als)-Hbl-Qz, showing the temperature of ~520°C. One of the important features is the ubiquitous occurrences of garnet either in pegmatite and Bt schists, which is spessartine-rich (XMn0.6, XFe 0.27, XCa 0.09, XMg 0.04) in the former, and almandine-rich (XMn0.24, XFe 0.65, XCa 0.04, XMg 0.07) in the latter. A slight zoning of garnet is observed in pegmatite from Mn-rich core to Alm-rich rim.

Based on the observation and analyses, the following scenario is considered on the generation and transportation of supercritical fluid from the melt to the crust. Qz diorite intruded into the upper crust (700-750°°C in 0.37-0.42 GPa) and the country rock would had been suffered from contact metamorphism (610-660°C). At the late stage of solidification, pegmatite was formed within the Qz diorite body, and some propagated into the metamorphic rocks (~520°C). These features suggest that pegmatites and later stage vein systems play important roles on transporting fluid in the high-T crusts.

[References]
[1] Wannamaker, et.al., 2009, Nature, 460 (7256), 733–736.
[2] Anderson & Smith, 1995, American Mineralogist, 80, 549-559.
[3] Holland & Blundy, 1994, Mineral and Petrology, 433–447.

Poster #25

Solar wind noble gases in the Rumuruti chondrite PRE95410 and heliocentric distance of the meteorite parent body: implication to inward migration

T. OBASE[1], D. NAKASHIMA[1], T. NAKAMURA[1], K. NAGAO[2]

[1] Department of Earth Science, Graduate School of Science, Tohoku University.
[2] Division of Polar Earth-System Sciences, Korea Polar Research Institute, Korea.

Introduction: Many Rumuruti chondrites (RCs) are solar wind (SW) noble gas-rich regolith breccias showing typical dark/light structures [1]. These characteristics indicate that they were mostly derived from near-surface regions of the meteorite parent bodies. The surface materials were exposed to both SW and galactic cosmic rays (GCRs). GCRs penetrate a few meters from the surface and produces cosmogenic noble gases in the surface materials via spallation. After ejection from the parent body, the meteoroid exposed to GCRs again during transit to the Earth in space. The cosmic ray exposure ages for these two exposure stages can be calculated separately from a correlation of SW and cosmogenic noble gas concentrations [2]. From those SW-rich meteorites, some studies attempted to estimate the heliocentric distances (distance from the Sun) of meteorite parent bodies [e.g.2,3] by comparing SW noble gas implantation rates between meteorites and lunar regolith, as SW flux is inversely related to the square of heliocentric distance. In this study, we modified the previous estimation model [3], measured concentrations and isotopic ratios in the SW-noble gas rich RC Mt. Prestrud (PRE) 95410, and estimated the heliocentric distance of PRE95410 parent body. We re-estimated the heliocentric distances of parent bodies of two Enstatite chondrites (EC) [3], Ordinary chondrite (OC) [4], and Howardite [4] from noble gas data previously reported.

Method: Noble gases in PRE95410 were analyzed by modified VG-5400 (MS-III) noble gas mass spectrometer at the Geochemical Research Center, University of Tokyo. Each samples were heated at 1700 ºC, 20min for total gas extraction. The concentrations and isotopic ratios of He, Ne, and Ar were measured as well as concentrations of ^{84}Kr and ^{132}Xe.

Result: We estimated the exposure ages on PRE95410 parent body (>23±5 Myr), in space (9.5±1.3 Myr), and the heliocentric distance of the parent body (<1.34±0.39 AU). The heliocentric distance is similar to that of re-estimated EC parent body(ies) (<1.84±0.50 for MAC88136, <1.39±0.39 for ALH85119).

Meteorite Name	Heliocentric Distance (AU)	Meteorite Group	Noble gas data
PRE95410	<1.34±0.39	RC	This study
ALH85119	<1.40±0.39	EC	[3]
MAC88136	<1.86±0.51	EC	[3]
Fayetteville	<2.03±0.50	OC	[4]
Kapoeta	<2.74±0.48	How	[4]

Table 1. Estimated heliocentric distances of meteorite parent bodies. How = Howardite.

Discussion: The exposure age on PRE95410 parent body is greatly shorter than a typical exposure age of lunar regolith (~400Myr) [5]. This probably suggests that the exposure on the parent body occurred under an active environment where collisions to the meteorite parent body were much more numerous and hence regolith formation rates were much higher.

Based on spectral analysis, many asteroids show links to three major chondrite groups: ECs, OCs, and Carbonaceous chondrites (CCs). As their distances from the Sun are roughly E<O<C [6], they probably formed in this order. Since RCs show intermediate chemical features between OCs and CCs, formation of RC parent body probably took place between OCs and CCs forming regions [7]. Therefore, the similar heliocentric distances of the PRE95410 parent body and EC parent body may indicate that the PRE95410 parent body has migrated into the inner part of the solar system from the original region before the exposure on the parent body.

[References]
[1] Bischoff A. (2011) *Chem. Erde-Geochem*. 71, 101-133.
[2] Wieler R. et al. (1989) *GCA*, 53, 1441-1448.
[3] Nakashima D. et al. (2006) *MAPS*, 41, 851-862.
[4] Pedroni A. (1989) Diss. Nr. 8880 ETH Zürich.
[5] Mckay D.S. et al. (1989) *Asteroids II*, 98-127.
[6] DeMeo F.E. and Carry B. (2014) *Nature*, 505, 629-634.
[7] Miller K.E. et al. (2017) *GCA*, 209, 24-50.

Poster #26

Structures of basaltic glass under high pressure by in-situ x-ray and neutron diffraction investigations

TOMONORI OHASHI[1], TATSUYA SAKAMAKI[1], TAKANORI HATTORI[2], ASAMI SANO-FURUKAWA[2], KEN-ICHI FUNAKOSHI[3], AKIO SUZUKI[1]

[1] Department of Earth Science, Graduate School of Science, Tohoku University
[2] J-PARC Center, Japan Atomic Energy Agency
[3] Comprehensive Research Organization for Science and Society

There have been a lot of structural investigations of silicate melts and glasses under pressure. However, most of them deal with those of simple compositions, such as $CaSiO_3$, $NaAlSi_3O_8$ and Mg_2SiO_4. The aim of this study is to determine the precise structure of silicate glass, which contains several kinds of metal and network-forming cations.

Our sample was made from 6 kinds of reagent powder (SiO_2, Al_2O_3, Fe_2O_3, MgO, Na_2CO_3 and $CaCO_3$). The mixed powder was melted by gas-mixing furnace, and then quenched. Structure determinations of basaltic glass have been conducted under high pressure using X-ray diffraction (XRD) and neutron diffraction (ND) techniques. XRD and ND experiments were conducted at NE5C beamline at PF-AR, and PLANET beamline at J-PARC, respectively.

The total structure factor, $S(Q)$ suggests that the position of the first sharp diffraction peak (FSDP) shifts to higher-Q region with increasing pressure. This shift indicates the intermediate-range structure of glass becomes compact. The radial distribution function, $G(r)$ shows the shrinkage of the average T-T length, and no detectable change of the average T-O length with increasing pressure (T means tetrahedrally coordinated cations, such as Si^{4+} and Al^{3+}). This result implies that drastic shrinkage of network structure involving a decrease in the mean T-O-T angle is the dominant structural evolution under experimental pressure conditions. Moreover, the second sharp diffraction peak, SSDP (Elliot, 1995) was observed in $S(Q)$ from the ND experiment. The intensity of SSDP enhanced, while that of FSDP weakened with increasing pressure. These trends indicate the disordering of the intermediate-range order (Salmon, 1994) and the diminution of the interstitial voids between TO_4 tetrahedra (Salmon et al., 2006), respectively. $G(r)$ of ND also indicates no extension of the T-O bond in the present study. Considering the T-O extension reported in basaltic liquid (Sakamaki et al., 2013), this difference seems to be due to thermal effect. Also, $G(r)$ of ND represents the Mg-O and Fe-O distances show increase two times at about 2.0 and 6.0–6.9 GPa. These changes is might be caused by the increase in their coordination numbers due to the polymerization of TO_4 tetrahedron. On the other hand, Ca-O and Na-O distances are less sensitive to the pressure. Since the Mg/Fe-O distance is shorter than the Ca/Na-O distance, the Coulomb force between Mg/Fe and O ions is larger than that of Ca/Na and O ions. Hence, Mg and Fe cations are easier to combine with non-bridging or isolated O anions than Ca and Na.

[References]
[1] S.R. Elliott, Phys. Rev. B **51(13)**, 8599–8601 (1995).
[2] T. Sakamaki, A. Suzuki, E. Ohtani, H. Terasaki, S. Urakawa, Y. Katayama, K. Funakoshi, Y. Wang, J.W. Hernlund, and M.D. Ballmer, Nat. Geosci. **6**, 1041–1044 (2013).
[3] P.S. Salmon, Proc. R. Soc. Lond. A **445**, 351–365 (1994).
[4] P.S. Salmon, A.C. Barnes, R.A. Martin, and G.J. Cuello, Phys. Rev. Lett. **96**, 235502 (2006).

Poster #27

Source location determination based on seismic cross-correlations: application to simulated tremor using volcano-tectonic earthquakes

THEODORUS PERMANA[1], TAKESHI NISHIMURA[1], HISASHI NAKAHARA[1], EISUKE FUJITA[2], HIDEKI UEDA[2]

[1] Department of Geophysics, Graduate School of Science, Tohoku University.
[2] Research Institute for Earth Science and Disaster Resilience, Japan.

Precise determination of volcanic tremor source location has been a challenge in seismology due to the complexity of tremor waveform and difficulties in reading P- and S-wave arrival time, which is commonly done in conventional earthquake hypocenter method. Several studies conclude that tremor is a superposition of individual seismic events [1]. We assumed the same and developed a method for locating volcanic tremor source using a seismic network distributed over a small region. The reliability and uncertainty of the method are then assessed.

We combined source-scanning algorithm (SSA) using cross-correlation functions (CCFs) [2] and seismic interferometry technique. Tremor records are preprocessed using seismic interferometry processing routine [3] to obtain stacked CCFs for all station pairs. The CCF-based SSA maps the distribution of possible sources using the sum of the amplitudes of normalized CCF envelopes at predicted travel time differences calculated using a trial source and known 3D velocity model. Our method benefits from the increase signal-to-noise ratio in the CCFs from stacking and the unnecessity to read the arrival times, compute synthetic values or provide initial hypocenter information.

Reliability of the SSA is assessed by locating the hypocenter of volcano-tectonic (VT) events. The error, calculated as the distance from the estimated hypocenters to the 'true' hypocenters from a conventional method, is less than 2 km at 8-16 Hz. This frequency range is related to the dominant frequencies of S-wave phase in the VT events.

We verified our approach on using CCF stacking to locate tremor source by stacking the CCFs of VTs occurred in a small region. We found that the estimated source is located approximately at the centroid of the stacked VTs true hypocenter. Smaller stacking region and higher number of stacked VT events produce more accurate results. Finally, we simulated volcanic tremors as superposition of randomly occurred VT events and applied our method. The source locations are resolved with the uncertainty of less than 2 km.

We believe that our tremor location method can serve as an alternative tool for volcano monitoring, especially to locate seismic events with complex waveform and no clear arrival times.

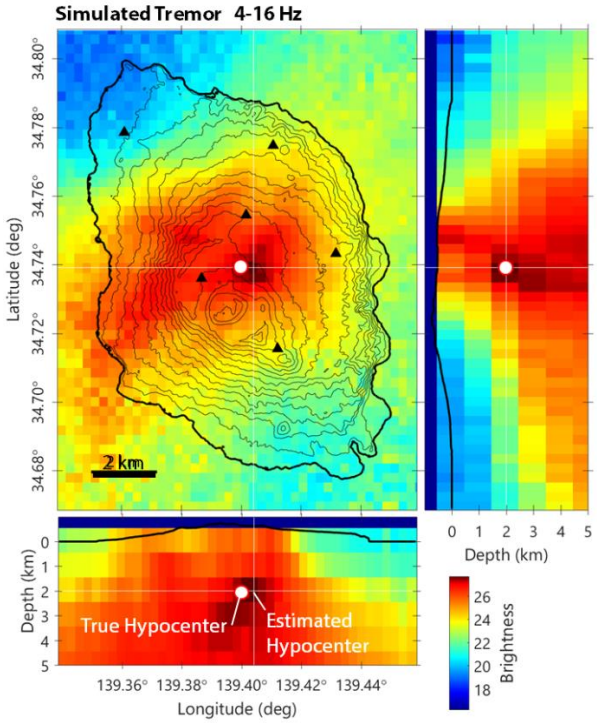

Fig 1. Result of CCF-based SSA from a simulated tremor. The estimated source location is the maximum of this map.

[References]
[1] Fehler, M.C., 1983. *J. Geophys. Res.*, 88(B4), 3476-3484.
[2] Droznin *et al.*, 2015. *Geophys. J. Int.*, 203(2), 1001-1010.
[3] Bensen *et al.*, 2007. *Geophys. J. Int.*, 169(3), 1239–1260.

Poster #28

Reexamination in northern Haramachi Segment of Futaba Fault delineation and its activity

ANGGRAINI PUJI[1], TOSHIFUMI IMAIZUMI[1],
SHINSUKE OKADA[2]

[1] Department of Earth Science, Graduate School of Science, Tohoku University
[2] International Research Institute for Disaster, Tohoku University.

Large crustal deformations have occurred in the Northeast Japan arc due to the earthquake off the Pacific coast of Tohoku (Mw 9.0) on March 11, 2011. Along with this massive earthquake occurred in the Japan Trench, the condition for failure on the Northeast Japan arc and surrounding active faults across Japan has changed (Toda, 2011). In addition, the Headquarter of Earthquake Research Promotion conducted a long-term evaluation of Active Fault (HERP, 2011) after the devastated event and have concluded that there are at least five major active fault zones that now may have high probability of earthquake occurrence, including Futaba Fault Zone which distributed in the forearc region of Northeastern Japan arc along the eastern margin of the Abukuma Mountains that has a left-lateral strike slip fault with the western uplift component with NNW-SSE trend (HERP, 2005).

Limited investigation has been conducted on Futaba Fault Zone. The previous study that delineates the fault line was conducted using big scale of topographic map and the examination of fault activity was estimated mainly only from the trenching and boring investigation in the Tochikubo area, which is at the central part of Haramachi segment (Kaneda, 2013; Fukushima-ken, 1999). Thus, the updated study is considered necessary to examine the active deformation thoroughly.

In this study, we focus on the area around Soma City, from Uda River to Hatsuno region in Fukushima Prefecture which is the location of the northern Haramachi segment of Futaba Fault that is lacking detail investigation from the previous study. We examined the geomorphic features of active faults in the northern part of Haramachi segment by utilizing 2m-mesh DEM and several types of topographic anaglyph image (slope, negative openness, and positive openness) from Yokoyama Geo-spatial Information Laboratory. Subtle geomorphic features such as deformed terrace risers, deflected drainages, and small fault scarps can now be identified. Repeated field survey was conducted to check the correlation of the terrace surfaces from GIS observation. Several new fault strands are also identified in this study, which is supported by the fault outcrop found in the field that confirms the evidence of displacement.

The most prominent fault scarp was observed near Uda River and Shiode Mountain area which displaced the lowest fluvial terrace surface indicating quaternary faulting. In attempt to validate the timing of the quaternary deformation, borehole survey on this terrace thread was conducted to collect the material suitable for ^{14}C dating. The sample is now being analyzed using AMS method in IAAA laboratory, Fukushima Prefecture. The calibrated age that will be produced will ideally be determined as the minimal age of recent faulting of the Haramachi segment, Futaba Fault.

[Reference]

[1] Kaneda, H., Goto, H. and Hirouchi, D.: *Active Fault Map in Urban Area, Futaba Fault Zone and its vicinity, Watari, Souma, Minamisouma (Scale 1:25,000) Reference Manual*. Geospatial Information Authority of Japan. D1-No.643. 18 pp. 2013. (in Japanese)

Poster #29

Cretaceous OIBs and MORBs into the Tokoro accretionary complex, NE-most of Japan

SHUNTA SAKAI[1], NAOTO HIRANO[2], SHIKI MACHIDA[3]

[1] Division of Earth and Planetary Materials Science, Tohoku University.
[2] Center for Northeast Asian Studies, Tohoku University.
[3] Ocean Resources Research Center for Next Generation, Chiba Institute of Technology.

The Tokoro Belt, Late Cretaceous accretionary complex at Eastern Hokkaido of Japan, is mainly composed of greenstones with tectonic blocks of bedded chert and limestone (Nikoro Group) with some forearc sediments. The greenstones (mainly basaltic or metabasaltic rocks) within an accretionary complex possibly provide information about igneous activities on subducted paleo-oceanfloor. In previous studies (Bamba, 1984; Yamasaki and Nanayama, 2017), the Nikoro Group greenstones were simply devided into the MORB-dominated eastern part and OIB-dominated western part on the basis of the chemical compositions of greenstones and their mode of occurrences with simultaneously accreted cherts and limestones. However, they reported a limited number of analytical elements of only a few greenstones; thus we report new geochemical major and trace elements of greenstones of Nikoro Group to reconsider their origins.

As mentioned above, geochemical compositions of the western Nikoro Group designate the typical composition of tholeiitic OIB. The greenstones in eastern Nikoro Group are further divided each into their localities on the basis of geochemical variation of them; moreover, the new data in this study show more detailed divisions. The eastern Nikoro Group particularly resulted from the underplating process both of MORB and OIA (oceanic island alkaline basalt) at the deeper part of subduction zone. This study proposes a new model about the origin of Tokoro Belt on the basis of the geochemistry of greenstones with geological data as follows; 1) tectonic structures of the greenstones and chert, 2) microfossil ages of chert and limestone associated with greenstones, 3) variation of metamorphic grades, 4) the exposing volume of MORB, and 5) mode of occurences of chert and limestone.

[References]
[1] Bamba Takeo., 1984, The Tokoro Belt, a Tectonic Unit of the Central Axial Zone of Hokkaido. Journal of the Faculty of Science, Hokkaido University. Series 4, Geology and mineralogy. 21, 21-75.
[2] Yamasaki, T. and Nakayama, F., 2017, Enriched mid-ocean ridge basalt-type geochemistry of basalts and gabbro from the Nikoro Group Tokoro Belt, Hokkaido, Japan. Journal of Mineralogical and Petrological Sciences. 112, 311-323.

Poster #30

Mechanism of olivine-spinel transformation and microstructural development under differential stress by phase field method

SANDO SAWA[1], JUN MUTO[1], HIROYUKI NAGAHAMA[1]

[1] Department of Earth Science, Graduate School of Science, Tohoku University

Olivine is the most abundant material in the upper mantle and undergoes phase transformation to wadsleyite and ringwoodite at about 410 km and 520 km depths, respectively. The phase transformation affects the mantle rheology (e.g. deep-focus earthquake and slab deformation). There are two nucleations during the olivine-spinel transformation (intra-crystalline nucleation and nucleation at the grain boundary). The mechanism of intra-crystalline nucleation has the following three stages: (1) $(100)_\alpha$ stacking faults form in olivine crystal, (2) thin ringwoodite "platelets" nucleate on these stacking faults coherently, (3) the platelets grow semi-coherently and ringwoodite/wadsleyite nucleate at the platelet interfaces incoherently [1]. The mechanism of nucleation at grain boundary is incommensurate phase transformation and has two cases: (1) the nucleation rate is fast but the growth rate is slow, (2) the nucleation rate is slow but the growth rate is fast [2]. The two types of nucleation often occur simultaneously depending on pressure- and temperature-conditions and it's difficult to reveal each kinetics. Therefore, it is useful to conduct numerical experiments which are capable of treating two mechanisms independently. As the numerical experiments, we adopt Phase Field Model (PFM) to model microstructural development associated with olivine-spinel phase transformation under differential stress condition. In this study, we simulate (A) the growth of phase at the grain boundary when the nucleation rate is slow and the growth rate is fast (GGB model), and (B) the semi-coherent growth of "platelet" by intra-crystalline nucleation (GIN model) because the PFM method can't simulate the nucleation. In the PFM, we configure the order parameter which describes the distribution of two phases. The phase boundary is described as a field where the order parameter continuously changes between two phases. Therefore, PFM is a powerful tool for the simulation of microstructural development with complex morphological features. By conducting numerical experiments of two mechanisms independently, we reveal each kinetics of both mechanisms.

Using the PFM, we conduct numerical experiments of germanate olivine as an analogue material at conditions of confining pressures of 1 ~ 5 GPa, temperatures of 1000 K ~ 1400 K, strain rate of 10^{-4}~ 10^{-7} s^{-1}, with a various grain size ranging from 100 μm to 1 mm under various ranges of differential stresses. The reason for using germanate olivine is that there were many previous studies using it, and we can compare our results with those results.

As a result, the volume fraction of spinel phase in the GGB model is larger than that in the GIN model. Furthermore, semi-coherent growth rate of platelet is fast near the phase boundary because shear stress is high there (GIN model). On the other hand, the growth rate of spinel phase nucleated at the grain boundary is fast far from the phase boundary because the overpressure is high and Gibbs free energy is relatively high comparing to elastic strain energy (GGB model). When the initial olivine grain size is larger, the phase transformation is difficult to occur in this study. In the GGB model, small grains of spinel phase are difficult to grow because the interface energy of small grains is smaller than that of large olivine grains. Meanwhile, in the GIN model, it is uncertain that why spinel grains do not grow when olivine grain size is larger. When the strain rate is slower, the effect of time when olivine is exposed to high temperature and pressure at the stable field of spinel phase is stronger than that of differential stress. Therefore, in the olivine-spinel phase transformation, semi-coherent growth of spinel platelet is not so important and the growth of spinel incoherently is more important.

[References]
[1] Kerschhofer et al. (2000) PEPI, 121, 59–76.
[2] Brearley et al. (1992) PCM, 18, 343–358.

Earth, Sea and Sky III:
International Joint Graduate Program Workshop in Earth and Environmental Sciences
co-hosted by The International Joint Graduate Program in Earth and Environmental Sciences (GP-EES, Tohoku University) and JSPS-DFG Japanese-German Graduate Externship for Research on Deep Earth Volatile Cycle
May 27-29, 2018. Tohoku University, Aobayama Campus

Poster #31

Evaluation of mining effects to river water in abandoned mining area by statistical analysis

KENGO SAWAYAMA[1], NORIYOSHI TSUCHIYA[1]

[1] Graduate School of Environmental studies, Tohoku University

1. Introduction

Pollution of river environment by heavy metals has been a big problem in the world. River environment pollution by heavy metals cause soil pollution, groundwater pollution and effect to aquatic lives not only in the mining area but also in the downstream of mine[1)]. Traditional approaches to the assessment and management of mine water pollution has been to quantify and remediate any environmental impacts occurring as a result of distinct point source discharge from abandoned mine. This study evaluates mining effects quantitatively to heavy metals in river environment.

2. Methodology

Ohitachi Mine (Fig. 2), research area in this study, is 10km west from Odate city in Akita prefecture, and Cu, Pb and Zn mine on working. This area is one of the Hayaguchibashi, monitoring point of environmental standard, and one of blanch of Yoneshiro River. This mine was closed at 1960s, and abandoned mine pollution prevention work was done at 1976 and 1978. Now, mine drainage from main adit is treated. Hayaguchigawa formation, Kuroishizawa formation and Fujikuragawa formation (Neogene Tertiary) are located in this area. In this study, we developed the environmental assessment method using this region as a model field. Samples, pH and temperature of river water data were collected at June 2014, October 2014 May 2015, May 2016 and May 2017. Water samples were filtered to remove suspension (> 0.45μm) before added HNO_3, 1 wt% of total volume. Dissolved heavy metals (Cu, Pb, Zn, Cd and As) were measured by ICP-MS. Mass balance analysis was held for estimation of the emission. Load is obtained by multiplying the Zn concentration and the flow late.

3. Result and Discussion

By mass balance analysis (Fig. 2), this area has two main emission of Zn except the treatment facility (M8 – M9). One is leaching around the mainstream (M5 – M8). Iron precipitation was observed bottom of river in this area. The other is blanch just before the treatment facility (- D12) . Untreated adit observed in this area. These are estimated to be the main source of Zn in this area.

4. Conclusion

Environmental impact assessment was conducted at the Ohitachi Mine (Cu-Zn-Pb) located in Odate, Akita Prefecture, Japan, as a model field. By mass balance modeling, emission areas were detected. So, it is important to calculate the artificial effect for environmental assessment.

[References]
[1] X. Zhang, L. Yang, Y. Li, H. Li, W. Wang and B. Ye : Environmental Monitoring and Assessment, 184 (2012), 2261-2273.
[2] E. Gozzard, W. M. Mayes, H. A. B. Potter and A. P. Jarvis : Environmental Pollution, 159 (2011), 3113-3122.

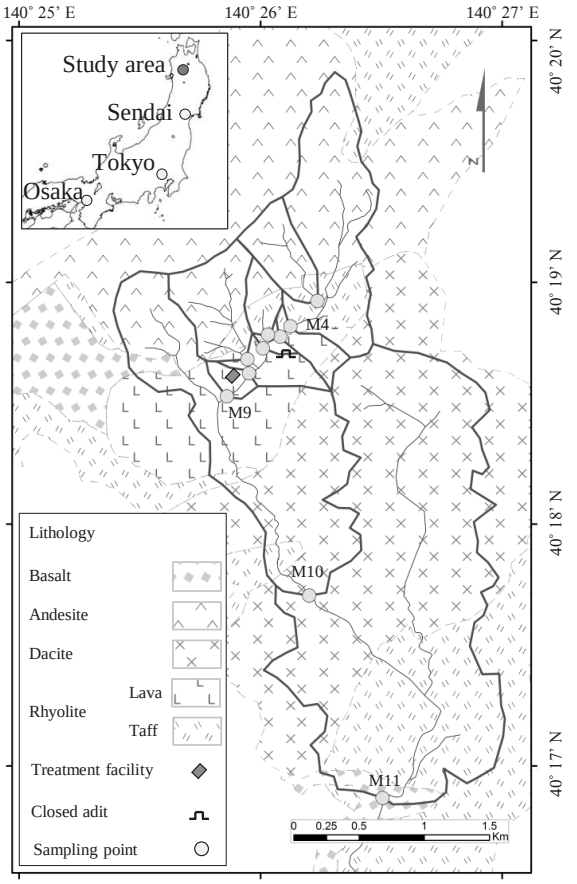

Fig. 1 Mine facilities on lithological map (Simplified after Hirayama and Sumi, 1969)

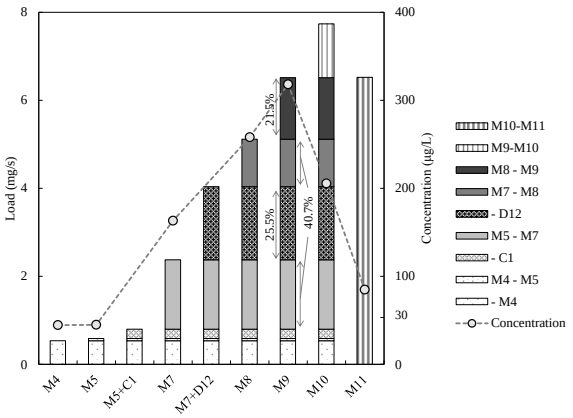

Fig. 2 Zn Concentration in river water

Poster #32

Interaction of peridotite with Ca-rich carbonatite melt at high pressure: Implication for merwinite formation in the upper mantle

IGOR SHARYGIN[1,2], ANTON SHATSKIY[1,3], KONSTANTIN LITASOV[1,3], ALEXANDER GOLOVIN[1,3], EIJI OHTANI[4], NIKOLAY POKHILENKO[1,3]

[1] Sobolev Institute of Geology and Mineralogy, Siberian Branch of Russian Academy of Sciences
[2] Center for Northeast Asian Studies, Tohoku University
[3] Department of Geology and Geophysics, Novosibirsk State University
[4] Department of Earth Science, Graduate School of Science, Tohoku University

Mineral inclusions in diamond can grow at the same time as the diamond (syngenetic), or as precursors to the diamond (protogenetic). They provide information about mineralogy and the P-T conditions of the surrounding mantle at the time of diamond growth. Diamonds from several localities reveal the existence of a deep, Ca-rich diamond host lithology other than peridotite and eclogite (Zedgenizov et al. 2014).

Recently, merwinite, $Ca_3MgSi_2O_8$, was discovered as inclusion in diamond from Juina province, Brazil (Zedgenizov et al., 2014). In addition, this diamond contains inclusions of calcite, olivine and walstromite-structured $CaSiO_3$. According to available experimental data, under mantle conditions, merwinite can only be formed in a specific Ca-rich and Mg- and Si-depleted environment that differs from dominant mantle rocks, peridotite and eclogite. Zedgenizov et al. (2014) suggested that such chemical conditions can occur when Ca-rich carbonatite melt, derived from subducted oceanic crust, infiltrates overlying peridotite. Interaction of Ca-rich carbonatite melt with reduced ambient peridotitic mantle could cause formation of Ca-silicates and diamond. To test this hypothesis, we modeled the interaction between olivine and orthopyroxene, main constituent minerals of peridotite in the upper mantle, and alkali-rich Ca-carbonate melt at high pressures (Sharygin et al., 2018).

In the first set of experiments, we studied the reaction between powdered Mg-silicates, olivine and orthopyroxene, and a model Ca-carbonate melt (molar Na:K:Ca = 1:1:2), in a homogeneous mixture, at 3.1 and 6.5 GPa. In these equilibration experiments, we observed the formation of a merwinite + olivine-bearing assemblage at 3.1 GPa and 1200 °C and at 6.5 GPa and 1300–1400 °C. The melts coexisting with this assemblage have a low Si and high Ca content (Ca# = molar 100 × Ca/(Ca + Mg) > 0.57). In the second set of experiments, we investigated reaction rims produced by interaction of the same Ca-carbonate melt (molar Na:K:Ca = 1:1:2) with Mg-silicate, olivine and orthopyroxene, single crystals at 3.1 GPa and 1300 °C and at 6.5 GPa and 1400 °C. The interaction of the Ca-carbonate melt with olivine leads to merwinite formation through the expected reaction: $2Mg_2SiO_4$ (olivine) + $6CaCO_3$ (liquid) = $Ca_3MgSi_2O_8$ (merwinite) + $3CaMg(CO_3)_2$ (liquid).

Thus, our experiments confirm the idea that merwinite in the upper mantle may originate via interaction of peridotite with Ca-rich carbonatite melt. It is remarkable that the interaction of the Ca-carbonate melt with orthopyroxene crystals does not produce merwinite both at 3.1 and 6.5 GPa. This indicates that olivine grain boundaries are preferable for merwinite formation in the upper mantle.

It is believed that carbonatite melts are highly efficient metasomatic agents in the mantle, and chief transport agents of carbon from the mantle to the crust and, ultimately, to the atmosphere because of their unique chemical and physical properties (Dasgupta and Hirschmann, 2010). This study demonstrates that the merwinite in diamond is further evidence of presence of carbonatite melts in the mantle.

[References]
[1] Zedgenizov, DA et al. (2014) *Am Mineral* 99, 547–550.
Sharygin, IS et al. (2018) *Contrib Mineral Petrol* 173, 22.
Dasgupta, R, Hirschmann, MM (2010) *Earth Planet Sci Lett* 298, 1–13.

Poster #33

S-wave velocity and attenuation structure as estimated from deconvolution analysis at CHBH10, in Chiba prefecture, KiK-net station

TSUYOSHI SHIBATA[1], HISASHI NAKAHARA[1]

[1] Department of Geophysics, Graduate School of Science, Tohoku University.

Shallow shear-wave velocity and attenuation structure strongly affects amplification characteristics of earthquake ground motion. Fukushima et al. (2016) estimated S-wave quality factor (Qs) beneath KiK-net borehole seismic stations from the spectral ratios between incident and surface reflected waves that appear on the deconvolution records between borehole and surface receivers. However, they didn't use other phases on the deconvolution traces that are reflected from layer boundaries between the surface and the borehole receivers, though these phases have important information about S-wave velocity and attenuation structure. Therefore, we try to estimate layered S-wave velocity and attenuation structure by modeling all parts of these deconvolution records.

We chose CHBH10 station in Chiba prefecture for our analysis because the depth of the borehole is 2000m so that the theoretical two-way shear-wave travel time between the surface and borehole receivers is longer than 0.5 seconds. We selected epicentral distances of smaller than 150km, peak ground accelerations at the surface of smaller than 100gal and the cosine of the incident angles at the borehole of larger than 0.995. Incident angles were calculated using the JMA2001 velocity structure (Ueno et al. 2002). First, we deconvolved borehole records by surface records for the 20s-long time window starting from the S-wave onset. Deconvolution was performed in the frequency domain, and the spectra were smoothed for stabilization by Parzen window with a width of 0.24Hz. Then we calculated S-wave quality factor Qs from the incident and reflected waves on these deconvolution records following the method of Fukushima et al. (2016). Finally, we estimated layered shear wave velocity structure with the estimated Qs so as to explain the stacked deconvolution record. Referring to the velocity logging data, we set 7 layers. We used Markov chain Monte Carlo method for optimization. After 100,000 iterations, we judged that the convergence was attained. The solutions showed S-wave velocity ranges from about 150m/s to 1000m/s at depths shallower than 1500m. The best-fit model explains the observed deconvolution record well and its misfit get smaller by 89.9% than that for the model using the velocity logging data.

[References]
[1] Fukushima, R., Estimatin S-Wave Attenuation in Sediments by Deconvolution Analysis of KiK-net Borehole Seismograms, Bull. Seism. Soc. Am. Vol.106, pp552-559, 2016.
[2] Silva, W., Body Waves In A Layered Anelastic Solid, Bull. Seism. Soc. Am. Vol.66, pp1539-1554, 1976.

Poster #34

Pumpellyite-bearing retrograde mineral assemblage of the Yunotani eclogite and the areal extension of eclogite-facies metamorphism in the Omi area, Japan

YUZUKI SHINJI[1], TATSUKI TSUJIMORI[1 2]

[1] Department of Earth Science, Graduate School of Science, Tohoku University
[2] Center for Northeast Asian Studies, Tohoku University

Paleozoic glaucophane-bearing eclogites occur as mafic layers within a unit of paragonite- and garnet-bearing pelitic schist of the Omi Schists in the Yunotani valley, Omi area, Hida Mountains (Fig.1). Previous studies suggested a so-called 'hairpin'-type metamorphic evolution in which the epidote-blueschist-to-eclogite prograde mineral assemblage was recrystallized in the epidote-blueschist-facies. Our new observations, however, found retrograde pumpellyite coexisting with secondary glaucophane. The calculated phase diagram suggests that the pumpellyite + glaucophane assemblages is stable at a low temperature and pressure portion of the lawsonite-glaucophane stability. This is the second example of the occurrence of pumpellyite + glaucophane mineral assemblage in the Hida Mountains; the assemblage has been known only in the Kuzuryu area. The inferred retrograde pressure-temperature (P–T) path after the eclogite-facies metamorphism is similar to that of Paleozoic garnet-glaucophane schist with relict eclogite-facies mineral inclusions of the Osayama serpentinite mélange, Chugoku Mountains. These retrograde paths after eclogite-facies metamorphism in both Omi and Osayama requires a significant cooling and hydration during the exhumation history.

We have also examined the areal extension of eclogite-facies metamorphism in the Omi area using mineral assemblages of the pelitic schists. Previous studies of the Yunotani Valley revealed that the eclogite-hosted pelitic schist was characterized by the mineral assemblage garnet + paragonite + phengite ± ferroglaucophane + rutile + quartz. Our new exploration in the Kanayamadani Valley, located about 3 km south-east of the Yunotani Valley, confirmed abundant paragonite- and garnet-bearing pelitic schist. The calculated stability of the mineral assemblage in a P–T pseudosection overlaps with a P–T condition of the Yunotani eclogites. This supports the previous prediction of the areal extension of 'Eclogitic Unit' ; our study revealed that the Eclogitic Unit extends at least 3 km from the Yunotani to the Kanayamadani Valley.

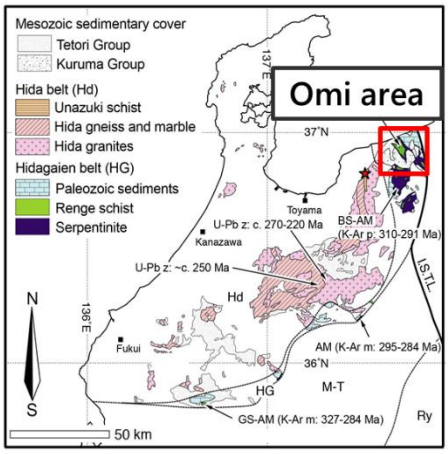

Fig. 1 Distribution map of Paleozoic and Mesozoic rocks in the Hida Mountains, Japan (Omi area) (modified after Tsujimori, 2002)

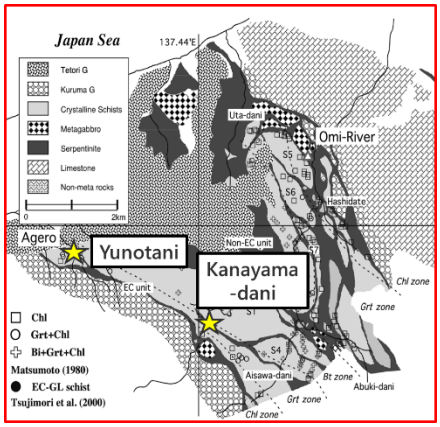

Fig. 2 Geologic map of the Omi area (modified after Matsumoto et al., 2011)

[References]
[1] Tsujimori, T. (2002) IGR, v. 44, p. 797-818.
[2] Matsumoto, K., Sugimura, K., Tokita, I., Kunugiza, K. Maruyama, S. (2011) J. Geography (Chigaku Zasshi), v. 120, p. 4-29.

Poster #35

Forecasting coastal front by numerical simulation

KENTO SUZUKI[1], TAKESHI YAMAZAKI[1]

[1] Department of Atmospheric science, Graduate School of Science, Tohoku University

1. Introduction

As defined by AMS*, Coastal front is a shallow (typically < 1km deep) mesoscale frontal zone marked by a distinct windshift and enhanced thermal contrast (~5-10°C /km). It develops in coastal areas when the land is colder than the ocean. During the winter, the coastal front may mark the boundary between snow and rain. Furthermore, mountains (e.g. the Japan alps, Ou mountains) play role in Cold-Air Damming (CAD) formation on the land side and coastal front development. Numerical simulation cannot realistically forecast coastal front accompanied by CAD because it is a local phenomenon. The purpose of this experiment is to reproduce coastal front more realistically by using very high-resolved model.

2. Overview of Case study

We conducted a case study on 18th January, 2016. On that day, cyclone passed the south coast of Japan and it brought about heavy snowfall to Sendai region. Strong coastal front was formed between easterly warmer wind from Pacific Ocean and colder wind from the mountainous region.

3. Model configuration

We used JMA-NHM (Japan Meteorological Agency-Non hydrostatic Model) in this experiment. We conducted 1km horizontal grid scale simulation in Tohoku region. I used two types of Planetary Boundary Layer (PBL) schemes: MYNN3 scheme, which is currently used for JMA weather forecast, and Deardorff scheme, which is suitable for very high-resolved model (<1km).

4. Result

Observation shows that northerly wind changed into strong easterly wind around 10a.m. and it caused rapid temperature rise. (figure 1) This rapid change means the passage of local front. Deardorff scheme simulated wind and temperature change more realistically. In figure 2, Deardorff scheme shows distinct windshift in the east side of Sendai Weather Observation.

5. Conclusion

The coastal front determined the surface temperature and Deardorff scheme represented more accurate temperature change and snowfall accumulation on 18th 2016. We need more case analysis to examine which PBL scheme is suitable for reproducing coastal front. Furthermore, we plan to use more high-resolved model for verifying the local front.

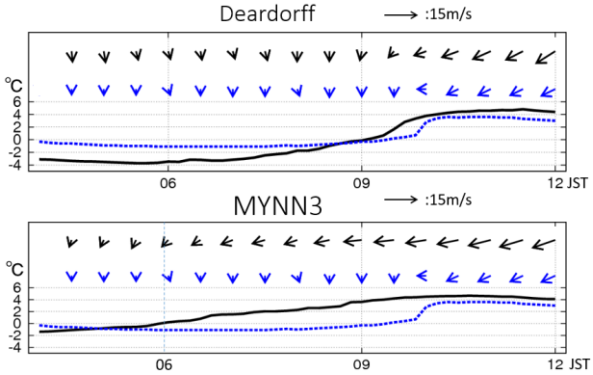

Figure 1. Temperature and wind shift on 18th, January 2016 Blue line and arrows are observed temperature and wind. Black line and arrows are model output at Sendai Weather Observatory.

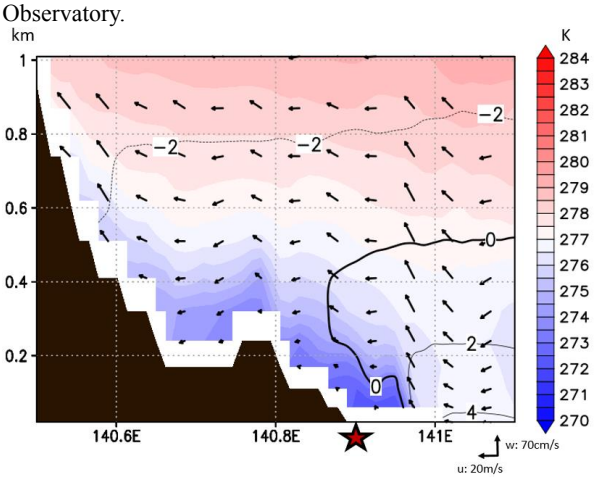

Figure 2. Vertical sectional view through Sendai region at 9:00, 18th January, 2016 by using Deardorff scheme. Shade shows potential temperature and contour shows the air temperature. The arrows indicate zonal and vertical components of winds. Red star is the location of Sendai Weather Observatory.

[References]
[1] *American Meteorological Society: Glossary of Meteorology, http://glossary.ametsoc.org/wiki/Coastalfront

Poster #36

Distribution of localized fluid inferred from S wave reflectors beneath the earthquake swarm in Yonezawa-aizu area, NE Japan

MANAMI SUZUKI[1], AKIKO HASEMI[2], TOMOMI OKADA[1], TORU MATSUZAWA[1], NORIHIKO UMINO[1], NORIKO TSUMURA[3], TADASHI YAMASHINA[4], GROUP FOR THE AFTERSHOCK OBSERVATIONS OF THE 2011 OFF THE PACIFIC OF TOHOKU EARTHQUAKE

[1] Department of Geophysics, Graduate School of Science, Tohoku University.
[2] Department of Earth and Environmental Sciences, Graduate School of Science, Yamagata University.
[3] Department of Earth Science, Graduate School of Science, and Engineering / Facultly of Science, Chiba University.
[4] Kochi Earthquake Observatory, Faculty of Science, Kochi University.

In order to understand the mechanism of inland earthquake occurrence, it is necessary to consider the influence of crustal fluid [Hasegawa et al., 2012]. Triggered shallow microearthquake swarm started at 7 days after the 2011 off the Pacific coast of Tohoku Earthquake in prefectural border between Yamagata and Fukushima prefectures, where the seismic activity was low before the Tohoku-Oki earthquake. Some previous studies, suggest that the cause of the triggered seismicity occurred due to increase of fluid pressure [e.g, Okada et al., 2015].

The objective of this study is to estimate the areas of fluid by investigating distribution of S wave reflectors, which are considered to indicate the localized (sill-like) distribution of fluid. As a previous study, Hasemi et al., [2016JpGU] found reflected S waves in seismograms recorded at the Hi-net stations of NIED. In this study, we use temporary seismic network deployed by Kochi University, Chiba University, and Tohoku University, to investigate more detailed distribution of reflectors in addition to the Hi-net stations. We used waveforms observed at these stations from 4798 events in the period from May 2011 to February 2012. We used hypocenter locations obtained by the double-difference method [Waldhauser and Ellsworth, 2000]. We applied the automatic amplitude control (AAC) correction and the normal moveout (NMO) correction [Inamori et al., 1992] to these waveform data, and we made some reflection profiles of seismograms along various lines for each station. These profiles were set passing above each cluster. As a result, we confirmed continuous S wave reflectors beneath the earthquake swarm for each profile; in the northeastern part of this area, reflector is located at a depth of 13-14 km, and in the southwest part it is located 20-21 km, in central part is located 13-15km.

[References]
[1] Hasegawa A, Nakajima J, Uchida N, Yanada T, Okada T, Zhao D, Matsuzawa T, Umino N. (2012): Mechanism Generating Earthquakes in Subduction Zones: Vital Role of Geofluids in Earthquake Generation. *Journal of Geography*, **121** (1), 128–160.
[2] 長谷見晶子・高橋承之・岡田知己 (2016): 山形県米沢-福島県会津の誘発地震域における反射波の検出. 日本地球惑星科学連合大会 2016 年大会予稿集, SSS26-02.
[3] Inamori T, Horiuchi S, Hasegawa A. (1992) Location of mid-crustal reflectors by a reflection method using aftershock waveform data in the focal area of the 1984 Western Nagano prefecture earthquake. J Phys Earth **40**, 379–393.
[4] Okada T, et al. Hypocenter migration and crustal seismic velocity distribution observed for the inland earthquake swarms induced by the 2011 Tohoku-Oki earthquake in NE Japan: implications for crustal fluid distribution and crustal permeability. (2015) :Geofluids, **15**, 293–309.
[5] Waldhauser. F., and W. L. Ellsworth. (2000) :A double-difference earthquake location algorithm: Method and application to the northern Hayward fault, California, Bull. Seismol. Soc. Am., **90**(6), 1353–1368.

Poster #37

Dark inclusion in the NWA2900 carbonaceous chondrite: CI-like material with large hydrothermal diopside veins

MIKI TAKAHASHI[1], TOMOKI NAKAMURA[1], TAKAZO SHIBUYA[2], MIKE ZOLENSKY[3]

[1] Division of Earth and Planetary Materials Science, Graduate School of Science, Tohoku University.
[2] Japan Agency for Marine□Earth Science and Technology (JAMSTEC).
[3] Astromaterials Research and Exploration Science, NASA Johnson Space Center.

■Purpose

Since dark inclusions differ from the host rocks of the meteorites mineralogically and compositionally, it is possible that they have a unique origin different from the host rocks and also from any kinds of meteorites coming to the earth. Because dark inclusions accreted onto the host-rock parent asteroids that are much smaller than the Earth and therefore they escaped high-speed impact upon accretion and thus survived even if they are fragile material. In this study, we have studied mineralogy of the dark inclusion (1.0 × 2.5 cm size) in the NWA 2900 which is classified as a CV3 carbonaceous chondrite[1], and found that the inclusion formed via hydrothermal alteration at temperature higher than that experienced by any other carbonaceous chondrites.

■Sample & Methods

The sample is the NWA2900 carbonaceous chondrite. Synchrotron radiation X-ray diffraction analysis was performed on undulator beam line 3A at the Photon Factory in High Energy Accelerator Research Organization. The sample was observed by a scanning electron microscope (JEOL JSM-7001F) to characterize textures and lithologies and analyzed for the chemical compositions of minerals with a FE-EPMA (JEOL JXA-8530F) of Institute for Materials Research, Tohoku University.

■Results & Discussion

As a result of petrological and mineralogical observations and analyses of the host rock, it was found that this meteorite is classified as a CK3 chondrite based on the following facts. Magnetite has high TiO_2 concentration (~1.0wt%), matrix olivine is equilibrated at high Fa# of ~ 34 and has high concentrations of NiO (~0.4wt%), and low-Ca pyroxene is vary rare in the host rock[2].

Large veins of diopside were found in the fine-grained dark inclusion. Each vein (~1cm long and ~100μm width) goes through an entire region of the dark inclusion and connects with other veins, forming a network structure. The veins consist mainly of crystalline diopside with high Wo contents (Wo>46), a small variation of Mg/(Mg+Fe) ratio (46.4>En>31.1). and low concentrations of minor elements such as Al_2O_3, Na_2O, MnO, Cr_2O_3, and TiO_2. These compositional features of diopside are consistent with hydrothermal origin of the veins. The high Mg/(Mg+Fe) ratios of diopside indicate formation at high temperature, which implies that the veins were precipitated from hydrothermal fluids of supercritical water[3].

On the other hand, the dark inclusion is embedded in an unbrecciated structure of the CK chondrite, which suggests that the inclusion has accreted to the CK chondrite parent asteroid together with chondrules and CAIs in the early solar nebula. Since the diopside veins occur only in the dark inclusion and terminate at the boundary to the host CK chondrite, the high-temperature aqueous alteration occurred early in the parent body or previous location of the dark inclusion prior to the formation of the CK parent asteroid. The dark inclusion is free of chondrules and consists mainly of fine-grained olivine, plagioclase, and framboid magnetite. The mineralogy and the presence of the diopside veins are consistent with high-temperature aqueous alteration. The dark inclusion found in this study indicates that high-temperature aqueous alteration took place in the earlier-formed, water-bearing small body that likely to have formed before chondrule formation.

[References]
[1] Chaumard et al., *Meteorit. & Planet. Sci.* 49, 419–452, 2014.
[2] Dunn & Gross, *Meteorit. & Planet. Sci.* 52, 2412-2423, 2017.
[3] Manning & Bird, *Contrib Mineral Petrol* 92, 432-447, 1986.

Earth, Sea and Sky III:
International Joint Graduate Program Workshop in Earth and Environmental Sciences
co-hosted by The International Joint Graduate Program in Earth and Environmental Sciences (GP-EES, Tohoku University) and JSPS-DFG Japanese-German Graduate Externship for Research on Deep Earth Volatile Cycle
May 27-29, 2018. Tohoku University, Aobayama Campus

Poster #38

Seasonality and co-variability of sea surface temperature front and low cloud cover in the mid-latitude North Pacific

NAOYA TAKAHASHI[1], TADAHIRO HAYASAKA[1], BO QIU[2], NIKLAS SCHNEIDER[2,3], KELVIN RICHARDS[3]

[1] Center for Atmospheric and Oceanic Studies, Graduate School of Science, Tohoku University
[2] Department of Oceanography, University of Hawai'i
[3] International Pacific Research Center, University of Hawai'i

1. Introduction

Oceanic low-level cloud plays an important role for determining shortwave radiation at sea surface. Properties of low clouds in the North Pacific (NP) change with not only meteorological condition but also sea surface temperature (SST). Previous studies showed that Low Cloud Cover (LCC) increase with a decrease in SST. They also said that there is positive feedback among low cloud, radiative flux, and SST(1).

In the mid-latitude NP, there are large-scale SST front where meridional SST gradient is very strong, which is important for formation of storm-track(2). Around SST front, meridional gradient of LCC is also strong, hereafter we will call it LCC boundary (Fig.1). It may have large impact on formation of SST front by generating meridional contrast of shortwave heating. However, relationship between SST front and LCC boundary is not well-known.

Objective of this study is to reveal seasonal variability and co-variability of SST front and LCC boundary, in particular, their positions. We also investigate lead-lag relationship of them and how one changes another property.

2. Dataset and Definition

We used monthly dataset of MODIS and OISST for determining LCC and SST, respectively. Both of them are based on satellite observations. Target area is central North Pacific (160°E-200°E and 35°-45°) where we can find easily front and boundary position. Available period of all datasets is from 2003 to 2016 (14 years).

To determine position of SST front, we defined it as latitude where meridional gradient of SST has minimum value for each month for each longitude bin (1° width). Position of LCC boundary is also determined by meridional LCC gradient, but we used its maximum value.

3. Result

First of all, we investigated seasonality and regional difference in SST front and LCC boundary properties. In western NP (160°E-180°E), strength of SST front weakens in summer. On the other hand, the strength in eastern NP (180°E-200°E) strengthens in summer. Variability of position of SST front in eastern Pacific is larger than that in western NP. These results imply relationship between ocean and low cloud is different between western and eastern NP.

Next, we investigated co-variability of position of SST front and LCC boundary for each season and region. The correlation is positive for all season in both regions. In particular, the correlation coefficient in summertime eastern NP is the highest (r=0.66) of all season. From lead-lag correlation between the positions, the results show that seasonal variation of position of SST front tends to be lagged from that of LCC boundary in summertime eastern NP, which implies low cloud controls SST in summertime eastern NP.

4. Discussion

Our results showed that low cloud variability may control SST variability, in particular, summertime eastern NP. To investigate feedback between low cloud and SST, we will discuss how much cloud radiative impact on oceanic temperature profile.

[References]
[1] Norris et al 1998, *J. Clim*, **11**, 2482-2490
[2] Nakamura and Kazmin 2003, *JGR*, **108**, 3078

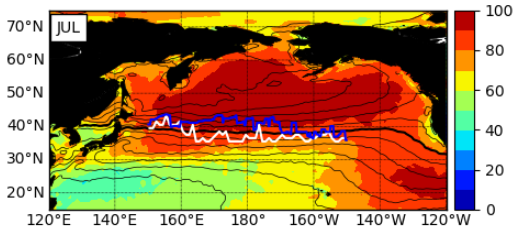

Fig.1: Climatological-mean of LCC (color: %) and SST (contour: °C, Thick black line: SST=16°C, interval of contour is 2°C) in July. Blue (White) line shows that position of SST front (LCC boundary : detailed in chapter 2).

Poster #39

Defining subsegments and testing their roles by comparing with actual rupture extent: an example from the Kamishiro fault, Japan

NAOYA TAKAHASHI[1]

[1] Department of Earth Science, Graduate School of Science, Tohoku University

Introduction

Earthquake magnitude largely depends on rupture length, and that makes fault segmentation crucial to seismic hazard assessment. Increasing number of earthquake records infers that a fault segment doesn't always behave persistently, thus rupture partially or with adjacent segments (e.g., Lefevre et al., 2018). DuRoss et al. (2016) have compiled paleoseismic data for the central Wasatch fault zone to compare with fault segments estimated from geological and geophysical properties and have found that subsegments may control the lengths of the partial and spillover ruptures. Although some subsegments are not long enough to generate a surface-rupturing earthquake by themselves, analyzing subsegments and their boundaries can provide insight into fault segmentation. Here we define subsegments of the Kamishiro fault, the northernmost segment of the Itoigawa-Shizuoka Tectonic Line active fault system (ISTL) in Japan, based on slip rate, topographic relief (crest profile in the hanging wall) and surface geometry of the fault trace. Then we discuss roles of subsegments by comparing with co-seismic slip distribution during the 2014 Nagano earthquake (Mw6.2, Japan Meteorological Agency, 2014). For the ease of this comparison, the study area is set to where the 2014 Nagano earthquake has ruptured.

Results

In defining subsegment, one has to detect discontinuities in the distribution of a geological or geophysical factor along fault strike. In this study, we extracted areas where a significant gap in slip rate distribution along fault strike, troughs in the crest profile, and an abrupt bend or a branching of the surface fault trace are observed as discontinuities. Based on discontinuities inferred from three factors, we defined four subsegments; referred to as ss1-4 from the north.

Discussions

To test whether defined subsegments play any roles during an earthquake, we compare defined subsegments with the co-seismic slip distribution of the 2014 Nagano earthquake (Ishimura et al., submitted). While at two of three subsegment boundaries no changes in the co-seismic slip distribution are observed, at one of three subsegment boundaries surface rupture terminated abruptly. This implies some subsegments boundaries can behave as a barrier to rupture propagation.

Considering analyses on historical rupture endpoints (e.g., Knuepfer, 1989), one of the key factors to reveal how a segment boundary behaves is the discontinuity of subsurface structure. Thus, to explain different behavior of defined subsegments we estimated a subsurface geometry of each subsegment based on results of field survey and the relocated aftershock distribution (Panayotopoulous et al., 2016). Consequently, changes in slip sense and dipping angle of a fault strand which was responsible for the 2014 earthquake are observed at the subsegment boundary where surface rupture terminated abruptly, while notable changes are not observed at the two other subsegment boundaries. This fact emphasizes the importance of considering continuities of subsurface structure in assessing fault segmentation.

[References]
[1] DuRoss, C. B., et al. (2016), Fault segmentation: New concepts from the Wasatch Fault Zone, Utah, USA, *J. Geophys. Res. Solid Earth*, *121*(2), 1131–1157.
[2] Ishimura, D., et al. Three-dimensional surface displacement and surface ruptures associated with the 2014 Mw6.2 Nagano earthquake by differential LiDAR data, Manuscript submitted for publication.
[3] Japan Meteorological Agency (2014), Information about Nagano-ken Hokubu earthquake occurred on 22 November 2014, at 22:08,[http://www.data.jma.go.jp/svd/eqev/data/mech/cmt/fig/cmt20141122220817.html].
[4] Knuepfer, P. L. K. (1989), Implications of the characteristics of end-points of historical surface fault ruptures for the nature of fault segmentation, in edited by D. P. Schwartz and R. H. Sibson, Fault Segmentation and Controls of Rupture Initiation and Termination, *U.S. Geol. Sur. Open-File Report* 89-315, 193-228.
[5]Lefevre, M., et al. (2018), Slip deficit and temporal clustering along the Dead Sea fault from paleoseismological investigations, *Scientific Reports*, *8*(1), 4511.
[6] Panayotopoulos, Y., et al. (2016), Seismological evidence of an active footwall shortcut thrust in the Northern Itoigawa–Shizuoka Tectonic Line derived by the aftershock sequence of the 2014 M 6.7 Northern Nagano earthquake, *Tectonophysics*, *679*, 15–28.

Poster #40

Evolutions of water mass anomalies in the upper North Pacific based on Argo

TONG WANG[1], TOSHIO SUGA[1]

[1] Department of Geophysics, Graduate School of Science, Tohoku University.

Water mass property in the upper layer (shallower than ~1km) of the North Pacific are described based on Argo data during 2004-2015, to interpret the evolutions of water mass anomalies in spatial and temporal domain.

Long-term changes of salinity and temperature at 137°E section have been detected through repeat hydrographic observation, with a salinity increase at the surface layer but a rapid freshening trend at the subsurface layers which are deeper than $\sigma\theta$ = 25 kg m-3 (Oka et al. 2017). However, it is still not clear how those changes evolved in space and time.

The Argo program provides a global dataset with spatially and temporally unbiased sampling since 2000s, and makes it possible to describe large-scale three dimensional water mass anomalies with seasonal variations for the first time (Riser et al. 2016). The Argo data used here has been interpolated to neutral density surfaces, because the isopycnally averaged gridded data preserves water mass structures better than traditional data gridded on pressure/depth surfaces (Kouketsu et al. 2016).

In this research, the distributions of temperature, salinity, pressure and thickness on each neutral density surface are given, as well as their zonal and meridional sections. Temperature and salinity at the shallower layer are increasing in general, while the layers under γ about 25 kg m^{-3} are freshening, which are consistent with the results from Oka et al. 2017. This subsurface layer in subtropical gyre is related with subtropical mode water, whose thickness anomaly also shows a positive trend. These long-term variations are possibly related to the strengthening of circulation caused by global warming.

Besides the long-term trend in basin-scale, the seasonal and interannual variations in different regions will also be discussed, to interpret the evolutions of the anomalies. For example, there is a pair of dipole signals in salinity anomaly over eastern subtropical Pacific, but the mechanisms remain unclear. In addition, Temperature-Salinity plane and its volumetric structure will also be analyzed, to find the connections between the property anomalies and the mode water mechanisms.

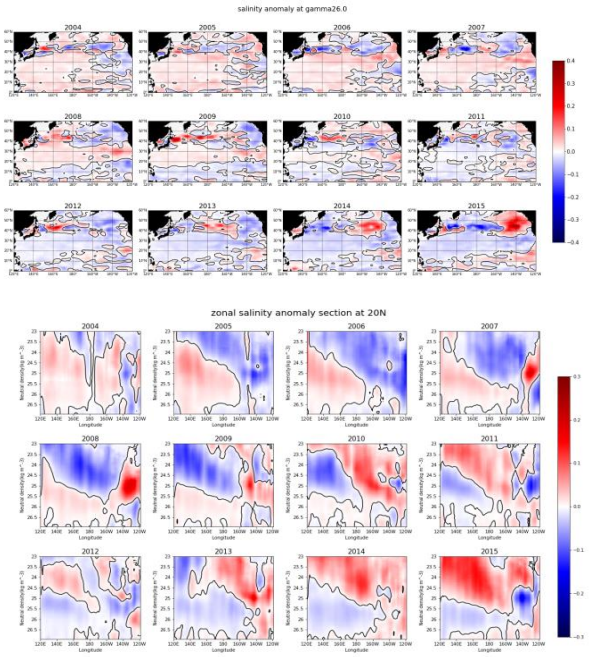

[References]
[1] Kouketsu S, Osafune S, Kumamoto Y, et al. Eastward salinity anomaly propagation in the intermediate layer of the North Pacific[J]. Journal of Geophysical Research, 2017, 122.
[2] Oka E, Katsura S, Inoue H, et al. Long-term change and variation of salinity in the western North Pacific subtropical gyre revealed by 50-year long observations along 137°E[J]. Journal of Oceanography, 2017:1-12.
[3] Riser S C, Freeland H J, Roemmich D, et al. Fifteen years of ocean observations with the global Argo array[J]. Nature Climate Change, 2016, 6(2):145-153.

Poster #41

Diagnostic of the development of seasonal stratification using potential energy anomaly in the North Pacific

RYOHEI YAMAGUCH[1], TOSHIO SUGA[1,2],
KELVIN RICHARDS[3], BO QIU[4]

[1] Department of Geophysics, Graduate School of Science, Tohoku University
[2] Research and Development Center for Global Climate, Japan Agency for Marine-Earth Science.
[3] International Pacific Research Center, University of Hawaii.
[4] Department of Oceanography, University of Hawaii.

The upper ocean in the warming season consists of a relatively thin mixed layer (ML) and seasonal stratification below the ML. Seasonal change in stratification is a ubiquitous feature in the whole of the North Pacific. In the warming season, the stratification develops as a result of heating, freshwater supply and wind forcing from the atmosphere, and the oceanic processes (e.g. horizontal/vertical advection). While the vertical structure of the seasonal stratification differs regionally, the property that develops during the warming season is general.

Heat, freshwater, momentum and chemical tracers exchanged between the atmosphere and ocean are transported into ocean's interior through the seasonal stratification and ML. Due to its maxima in stratification, current shear, and potential vorticity below the ML, the seasonal stratification characterizes the upper ocean as "difficulty in mixing" and exerts large influences on physical and biogeochemical processes during the warming season. Indeed, it is pointed out that the stability of the upper ocean column given by the seasonal stratification is closely related to spring bloom in the subpolar region (e.g. Dale et al., 1999). Moreover, the change in the strong seasonal stratification controls the vertical mixing intensity below the ML (e.g. Cronin et al., 2013) and the vertical mixing in the seasonal stratification is suggested as one of the important process providing nutrients to euphotic layer from subsurface in oligotrophic subtropical gyre (Sukigara et al., 2011). In general, direct measurements of vertical mixing in the seasonal stratification have sparse spatial and temporal coverage that could not describe the large-scale spatial distribution and its typical seasonal cycles.

In this study, we quantitatively investigated how the regional differences in the development of the seasonal stratification are set with the use of potential energy anomaly (PEA) as a metric to represent the strength of stratification based on Argo profiles and satellite-based atmospheric data.

The PEA budget analysis revealed that the seasonal stratification develops under an almost one-dimensional balance between the PEA increase (i.e. strengthening of the stratification) by atmospheric buoyancy forcing and the PEA decrease by vertical mixing within the water column in most of the North Pacific, except for regions of the western boundary current and equatorial current system south of 10°N. Moreover, it is found that the composition of buoyancy forcing (penetrating shortwave radiation and other non-penetrating components) contribute to making the meridional difference in the vertical structure of stratification; in the northern (southern) side of the North Pacific, the condition that the non-penetrating (penetrating) component dominates is favorable for the formation of a sharp (gradual) stratification.

The depth-averaged vertical diffusivity obtained from the residual of the PEA budget is in the range from 5×10^{-5} m^2/s to 5×10^{-4} m^2/s and its spatial and seasonal variability is found to be related to the amplitude of local wind forcing.

[References]
[1] Cronin, M. F., Bond, N. A., Farrar, J. T., Ichikawa, H., Jayne, S. R., Kawai, Y., Konda, M., Qiu, B., Rainville, L., & Tomita, H. (2013). Formation and erosion of the seasonal thermocline in the Kuroshio Extension recirculation gyre. *Deep Sea Research, Part II*, *85*, 62-74.
[2] Dale, T., Rey, F., & Hemidal, B. R. (1999). Seasonal development of phytoplankton at a high latitude oceanic site. *Sarsia*, *84*, 419-435.
[3] Sukigara, C., Suga, T., Saino, T., Toyama, K., Yanagimoto, D., Hanawa, K., & Shikama, N. (2011). Biogeochemical evidence of large diapycnal diffusivity associated with the Subtropical Mode Water of the North Pacific. *Journal of Oceanography*, *67*, 77-85.

Poster #42

Refractory lithophile composition of chondrites and their components: Implications for planetary compositions

TAKASHI YOSHIZAKI[1], WILLIAM F. MCDONOUGH[1,2,3], RICHARD D. ASH[2], TETSUYA YOKOYAMA[4]

[1] Department of Earth Science, Graduate School of Science, Tohoku University.
[2] Department of Geology, University of Maryland, College Park.
[3] Research Center for Neutrino Sciences, Tohoku University.
[4] Department of Earth and Planetary Sciences, Tokyo Institute of Technology.

Introduction: Historically, relative abundances of refractory lithophile elements (RLEs) are considered to be nearly constant among all classes of chondrites and the solar photosphere, at least within about 10%, leading to the assumption that the bulk RLE ratios of the terrestrial planets are chondritic [e.g., 1]. However, recent high-precision measurements revealed variations in some RLE ratios (e.g., Nb/Ta, Y/Ho, Zr/Hf) between chondrite groups and terrestrial samples [e.g., 4–6]. Although these observations may guide us to a better understanding of the building blocks of the planets, their detailed nature and origin are unclear.

Various stable isotope systems (e.g., O, Ti) in chondrites strongly suggest that the solar nebula was not isotopically homogenized when chondrite parent bodies accreted [e.g., 7]. Since enstatite chondrites (ECs) and the terrestrial samples are almost indistinguishable in most isotopic systems, they can be the main building blocks of the Earth [e.g., 8].

Chondritic components formed in the solar nebula before chondrite parent bodies can provide snapshots of spatial/temporal heterogeneities of chemical composition in the nebula. To reveal the variation in a variety of RLE ratios among solar system materials, and put constraints on its origin, we have performed a systematic analysis of RLE compositions of primitive ECs and their components. We also seek to understand the cosmochemical behavior of RLEs under reduced conditions in which ECs have formed.

Methods: Petrology, mineralogy and major element chemistry of thin sections of five unequilibrated ECs were analyzed using SEM and electron microprobes at Tohoku University. Trace element compositions of the samples were determined using a New Wave frequency- quintupled Nd:YAG laser system coupled to a Thermo Finnigan Element2 ICP-MS at University of Maryland (UMd). Chips of ECs were digested by combination of HCl, HNO_3, HF and $HClO_4$ acids at Tokyo Institute of Technology to measure their bulk compositions using the ICP-MS at UMd.

Results and Discussion: The EC chondrules show non-chondritic values with large variation in several RLE ratios. They are significantly depleted in Nb, with Nb/Ta being ~30% lower than the chondritic value [4]. They also show subchondritic mean Ti/Sc and Zr/Hf values. Most troilites in ECs have, on average, a factor of 5 enrichments in Ti, V and Nb relative to CI, whereas Zr and Ta abundances are 10 times less and Hf is undetected. Thus, the variations in RLE ratios in EC chondrules can be explained by subtraction of troilite from a chondritic reservoir before/during EC chondrule formation.

RLE composition of EC sulfides shows that some RLEs including Nb, Zr and Ti are become chalcophile at low fO_2. Although Münker et al. [18] recently argued that the incorporation of Nb-rich cores of highly reduced asteroids into the Earth's core, and their concomitant Ta enriched silicate portion into the silicate Earth, caused subchondritic Nb/Ta of the bulk silicate Earth, there is abundant evidence that the silicate Earth has chondritic Ti/RLE and Zr/RLE ratios. Therefore, RLE fractionation in the silicate Earth by subtraction of the RLE-bearing sulfide is unlikely, leaving us an enigmatic state regarding the role of Nb during the core formation.

Results of bulk rock measurements will be discussed in this talk.

[References]
[1] Wasson J.T. and Kallemeyn G.W. (1988) *Philos. Trans. Royal Soc. A.*, 325, 535–544.
[4] Münker C. et al. (2003) *Science*, 301, 84–87.
[5] Pack A. et al. (2007) *GCA*, 71, 4592–4608.
[6] Patzer A. et al. (2010) *MAPS*, 45, 1136–1151.
[7] Warren P.H. (2011) *EPSL*, 311, 93–110.
[8] Javoy M. et al. (2010) *EPSL*, 293, 259–268.
[18] Münker C. et al. (2017) *Nat. Geosci.*, 10, 822–826.
[19] Lodders K. (2003) *ApJ*, 591, 1220–1247.

Poster #43

Chemical reactions between Fe and H_2O up to megabar pressures and implications for water storage in the Earth's mantle and core

LIANG YUAN[1], EIJI OHTANI[1,2], DAIJO IKUTA[1], SEIJI KAMADA[1], JUN TSUCHIYA[3], NAOHISA HIRAO[4], YASUO OHISHI[4], AKIO SUZUKI[1]

[1] Department of Earth and Planetary Material Sciences, Tohoku University, Sendai, Japan.
[2] V.S. Sobolev Institute of Geology and Mineralogy, Siberian Branch, Russian Academy of Sciences, Novosibirsk, Russia.
[3] Geodynamics Research Center, Ehime University, Matsuyama, Japan.
[4] Japan Synchrotron Radiation Research Institute, Sayo, Hyogo, Japan.

We investigated the phase relations of the Fe-H_2O system at high pressures based on in situ X-ray diffraction experiments and first-principles calculations and demonstrate that FeH_x and FeO are present at pressures less than ~78 GPa. A recently reported pyrite-structured FeO_2 was identified in the Fe-H_2O system at pressures greater than ~78 GPa after laser-heating. The phase observed in this study has a unit-cell volume 8%-11% larger than that of FeO_2, produced in the Fe-O binary system reported previously, suggesting that hydrogen might be retained in a FeO_2H_x crystal structure. Our observations indicate that H_2O is likely introduced into the deep Earth through reactions between iron and water during the accretion and separation of the metallic core. Additionally, reaction between Fe and H_2O would occur at the core-mantle boundary, given water released from hydrous subducting slabs that intersect with the metallic core. Accumulation of volatile-bearing iron compounds may provide new insight into the enigmatic seismic structures observed at the base of the lower mantle.

Poster #44

Compressibility and structure of hydrous silicate melts from first-principles

LIANG YUAN[1], GERD STEINLE-NEUMANN[2], EIJI OHTANI[1], AKIO SUZUKI[1]

[1] Department of Earth and Planetary Material Sciences, Tohoku University, Sendai, Japan
[2] Bayerisches Geoinstitut, Universität Bayreuth, Bayreuth, Germany

Water is generally considered to be an important component in silicate melts. They can contain a substantial water content (up to 16 wt%) [1-2], particularly at low degree partial melting, while experiments typically explore hydrous silicate melt properties over a limited range of water content (typically below 10 wt%) [3-4].

In situ x-ray observations suggest an unusual polymerization transition at 3-5 GPa in hydrous silicate melts, assuming that OH^- hydroxyl preferentially bond to Mg^{2+} instead of Si^{4+} above this *P*, via the mechanism Si-O-Mg + Si-OH → Mg-OH + Si-O-Si [5]. Here we use first-principles molecular dynamics (FPMD) simulations to explore the following:

(1) Compressibility and static structure of molten $MgSiO_3$ and Mg_2SiO_4 containing up to 20 wt% H_2O;
(2) Validity of the assumption of a *P*-induced affinity for Mg^{2+} cation to water species suggested by experiments [5-6].

This work was supported by the JSPS Japanese–German Graduate Externship.

[References]
[1] Freitas et al., *Nat. Commun*. 8 (1), 2186 (2017).
[2] Litasov and Ohtani, *Phys. Earth Planet. Inter*. 134 (1-2), 105 (2002).
[3] Sakamaki, *Chem. Geol*. 475, 135 (2017).
[4] Mookherjee et al., *Nature* 452 (7190), 983 (2008).
[5] Yamada et al., *Earth Planet. Sci. Lett*. 308 (1-2), 115 (2011).

Participants List

	Name (First, Middle, Family)			Affiliation	E-mail
1	Sae		Aizawa	Dept. of Geophysics, Tohoku Univ.	aizawas@pat.gp.tohoku.ac.jp
2	Shun		Arai	Dept. of Earth Science, Tohoku Univ.	shun.arai.t4@dc.tohoku.ac.jp
3	Naoki		Araya	Dept. of Earth Science, Tohoku Univ.	n.araya@dc.tohoku.ac.jp
4	Masyitha	R.	Budiati	Dept. of Geophysics, Tohoku Univ.	retno@dc.tohoku.ac.jp
5	Fidel		Costa	Earth Observatory of Singapore, Nanyang Technological Univ.	fcosta@ntu.edu.sg
6	Shanaka		de Silva	College of Earth Ocean and Atmospheric Science, Oregon State Univ.	desilvas@geo.oregonstate.edu
7	Mindaleva		Diana	Dept. of Environmental Studies for Advanced Society, Tohoku Univ.	diana@geo.kankyo.tohoku.ac.jp
8	Sara		Emanuel	Dept. of Earth Science, Tohoku Univ.	saraemanuel17@gmail.com
9	Daniel		Frost	Bayerisches Geoinstitut, Univ. of Bayreuth	dan.frost@uni-bayreuth.de
10	Wakana		Fujita	Dept. of Earth Science, Tohoku Univ.	w.fujita@dc.tohoku.ac.jp
11	Kenichi		Goto	Dept. of Earth Science, Tohoku Univ.	kenichi.goto.q5@dc.tohoku.ac.jp
12	Tomomi		Hara	Dept. of Earth Science, Tohoku Univ.	tomomi.hara.r1@dc.tohoku.ac.jp
13	Mohammad		Hasib	Dept. of Geophysics, Tohoku Univ.	hasib@zisin.gp.tohoku.ac.jp
14	Takashi		Hirose	Dept. of Geophysics, Tohoku Univ.	hirose@zisin.gp.tohoku.ac.jp
15	Yongsheng		Huang	Dept. of Earth Science, Tohoku Univ.	huang.yongsheng.s8@dc.tohoku.ac.jp
16	Ayumu		Ishikawa	Dept. of Geophysics, Tohoku Univ.	ishikawa@zisin.gp.tohoku.ac.jp
17	Mochamad	R.	Iskandar	Dept. of Geophysics, Tohoku Univ.	riza@pol.gp.tohoku.ac.jp
18	Eranga		Jayawickrama	Dept. of Earth Science, Tohoku Univ.	eranga.j@dc.tohoku.ac.jp
19	Kasper	B.	Jensen	Dept. of Earth Science, Tohoku Univ.	jensen.kasper.bisgaard.q5@dc.tohoku.ac.jp
20	Hisamu		Kasahara	Dept. of Environmental Studies for Advanced Society, Tohoku Univ.	h.kasahara@geo.kankyo.tohoku.ac.jp
21	Yuki		Katsuragi	Dept. of Earth Science, Tohoku Univ.	yuki.katsuragi.r1@dc.tohoku.ac.jp
22	Stephen		Kirby	U.S. Geological Survey	stevenlyle@icloud.com
23	Fumiya		Maeda	Dept. of Earth Science, Tohoku Univ.	fumiya.maeda.p1@dc.tohoku.ac.jp
24	Sagar		Masuti	Asian school of Environment, Nanyang Technological Univ.	sagarshr001@e.ntu.edu.sg
25	William	F.	McDonough	Dept. of Earth Science, Tohoku Univ. / Dept. of Geology, Univ. of Maryland	mcdonoug@umd.edu
26	Keiko		Mori	Dept. of Earth Science, Tohoku Univ.	keiko.mori.q4@dc.tohoku.ac.jp
27	Hisashi		Nakahara	Dept. of Geophysics, Tohoku Univ.	naka@zisin.gp.tohoku.ac.jp
28	Yusuke		Netsu	Dept. of Environmental Studies for Advanced Society, Tohoku Univ.	netsu@geo.kankyo.tohoku.ac.jp

	Name (First, Middle, Family)			Affiliation	E-mail
29	Astin		Nurdiana	Dept. of Environmental Studies for Advanced Society, Tohoku Univ.	astin@geo.kankyo.tohoku.ac.jp
30	Tomoya		Obase	Dept. of Earth Science, Tohoku Univ.	tomoya.obase.s3@dc.tohoku.ac.jp
31	Tomonori		Ohashi	Dept. of Earth Science, Tohoku Univ.	tomonori.ohashi.s8@dc.tohoku.ac.jp
32	Satoshi		Okumura	Dept. of Earth Science, Tohoku Univ.	satoshi.okumura.d2@tohoku.ac.jp
33	Theodorus		Permana	Dept. of Geophysics, Tohoku Univ.	theodorusp@zisin.gp.tohoku.ac.jp
34	Anggraini		Puji	Dept. of Earth Science, Tohoku Univ.	puji.anggraini.rizkita.p1@dc.tohoku.ac.jp
35	Bo		Qiu	Dept. of Oceanography, Univ. of Hawaii at Manoa	bo@soest.hawaii.edu
36	Inna		Safonova	Novosibirsk State Univ.	inna03-64@mail.ru
37	Shunta		Sakai	Dept. of Earth Science, Tohoku Univ.	shunta.sakai.q6@dc.tohoku.ac.jp
38	Sando		Sawa	Dept. of Earth Science, Tohoku Univ.	sando.sawa.t1@dc.tohoku.ac.jp
39	Kengo		Sawayama	Dept. of Environmental Studies for Advanced Society, Tohoku Univ.	sawayama@geo.kankyo.tohoku.ac.jp
40	Igor		Sharygin	Sobolev Institute of Geology and Mineralogy / Center for Northeast Asian Studies, Tohoku Univ.	igor.sharygin@gmail.com
41	Tsuyoshi		Shibata	Dept. of Geophysics, Tohoku Univ.	shibata@zisin.gp.tohoku.ac.jp
42	Yuzuki		Shinji	Dept. of Earth Science, Tohoku Univ.	yuzuki.shinji.r2@dc.tohoku.ac.jp
43	Shusaku		Sugimoto	Frontier Research Institute for Interdisciplinary Science, Tohoku Univ.	sugimoto@pol.gp.tohoku.ac.jp
44	Kento		Suzuki	Dept. of Geophysics, Tohoku Univ.	kento.suzuki.p4@dc.tohoku.ac.jp
45	Manami		Suzuki	Dept. of Geophysics, Tohoku Univ.	manami.suzuki.p8@dc.tohoku.ac.jp
46	Miki		Takahashi	Dept. of Earth Science, Tohoku Univ.	miki.takahashi.p4@dc.tohoku.ac.jp
47	Naoya		Takahashi	Dept. of Earth Science, Tohoku Univ.	naoya.takahashi.t1@dc.tohoku.ac.jp
48	Naoya		Takahashi	Center for Atmospheric and Oceanic Studies, Tohoku Univ.	naoya.takahashi.r5@dc.tohoku.ac.jp
49	Marcel		Thielmann	Bayerisches Geoinstitut, Univ. of Bayreuth	Marcel.Thielmann@uni-bayreuth.de
50	Tatsuki		Tsujimori	Center for Northeast Asian Studies / Dept. of Earth Science, Tohoku Univ.	tatsukix@tohoku.ac.jp
51	Tong		Wang	Dept. of Geophysics, Tohoku Univ.	wangtong.330@gmail.com
52	Ryohei		Yamaguchi	Dept. of Geophysics, Tohoku Univ.	ryohei@pol.gp.tohoku.ac.jp
53	Takashi		Yoshizaki	Dept. of Earth Science, Tohoku Univ.	tacasy22@dc.tohoku.ac.jp
54	Liang		Yuan	Dept. of Earth Science, Tohoku Univ.	yuan.liang.s4@dc.tohoku.ac.jp
55	Georg	F.	Zellmer	Volcanic Risk Solutions, Massey Univ.	G.F.Zellmer@massey.ac.nz